OBSERVATIONS OF THE MEDIUM ENERGY COSMIC RAY FLUX

A thesis presented for the degree of

Doctor of Philosophy

by

Peter Ronald Gerhardy B.Sc.(Hons)

Department of Physics

University of Adelaide

January 1983

C O N T E N T S

SUMMARY

Since the discovery that cosmic rays with energies above about 10 GeV are not of solar origin, details of their origin, energy spectrum and composition have been of great importance to astrophysical and cosmological theories, especially regarding the highest energy astrophysical events. At primary particle energies above about 10^{14} eV, the nuclear interaction processes in collisions are not yet observable by man-made particle accelerators and so are not well understood. Details of the primary spectrum and composition at these energies remain unclear since cosmic ray primaries may only be observed by the secondary products of their interactions with the atmosphere. This difficulty is especially evident in the medium energy range between about 10^{15} eV and 10^{17} eV where there appears to be a change in the spectrum. The aim of this project was to study the cosmic ray flux in this energy range by means of the secondary products at sea level using the Buckland Park Extensive Air Shower Array in order to unravel details of the flux including arrival directions, energy spectrum and composition.

For much of the author's candidature, he was responsible for the routine running of the Buckland Park array and the analysis of the data recorded by it. Details of the components of this array, its response to the air shower flux, and the data analysis procedures are described.

Observations of the primary spectrum from the sea level products are made in terms of the number of secondary particles produced - the shower size spectrum. This spectrum may be inferred from assumptions about the shower structure or alternatively from measurements of the array density spectrum. Results from both techniques are given.

Clearly, the structure of the shower at sea level is determined by its development in the atmosphere. The shower development was studied by means of parameters measured at ground level. These include the shower absorption and attenuation lengths, and the lateral distribution age parameter. The results of the determination of these parameters are given.

Measurements on the isotropy of the cosmic ray flux were made using the collected data from a period of three years. Results of these measurements are described by harmonic analyses of the data in both sidereal and solar times, as well as side-bands. The declination distribution of the flux is described using the Buckland Park data and also by comparison with another observatory.

Finally, the results of all the measurements are discussed in terms of the information they provide and their influence on the primary cosmic ray flux.

STATEMENT

This thesis contains neither any material which has been accepted for the award of any other degree or diploma, nor, to the best of the author's knowledge and belief, any material previously published or written by any other person, except where due reference is made.

Peter R. Gerhardy

ACKNOWLEDGEMENTS

I wish to thank my supervisor, Dr. Roger W. Clay for his advice and help throughout my candidature. His encouragement, sense of humour and overwhelming enthusiasm have made this project a memorable and most enjoyable experience.

I am also grateful for the technical support received, especially from Neville Wild and Lindsay Hettner, and also at various times from the other technical and workshop staff of the Physics Department and Electronic Services for their invaluable help, Peter Wadey, George Joss and the staff of the Computing Centre, and also Anne White and Ann McLean for their tolerance and help.

For helpful discussions in congenial as well as occasionally trying circumstances and at times physical labour, I would also like to thank my fellow students, especially David Liebing, Jim Kuhlmann and Greg Thornton and Bruce Dawson, also the other members of the Cosmic Ray Group and C.R.G.G.C. (Int.) for their cooperation and friendship.

For the actual production of the thesis, I thank Judy Laing for her excellent drawings, Fred Lowe for his help with the printing and especially Jayne Trowse and Anne White for their patience and help during the late and early hours.

Finally, I would like to thank my parents for their encouragement and support without which this work would not have been done.

CHAPTER ONE

INTRODUCTION

1.1 The Primary Spectrum

In 1912, Victor Hess discovered that highly energetic and ionizing radiation was continually impinging on the earth's atmosphere from outside. Since then, the origin and composition of this cosmic radiation have been major puzzles in astrophysics. The astrophysical problem is especially concerned with determining a satisfactory mechanism which is capable of accelerating these particles to the enormous energies (up to at least 10^{20} eV) in the numbers observed. This problem has strenuously exercised the ingenuity of those concerned. Cosmological theories must also take account of cosmic radiation since the projected energy density of this radiation is not inconsiderable, and in fact is of the same order of magnitude as that of starlight or magnetic fields in the galaxy.

Over the years almost every type of high energy astrophysical process has been invoked for producing cosmic rays. Proposed cosmic ray sources have included supernovae and their remnants - black holes and neutron stars, radio and other energetic galaxies, the galactic centre, and globular

clusters. Frequently, these have been proposed as injection sources with further acceleration taking place by means of collisions with magnetic irregularities or 'clouds' propagating through the interstellar medium. The basic acceleration mechanism associated with these collisions is known as second-order Fermi acceleration (Fermi 1949). The total energy change is proportional to the cloud velocity squared, and involves both head-on and following collisions. There is a mean energy gain since head-on collisions are statistically more probable than following collisions. However, because energy is lost in following collisions, the acceleration of particles by this mechanism is slow. First-order Fermi acceleration, with the total energy gain proportional to the cloud velocity, involves only head-on collisions and is clearly a more rapid acceleration process. This mechanism is used in a number of current acceleration theories.

The most promising current theories involve shock wave acceleration of injected particles (Bell 1978a,b, Blandford and Ostriker 1978). Such shock waves, produced by supernovae or other energetic processes, may propagate large distances through the galaxy before they become inefficient accelerators. Relativistic particles are trapped in the shock front and may cross the shock many times, each time gaining energy by the Fermi first-order process. This mechanism gives rise to a power law spectrum for the energies produced with an index in close agreement to that observed in galactic cosmic rays (Bell 1978).

Key indicators of the original particle source come from the measurements of the isotopic and chemical composition of the particles. Unfortunately these measurements have only been made for energies below about 10^{12} eV. When compared with other available composition measurements such as those of the local galactic (from meteorites), solar corona and solar wind, the galactic cosmic ray composition is found to be close to that from solar energetic particles (Casse 1981), suggesting that at least at low energies the flux injected for acceleration comes from solar-like stars.

For higher energies no such data are available. However supernovae, pulsars and the stellar winds from hot OB star associations are favoured as candidates for producing the injection component. Ostriker and Gunn (1969) have suggested a mechanism whereby pulsars can accelerate particles. They predicted a peak in the energy spectrum above 10^{15} eV depending on composition. The injected particles could then be further accelerated by the supernova shock wave. A mechanism for particle acceleration to very high energies in the very early stages of supernova collapse has also been suggested by Colgate and Johnson (1960).

Once accelerated, the particle (if galactic) propagation is determined by the galactic magnetic field. Up to about 10^{17} eV, the particles are effectively confined to the galaxy since the radii of gyration of lower energy particles are of less than galactic dimensions. The

propagation mode along the magnetic field lines is also strongly influenced by the presence of the partially ionized interstellar medium (e.g. see Longair 1981). In this case, the streaming velocity of the cosmic ray flux is restricted by scattering from Alfven and hydromagnetic waves set up in the plasma by the interaction of the particles themselves with the magnetic field. If there is a significant neutral gas component, the Alfven waves may be damped by kinetic energy losses to the neutral gas so that the particles can diffuse more rapidly. However, in a highly ionized gas the cosmic ray streaming is restricted to the Alfven speed. This also provides an effective containment mechanism.

Many of the results from investigations of the various components and products of cosmic radiation have only deepened the mystery of its origin and opened further possibilities for the solution. After about 70 years of detailed and careful study some features of the primary radiation are now becoming clear.

The primary cosmic ray energy spectrum can conveniently be divided into three parts (ignoring solar cosmic rays which, although the most numerous, occupy only the lowest energies - less than about 10^{10} eV):

(i) less than 10^{14} eV at which energies the primary particles can be observed directly or by their penetrating products;

(ii) between 10^{14} eV and 10^{17} eV where it is necessary (due to the low flux) to employ

large detectors at ground level which observe secondary products and where the 'knee', the most obvious feature of the cosmic ray spectrum is observed;

(iii) greater than 10^{17} eV, the realm of the highest energy cosmic rays where the extremely low flux dictates the use of detectors with sensitive areas of the order of several square kilometres or larger.

Figure 1.1 indicates the general form of the cosmic ray energy spectrum, although experimental evidence from the various groups studying the spectrum is far from conclusive about the details.

1.1.1 The Low Energy Range

In the low energy interval (below 10^{14} eV), due to the possibility of direct observations, the spectrum appears to be most settled although discrepancies between the results obtained using different techniques still exist. There are three general methods of making observations in this region. Firstly, direct measurements may be made on the primary flux. This technique involves the use of detectors (flown above most of the atmosphere) mounted on high altitude balloon rigs or on satellites. Probably the most definitive of these experiments were those of Grigorov et al (1971), who flew the PROTON series of satellites. Using large ionization calorimeters

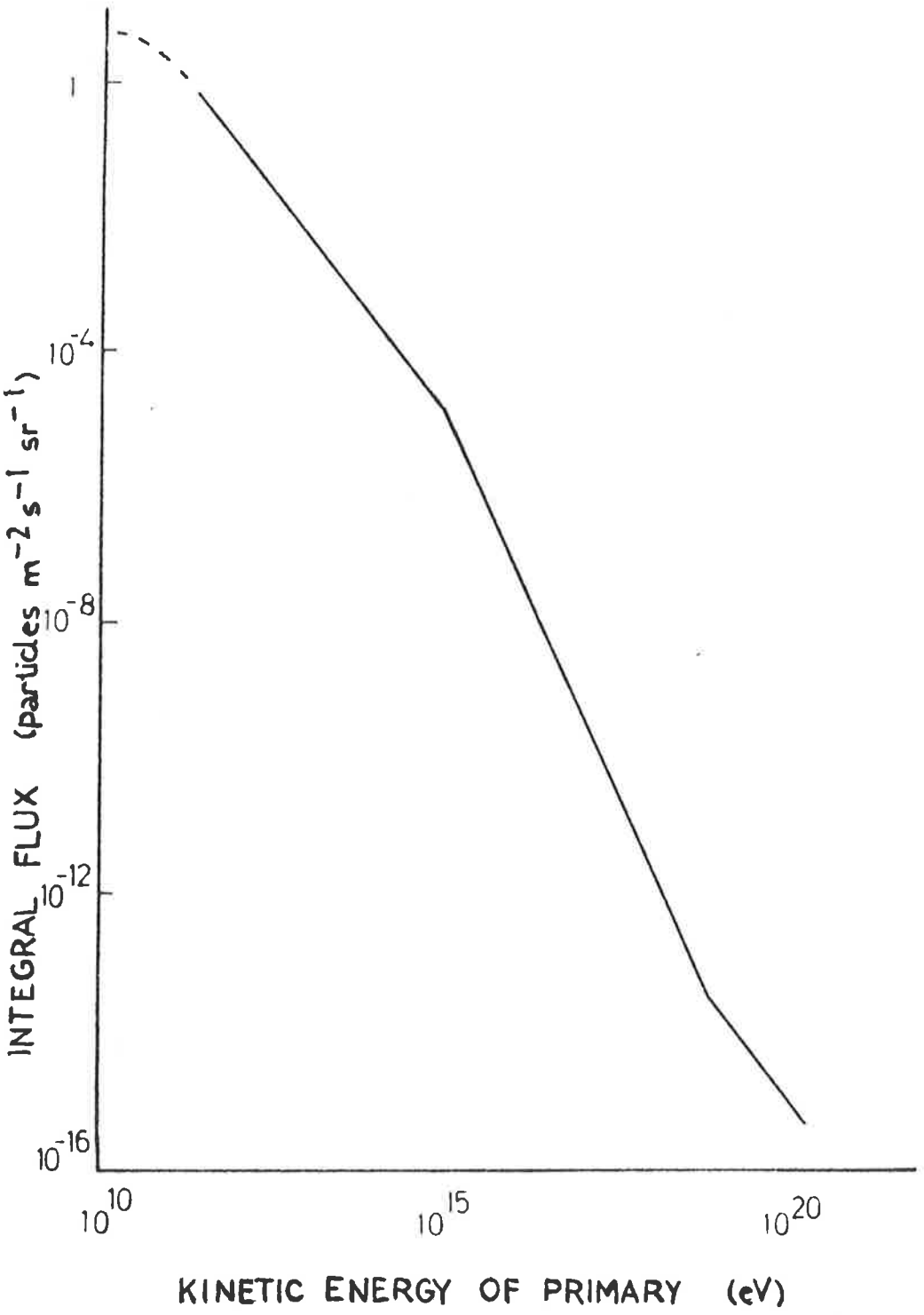

Figure 1.1 The Cosmic Ray Integral Energy Spectrum

(Grigorov et al 1965), they were able to study the compositions and the energies of the detected primaries up to the medium energy range.

In calorimetry experiments, the primary particles impinge on a number of different types of detectors such as proportional counters, spark chambers, scintillators and Cerenkov detectors sandwiched between various nuclear targets and absorbers. These all ensure that the charge and energy of the primary particles can ~~by~~ be measured through the production of nuclear and electromagnetic particle cascades which finally result in the deposition of the total energy of the primary particles in the calorimeter. By monitoring the deposition process, the energies and composition of the primaries can be estimated. This type of experiment is limited to a maximum detectable energy, firstly by the size of the calorimeter which ensures that substantially all of the energy is collected and secondly by the low flux of the higher energy primary particles increasing the statistical limits on intensity measurements.

Similar types of experiment (e.g. Gregory et al 1981, Kuzmichev et al 1981) can also be carried out using passive recording techniques. In these, interactions and cascades are produced in a similar manner, but the energy deposition process is recorded using various nuclear and X-ray films and emulsions.

Although both types of calorimetry experiment require

very careful calibration and interpretation, they constitute the only direct measurement technique on the cosmic ray flux.

The second source of information in this energy range is the study of penetrating particles at ground level produced by nuclear interactions between the incoming primary cosmic rays and atmospheric nuclei. These penetrating particles are charged muons coming from the decay of kaons and pions produced in the interactions. There is a close relationship between the detected particles (which if they have high enough energy, only lose energy by ionization in their passage through the atmosphere) and the primary particles. At lower energies, the decay of the muons to electrons and neutrinos becomes important.

These particles are monitored in a number of different ways, including large muon spectrometers such as that used by the DEIS collaboration (Allkofer et al 1977a,b) and underground detectors (e.g. Bergeson et al 1975a, Cini 1976). Similar types of elements such as scintillators, Cerenkov counters and spark chambers are used in both types of experiment, although these are combined with magnets to measure the muon charge in the spectrometers.

Calculations relating the energy spectrum of the muons to that of the primary particles ~~were~~ have been ~~first~~ performed by Ramana Murthy and Subramanian (1972a), using a postulated primary nucleon spectrum with the measured muon momentum spectrum and particle accelerator data to test the Feynman

scaling theory (Feynman 1969) of nuclear interactions. Since then, the technique has been turned around and used to calculate the primary nucleon spectrum from the muon data using accelerator data with models of nuclear interactions such as Feynman scaling and CKP (see Brooke et al 1964). Recent calculations (Das and De 1980) set the ratio between muon energy and the energy of the parent primary at about 10 (as a rough rule of thumb). In detail, two techniques can be used in attempting to derive the primary nucleon spectrum. Either the spectrum of parent mesons is deduced from the muon data and hence the primary nucleon spectrum, or a primary nucleon spectrum is assumed and this is used to calculate a muon spectrum which is then fitted to the measured data. Unfortunately, the results of these two techniques do not always agree (see Klemke et al 1981 and Mitsui at al 1981). Hence Hillas (1981) notes the difficulty of the 'inverse problem' - calculating the most probable primary spectrum from the spectrum of the secondary products. This problem applies not only to this energy range and data collection technique, but in all cosmic ray experiments where direct measurements on the flux are not possible.

Ramana Murthy and Subramanian (1972b) also pointed out that the ratio of the number of positively to that of negatively charged muons is sensitive to the fraction of protons in the primary spectrum and can therefore be used to study changes in the chemical composition of the flux (e.g. from a pure proton beam to a mixture with other nuclei). Measurements of the rates of doubles, triples, and higher

multiplicities of coincidences (Lowe et al 1973) can also be used to study the composition (Elbert et al 1973). It should be noted however, the composition results from these types of calculations are also dependent on the model of nuclear interactions used (in the same way as energy spectrum calculations).

Studies of the cascades (known as extensive air showers) resulting from the interactions between the cosmic ray primaries and atmospheric nuclei provide the third source of information about the primary flux in this energy range. This technique is also the only viable method in the higher energy intervals. However at these low energies the detectors must be placed at high altitudes to detect useful numbers of secondary particles. Arrays of detectors (e.g. scintillators or proportional counters) are spread out (on a scale distance of about 10 metres) at mountain altitudes to measure coincidences of the secondary particles and hence monitor the cosmic ray primaries which produced them.

In experiments of this type, the individual detectors sample the cascade products and hence, assuming some lateral distribution of the secondary particles, estimate a ground parameter, generally N_e - the number of particles (electrons) at ground level. Erlykin et al (1973) at the Tien-Shan observatory (altitude 3340 metres) have used these data in conjunction with simultaneously measured muon data to investigate whether the primary composition is changing in the region of about 10^{13} eV. At this energy, their calculations

were consistent with the composition measured at lower energies.

Figure 1.2 (from Hillas 1981 and references therein) gives a compilation of various primary energy spectra and composition measurements over the whole cosmic ray spectrum. One very interesting feature of these measurements is the apparent rising proportion of iron nuclei in the compilation. The increasing slope of the proton-only spectrum has been measured in all of the PROTON experiments of Grigorov et al (1971), however it is believed (Hillas 1980) that this observation may be due to the difficulty of particle identification and should have no effect on the all-nuclei spectrum. Measurements of a sharp cut-off in the all-nuclei spectrum in the same experiments at above 10^{14} eV may be due to the incomplete containment of the cascade products in the calorimeters at these energies (Watson 1974).

1.1.2 The Medium Energy Range

As stated earlier, the only useful method for investigating the primary cosmic ray spectrum above 10^{14} eV is by observing the products of the interactions between the primary particles and atmospheric nuclei. To some extent, the whole atmosphere above the detector can be considered as performing the function of the ionization calorimeter of satellite and balloon borne experiments, with over 90% of the incident energy deposited as ionization in the atmosphere. In

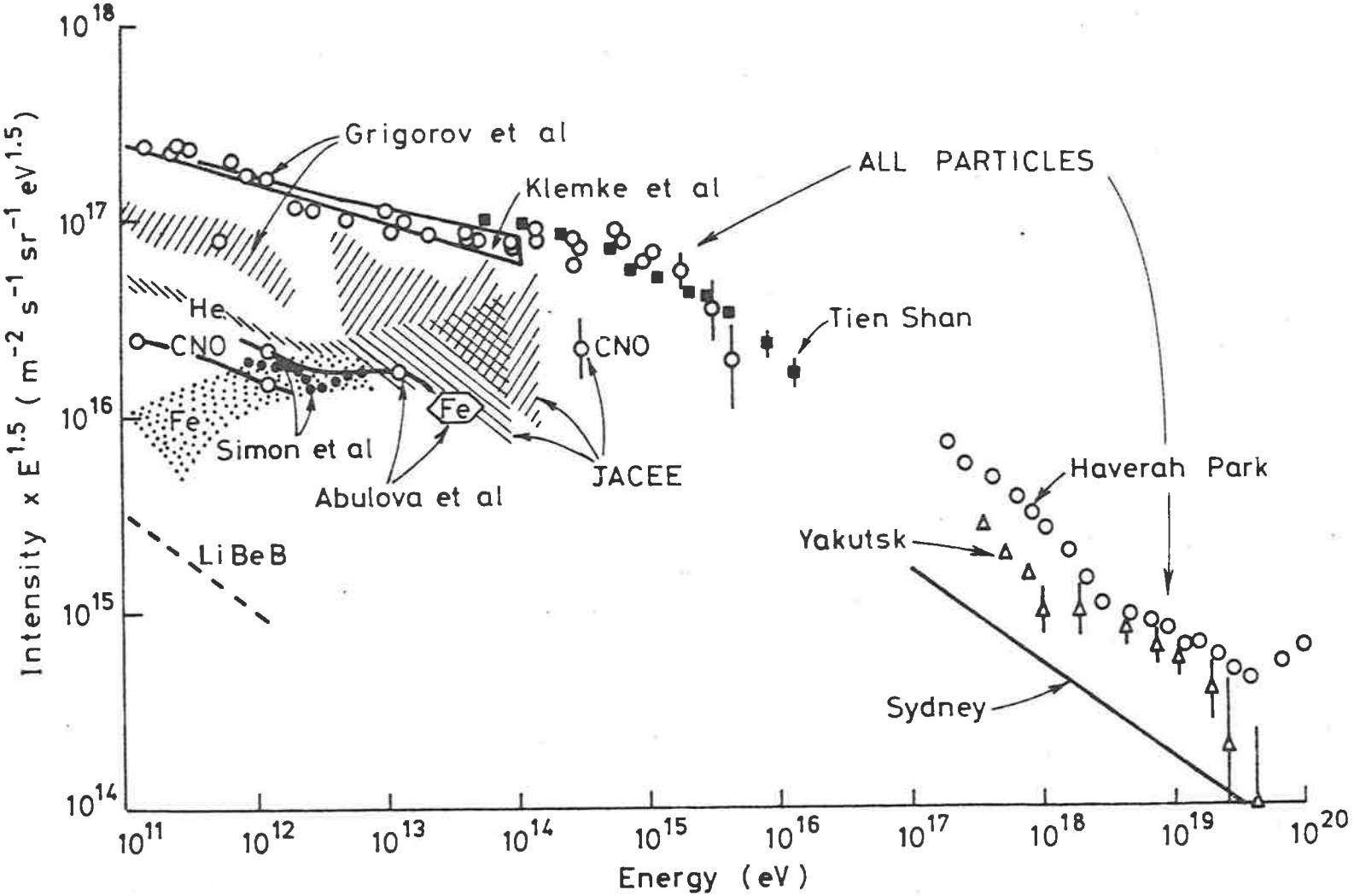

Figure 1.2 A compilation of energy spectrum results (after Hillas 1981)

this case the resultant cascade cannot be monitored over its whole development, but is observed over only a limited range which depends on the altitude and zenith angle resolution of the observatory. Measurements of the extensive air shower size, N_e, at various zenith angles but at constant shower rate, are essentially equivalent to observations of the same average shower (and hence average primary particle) at different depths in the atmosphere. Information on the composition and the nuclear physics involved in the shower development may therefore be obtained by this process. Since direct measurements of the energy and composition spectrum are not feasible, this information must be used in conjunction with some model of the nuclear interactions to derive the primary spectrum.

For a given shower, to derive the energy of the incident primary, a theoretical curve of shower size as a function of atmospheric depth (or zenith angle) at constant intensity is fitted to the measured data, using a suitable nuclear interaction model (e.g. Feynman scaling with rising interaction cross sections (Hillas 1979b)). The integral of this curve is then proportional to the energy dissipated in the atmosphere, so that, after allowance is made for the remaining energy (for example in neutrinos), the primary energy can be estimated. Alternatively, and somewhat less accurately, these shower development curves are used to determine an estimate of the shower size at maximum, and this is multiplied by a predetermined energy per particle to give the primary energy (Kempa et al 1974, Bradt et al 1965).

Because of the composition uncertainty, it is clear that these calculations of the energy spectrum are open to speculation.

Results reported from air shower experiments generally give the rate of detection of extensive air showers as a function of shower size, because of the composition uncertainty producing uncertainty in the determination of the energy per nucleus. The ratio of the shower size to the energy of the initiating primary particle is roughly 10^{-10} at energies near 10^{15} eV (Cocconi 1961).

Most recent attempts to evaluate the mass composition of the primary cosmic radiation in the medium energy range have come from the interpretation of atmospheric Cerenkov radiation measurements made on extensive air showers. Since Cerenkov radiation is produced by relativistic particles throughout the development of the air shower, the amount of Cerenkov radiation detected at a given distance from the shower core can be related to the shower growth and decay. In fact, there is a one-to-one correspondence between the Cerenkov pulse shape and the shower development curve. Kalmykov et al (1979) calculated the relationship between the full width at half maximum of the Cerenkov pulse at a core distance of 300 metres and the height of maximum of the shower size (at primary energies between $5*10^{16}$ eV and 10^{18}eV). These calculations were extrapolated by Thornton and Clay (1979) who used them with their own Cerenkov measurements at smaller core distances to postulate a change in mass composition from heavy to light nuclei in the region of the

energy spectrum knee. Similar measurements were also carried out by Hammond et al (1978) using their own calculations over a wide energy range. The compilations of atmospheric depth of shower size maximum of Linsley and Watson (1981a,b) and Hillas (1981) compared with various models of nuclear interactions appear to support the possibility of composition changes in the medium energy interval. These workers concluded that if a change in composition from iron nuclei to protons was assumed at near 10^{15} eV, then Feynman scaling could be applied to the nuclear interactions up to the highest energies with good results. However, if the composition was assumed to be the so-called mixed or conventional composition measured directly at low energies, none of the nuclear interaction models could be stretched to fit the depth of maximum data.

Other evidence for the predominately heavy composition near the spectrum knee (at about 10^{15} eV) comes from Cowsik et al (1981) who investigated the arrival time distribution of hadrons associated with air showers. Using Monte Carlo simulations, they found that their data was best fitted by a composition which had an increasing proportion of heavy nuclei at this energy. However, the difficulties of the composition at these energies are not yet overcome, due to some as yet unexplained results, such as those of Nikolsky et al (1979,1981) whose muon data indicates a mixed composition. The possibility of nuclear interaction characteristics changing radically in this energy region has not yet been excluded.

There have been a number of explanations of the form of the energy spectrum in this region. Karakula et al (1974) derived the spectrum of cosmic rays produced by pulsars from the pulsar acceleration model of Ostriker and Gunn (1969). Using experimental data on pulsars, they postulated the so-called 'pulsar bump', where the contribution from pulsars is added to a background flux. The proposed spectrum shape with accelerated protons is an excellent fit to the measured spectrum, although this composition produces difficulties when compared to the depth of maximum data. The cut-off energy for the acceleration mechanism goes as:

$$E_{max} \sim A^{1/3} \cdot Z^{2/3} \qquad (1.1)$$

and so the situation is not improved for heavy nuclei acceleration.

An alternative model is the 'leaky box' propagation model (e.g. Peters 1961, Cowsik and Wilson 1973) which is in essence energy-dependent particle diffusion. The basis of this model is that the primary cosmic rays, at least up to about 10^{17} eV, are accelerated by sources inside the galaxy, with the component spectra having similar slopes. These particles are contained in the galaxy by the galactic magnetic field. At appropriate energies, the radii of gyration of the various composition components become large enough to increase leakage from the galaxy, giving rise to a change in slope of the all-nuclei spectrum. This model was rejected by Hillas (1979a) on the basis of a mixed composition (from lower energy

data) and the requirement that leakage of the composition components should begin at the same magnetic rigidity. However, Cowsik et al (1981) have proposed a fairly simple model, including an extragalactic proton component to agree with higher energy depth of maximum data, which not only gives constant rigidity cut-offs, but also predicts an enhanced heavy component between about 10^{14} eV and 10^{17} eV.

1.1.3 The High Energy Range

At the highest energies, measurements of the primary energy spectrum can only be made by the very limited number of giant air shower arrays. These use essentially the same techniques as at the medium energies (although the new Fly's Eye detector (Bergeson et al 1975b,c,d) is radically different) having, however collection areas of the order of a number of square kilometres to enable detection of low flux primaries at a reasonable rate. Energy spectra from the various arrays are calculated from the measured ground parameters and nuclear interaction models in a similar way to that at lower energies. The ground parameters used, though, are not necessarily the measured shower size and depend on the type of the individual detectors used in the array. Examples of these alternative ground parameters are ρ_{600}, the particle density at 600 metres used at the Haverah Park array (e.g. Andrews et al 1971, Hillas et al 1971), and Q_{400}, the Cerenkov radiation flux at 400 metres used at the Yakutsk array (e.g. Dyakonov et al 1973, Krasilnikov et al 1977).

These parameters may be chosen to be relatively insensitive to the nuclear model used and the mass of the primary particle and this enables accurate estimates of the primary energy to be obtained. Spectra measured by a number of groups are shown in figure 1.2.

As in the medium energy range, the mass composition of the primary particles must be inferred from the extensive air shower properties measured at ground level. Depth of maximum measurements made by the Durham group at Dugway (Andam et al 1981) and Haverah Park (Hammond at al 1978) are the most complete and indicate a trend to lower masses than those inferred at lower energies. Dyakonov et al (1981) used lateral distribution measurements of the Cerenkov flux at sea level to deduce the depth of shower size maximum. Their results, although not in good agreement with those of Andam et al, also imply lower average mass. A number of other experiments, as well as these, have been summarized by Linsley and Watson (1981a) who concluded that the mean mass of primaries above $6*10^{16}$ eV was consistent with a nearly pure proton flux.

The energy spectrum above 10^{17} eV is particularly interesting since a number of predictions have been made about interactions at these energies. In 1966, it was predicted (Greisen, Zatsepin and Kuzmin) that the primary energy spectrum should cut off very sharply at a few times 10^{19} eV due to photo-pion production by high energy protons interacting with photons from the 3K cosmological radiation.

Data from Haverah Park (Bower et al 1981), the array with the best collection statistics, shows no such cut-off, but rather a flattening of the spectrum at the highest energies. This has been interpreted as placing a maximum age on these primaries (alternatively, a limit on the distance traversed by them). Until recently, the Yakutsk data showed a similar flattening, however this does not appear in their recent data (see Hillas 1981). Southern hemisphere data from the Narrabri array (Bray et al 1981) also does not show the feature measured at Haverah Park, though, due to serious calibration problems, their results must be considered as very preliminary. It has been pointed out also (Hillas 1981), that due to the large anisotropies in arrival directions measured at the highest energies (Pollock 1978, Lloyd-Evans 1982) and also relatively low statistics, it is important, when measuring the spectrum, also to specify the region of sky being observed.

Another effect predicted to change the primary spectrum at high energy (Greisen 1966) is the photo-disintegration of heavy nuclei by interactions with the microwave background at a threshold of $5*10^{18}$ eV per nucleon and a mean path length for the effect of much less than galactic dimensions. This is in agreement with the measured predominance of light primary particles at high energies. At energies greater than $7*10^{17}$ eV, proton primaries can also interact with the thermal stellar background in pair production processes. A dip which has been observed in the Haverah Park spectrum (Bower et al 1981) has been interpreted

as possibly being a consequence of this effect.

1.2 Extensive Air Showers

Since this thesis is concerned with measurements on the cosmic ray flux using their secondary products at ground level, a brief account of the processes occurring in extensive air showers will now be given.

It was shown earlier that the Earth's atmosphere can be considered to be an ionization calorimeter or absorber with a thickness of about 1000 g cm^{-2}. Because of this, the probability of detecting a primary cosmic ray particle at sea level is very low, the flux above 10^{16} eV being only about 1 particle per square metre per year. However, it is the presence of this absorber which makes cosmic rays above 10^{15} eV detectable at all with a reasonable rate, since interactions of the primary particle with atmospheric nuclei produce a cascade of secondary particles, which, at sea level (largely due to the Coulomb scattering of these secondaries) is of the order of 100 metres in lateral extent. Therefore, if some assumptions can be made about the extent and development of the air shower, information is available about the primary particle from sample measurements made on the secondary particles at ground level.

Under these circumstances, a detector system with very large effective collecting area may be constructed from a

number of relatively small detectors which sample the shower. In general, an air shower detection system is built up from a number of widely spaced detectors, such as scintillators, which are set up so that coincident events (i.e. particles simultaneously traversing more than one detector) are recorded.

Extensive air showers (EAS) consist of three main components which are related by the energy flow into them from the interactions of the primary particle with atomic nuclei in the atmosphere. These are, the nuclear component, the muon component and the electromagnetic component. The Cerenkov component, produced by superluminal particles in the shower traversing the atmosphere, is interesting since, ignoring scattering and absorption, it carries information from all parts of the shower development and can be very useful in calorimetric techniques. However, it carries a negligible proportion of the shower's energy and will not be discussed here.

1.2.1 The Nuclear Component

When a cosmic ray primary particle impinges on the atmosphere, it collides with an atmospheric nucleus, losing some of its energy and producing some high energy hadrons. Some of these, as well as the primary particle will then continue on down through the atmosphere, with further interactions producing further secondaries, and distributing

energy to the other components of the shower. These nuclear-active particles comprise the nuclear core of the shower with about 1% of the shower particles. Since air shower energies are, at this time, well above those energies accessible to man-made accelerators, the details of the collisions are unclear, however semi-empirical models such as scaling (Feynman 1969) and CKP (see Brooke et al 1964, Wdowczyk 1973) with modifications such as rising interaction cross sections (Hillas 1979b), have been proposed to explain the measured results.

Two important parameters of the interactions for air shower measurements are the inelasticity, the amount of energy lost by the primary in collisions, and the interaction mean free path. Conventional models (CKP) for nucleons assign values of about 0.5 and 80 g cm^{-2} respectively to these, independent of energy (de Beer et al 1966). However if the rising proton-proton cross sections observed at accelerators below 10^{13} eV continue to air shower energies, the mean free path length may be considerably reduced. Since the atmosphere is only about 12 interaction lengths thick, it is clear from these values that the primary particle may retain an appreciable fraction of its energy to considerable atmospheric depths. Because of the relationship of the hadron cascade produced by the primary particle to the other shower components which are fed by it, the EAS will continue to grow until energy losses from it (as ionization in the atmosphere) become greater than the energy being fed into it. This shower maximum may occur quite deep in the atmosphere.

For multi-nucleon primary particles, a superposition rule (Khristiansen et al 1965) is conventional, so that a primary of mass number A and energy E is considered as A primary nucleons, each with energy E/A. The shielding effects of nucleons in the nucleus may present some problems to this model (Dixon and Turver 1974). Also, the interaction cross section for the first nucleus-nucleus interaction (increasing as $A^{1/3}$ (Waddington and Freier 1973)) is larger than for proton-nucleus collisons (Cleghorn et al 1968). Therefore it can be seen that EAS produced by massive primary particles should reach maximum development higher in the atmosphere, and also that fluctuations in the shower development should be less for heavy primary particles than for protons.

Energy lost in the inelastic collision process results in the production of particles, mainly pions, although other mesons and baryons may also be produced. On average, the pion charges are equally divided between +e, -e and 0. Neutral pions have a very short half-life (about 10^{-15} seconds) and decay almost immediately to a pair of photons. The charged pions continue on through the atmosphere interacting with atmospheric nuclei in the same way as the primary, producing further secondaries, until their energies are low enough (about $3*10^{10}$ eV) so that their decay to muons becomes more probable than further interactions. At the higher energies the Lorentz factor gives them extended half-lives (Hayakawa 1969). In conventional models, the pion collisions are catastrophic (i.e. inelasticity is 1) with an interaction

length of about 120 g cm^{-2}, however in quark models of hadron interactions this is not necessarily so (Gaisser 1977) and there is a close similarity between pion and nucleon interactions.

The multiplicity of the collisions, the number of secondary particles produced, is an important factor in the shower development, but there is as yet no general agreement as to its governing rule. Feynman scaling results in a logarithmic dependance (as ln E) on energy, while the CKP model proposes that the multiplicity is a fractional power law in energy (as $E^{0.25}$) and other models with multiplicities as high as $E^{0.5}$ have been suggested (e.g. Chantler et al 1982). Problems with the superposition model are due to shielding and fragmentation of heavy primaries and lead to supressed pion production (Gaisser et al 1982). This means that shower development fluctuations for these primaries will be larger than would otherwise be expected, although not large enough to upset the use of shower development measurements as a tool for composition investigations.

The transverse momentum distribution of the hadrons produced in the nuclear-active core is a good test of the accuracy of the extrapolations from accelerator data, since this distribution is almost independent of energy. Some recent measurements (e.g. Ashton and Nejabat 1981) however, have indicated that this is no longer true at energies above $2*10^{14}$ eV, suggesting a change in the nuclear interactions above this energy.

Due to their relatively high energies and large masses, the nuclear component is little affected by Coulomb scattering and most of the particles in this component are found within a couple of metres of the primary particle trajectory.

1.2.2 The Muon Component

Comprising less than about 10% of the total number of particles in the shower at ground level, the muon component is produced by the decay of (relatively) low energy mesons (mostly charged pions with some kaons). Because of their very long interaction length, these muons are unlikely to interact with atmospheric nuclei and so are sometimes known as the hard or penetrating component.

Although their half-life at rest is only about $2*10^{-6}$ seconds, their large Lorentz factor with which they are produced means that they can travel a large fraction of the atmosphere before decaying. Hence the muon flux from EAS observed at ground level is essentially the integral of the muon production of the whole hadronic cascade. Also, because of their mass, the muons are not deflected appreciably by the geomagnetic field and so travel effectively in straight lines from their point of origin. Apart from the low decay probability, the only losses occurring to the muon flux are ionization losses of about 2 MeV per gram per square

centimetre. It can therefore be seen from the characteristics of the longitudinal development of the nuclear cascade that the longitudinal development of the muon component will exhibit a rapid increase in numbers (following the nuclear cascade) and then after shower maximum, a relatively constant number of particles. The attenuation length of the muon component (defined by $N_\mu \sim \exp(-x/\lambda)$) is at least 1000 g cm^{-2} (e.g. Cranshaw et al (1958) reported 1400 g cm^{-2}).

The lateral spread of the muon component is due to the transverse momenta with which the muons and their parents are produced, and although in the laboratory frame this is comparatively small, due to the height of muon production, the lateral distribution of this component is rather flat. Hence muons may be found at large distances from the primary particle trajectory. To a rough approximation, muons found furthest from the shower core are those produced earliest in the shower development. Lowest energy particles will be found at the largest distances from the shower core because of the ionization losses over the muon trajectories.

Measurements of the muon component are usually made using spectrometers shielded by large thicknesses of atmospheric absorber (by having the acceptance directions at large zenith angles) or by underground construction. The shielding is required to discriminate the muon component from the more numerous electromagnetic component. Also, the high energy muons which must have come from very early in the EAS development can then be observed.

1.2.3 The Electromagnetic Component

By far the most numerous component, the electromagnetic component comprises about 90% of the number of shower particles at ground level for primary particles with energies greater than about 10^{14} eV. For lower energy primary particles, which (as can be seen from the slope of the energy spectrum) are the bulk of the cosmic ray flux, the electromagnetic component is absorbed high in the atmosphere leaving only unaccompanied muons, so that in fact the most numerous component of the cosmic ray flux at sea level is unaccompanied muons.

The electromagnetic component derives from the gamma ray photons produced in the neutral pion decay. Each of these very energetic photons produces an electromagnetic cascade by a process which, in contrast to that of the nuclear cascade is fairly well understood (see Nishimura 1967). After traversing a chacteristic distance (the radiation length, X_0) of about 38 g cm^{-2}, a photon produces an electron pair which in turn produces further photons by means of the bremsstrahlung process. In this way the cascade develops, and continues to grow until ionization energy losses become competitive with the pair production and bremsstrahlung processes at the critical energy (E_c, about 84 MeV). Since the gamma ray photons are continually being produced by neutral pions from the nuclear component, it can be seen that the EAS can be well

approximated by the superposition of a large number of electromagnetic cascades. When the nuclear cascade decays, energy is no longer fed into the electromagnetic component, and the EAS then decays with an attenuation length (defined as previously) which is chacteristic of the nuclear cascade (Hayakawa 1969).

Studies of EAS have shown that the lateral distribution of secondary particles in the shower can be described by:

$$\rho(r)=N_e.f(r)/(r_1)^2 \qquad (1.2)$$

where $\rho(r)$ is the particle density at distance r from the shower core, N_e is the shower size and f(r) is known as the lateral structure function. Multiple Coulomb scattering of electrons in the shower is by far the most important contribution to the lateral spread of the EAS. This process can be described in terms of the angle $d\theta$ through which a charged particle of energy E crossing a thickness of scatterer dt, is scattered by:

$$\langle d\theta^2\rangle=(E_s/E)^2.dt \qquad (1.3)$$

where E_s is 21 MeV (Cocconi 1961). This in turn gives rise to a unit of lateral displacement of the particles, known as the Moliere unit, r_1, given by:

$$r_1=X_0.E_s/E_c=9.5 \text{ g cm}^{-2} \qquad (1.4)$$

Obviously the actual distance involved is dependent on the atmospheric density.

A number of empirical lateral structure functions are used by the various research groups involved in EAS investigations (see Staubert 1968). The most commonly used function is the NKG function and its variations. Following the work of Moliere (1946), Nishimura and Kamata (1950,1951a,b) produced an analytical function describing the lateral spread of an electromagnetic cascade. Not surprisingly (for the reasons given earlier), the approximation of this function produced by Greisen (1956) also provides a good fit to the EAS lateral distribution. The NKG function,

$$f(r/r_1)=C(s)(r/r_1)^{s-2}((r/r_1)+1)^{s-4.5} \qquad (1.5)$$

where $C(s)=\Gamma(4.5-s)/[2\,\Gamma(s)\Gamma(4.5-2s)]$

describes the particle lateral distribution in terms of the lateral age parameter, s, which is a measure of the longitudinal shower development. This parameter varies in value between about 0.4 and 2.0 as the shower develops i.e. early in the shower development $s<1$, at shower maximum $s=1$, and after maximum $s>1$. Greisen (1956) also showed that the lateral spread of the EAS is influenced by atmospheric conditions two radiation lengths higher than those at the level where the shower is sampled. Thus the value of the Moliere unit used in the shower analysis can be somewhat

modified.

It can be seen from equation 1.3 that the mean scattering angle is inversely proportional to particle energy, so that in general lower energy particles will be found further from the shower core, and also, due to the trajectories produced by multiple scattering, lower energy particles will tend to lag longitudinally behind the higher energy particles at the shower front.

Hence the EAS can be represented as having a shallow disc shape with a radius of curvature of about a kilometre. This disc moves down through the atmosphere at about the speed of light and has, at sea level (for primary energy about 10^{15} eV), a useful lateral extent of about 100 metres and thickness of perhaps 5 metres. It should be noted that shower maximum for medium energy showers occurs fairly high in the atmosphere (see e.g. Thornton and Clay 1981), so that at sea level these showers are well past their maximum development.

CHAPTER TWO

THE BUCKLAND PARK EAS ARRAY

The Buckland Park Extensive Air Shower Array was used for the collection of all data for the experiments discussed in this thesis. Its synthesis and capabilities are described in this chapter.

2.1 Data Collection and Recording

In any experiment involving measurement, a knowledge of the characteristics of the measuring device is as important to the final results as the parameters to be measured. Measurements on the cosmic ray flux were carried out using the University of Adelaide's Buckland Park EAS Array situated on level ground at very close to sea level. The array is located at longitude 138° 28' E and latitude 34° 38' S, about 40 km north of Adelaide, South Australia.

Since 1978, the author has been responsible for the routine running, maintainance and calibration of the array and the analysis of the data from it. The design and some performance characteristics of this array have been described elsewhere (Crouch et al 1981, Gerhardy et al 1981), however since its performance is of crucial importance to the

experiments described here, the array will be described in some detail.

Developed from an array originally operated at Penticton in Canada by the University of Calgary, this array has been extended by the addition of a number of detectors to its present dimensions, now having an enclosed area of approximately $3*10^4$ m^2. It runs almost continuously, the only interruptions being stoppages for the changing of magnetic tapes on which the data is recorded, and equipment breakdowns. Figure 2.1 shows the plan of the particle array. Other EAS experiments being conducted at Buckland Park include measurements on the lateral (Kuhlmann and Clay 1981) and temporal structure (Liebing et al 1981) of the Cerenkov radiation associated with EAS. The Cerenkov detectors involved in these investigations will not be described here.

The particle array now consists of 12 scintillator detectors (5 fast timing and 12 density detectors), housed in semi-permanent galvanized iron huts. These are labelled A to K and R in figure 2.1. Detectors A to H are from the original array (which consisted of 8 sites - 5 fast timing and 5 density detectors) and each have a 1 m^2 by 5 cm thick block of NE102 plastic scintillator contained in a rectangular galvanized iron box and viewed from beneath by one or two photomultipliers. These are type RCA 8055 for the measurement of particle densities in the scintillators. Detectors A to E also contain fast rise time (about 4 ns) Philips XP1040 photomultipliers which are used for fast timing measurements

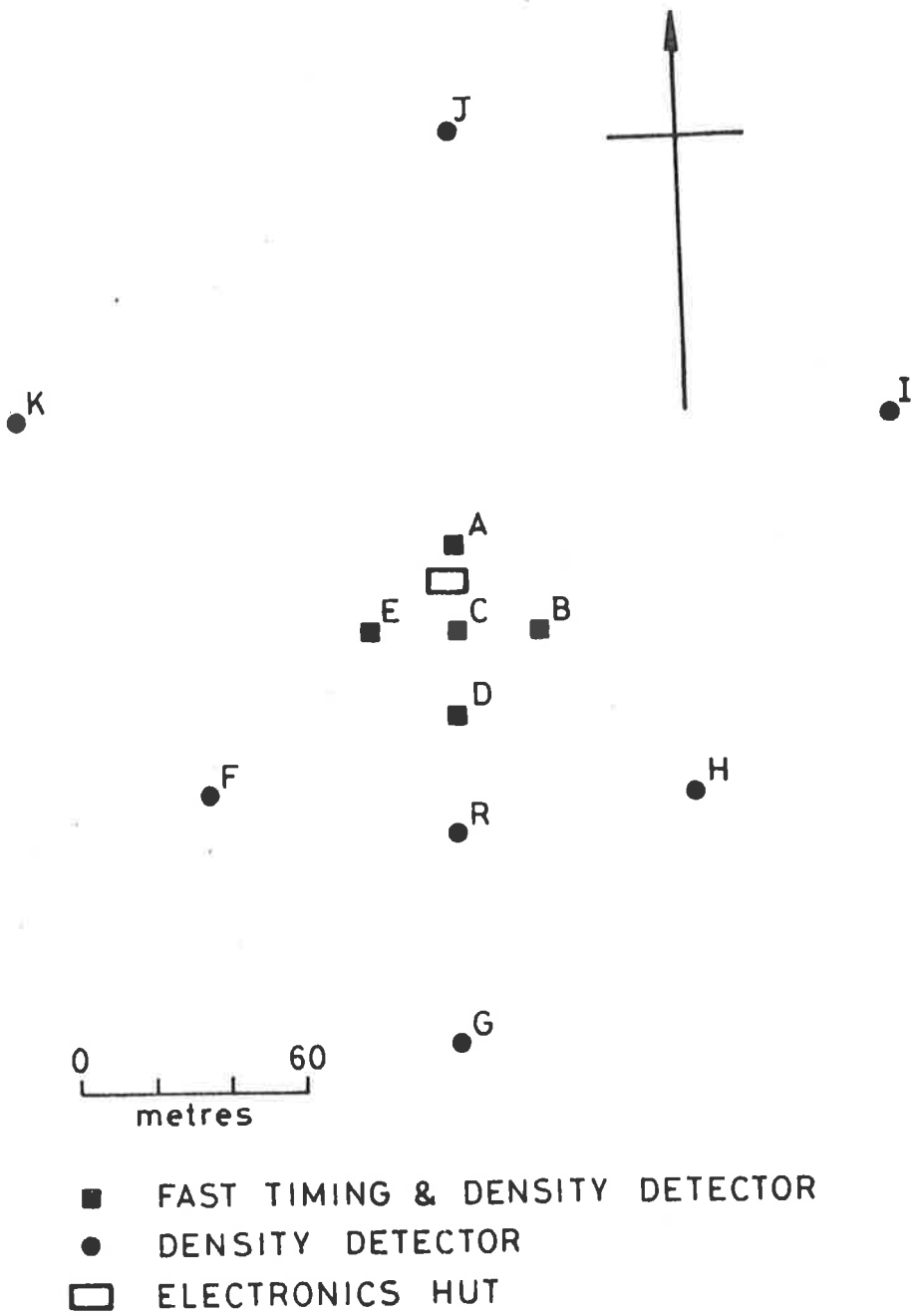

Figure 2.1 A plan of the Buckland Park EAS particle array

on the shower front to give directional information on the EAS. The new detectors, I, J and K are used only for particle density measurements and have 1 m^2 by 1 cm blocks (for financial reasons) of NE110 plastic scintillator housed in pyramidal aluminium enclosures (Clay and Gregory 1978) and viewed from above by RCA 8055 photomultipliers. Detector R (also for density measurements only) uses similar components to I, J and K detectors although the arrangement is slightly different. In this case, the scintillator is viewed from beneath in the variable light-tight enclosure used by Clay and Gregory in the design of the other new detectors. Apart from I, J and K detectors, the mass of the covering (including the enclosure and hut) above the scintillators is about 1 g cm^{-2}, while for I, J and K it is slightly more due to the photomultiplier and associated electronics.

Signals from the density detectors are amplified by charge-sensitive preamplifiers and line drivers. This process also shapes the pulses so that the energy deposited in a scintillator is proportional to the output voltage pulse height. Both density and fast timing signals are transmitted through coaxial cable (RG8A/U) to the array electronics hut for measurement and recording.

Temperature variations in the detectors are minimized by lagging with 'glass wool' 7.6 cm (A.C.I.) thick and a double sided reflective thermal insulator (Sisalation) covering. Various devices for the temperature control of the detectors have been investigated, however none is yet in

general use at Buckland Park. For each EAS detected, a sample detector (C detector) temperature is recorded, along with the atmospheric temperature and barometric pressure and also the temperature inside the (air-conditioned) electronics hut.

The pressure transducer used consists of an aneroid bellows, mechanically coupled to the core of a linear variable differential transformer (Texas Electronics 2012). Once conditioned, the signal from this device is digitized and recorded to an accuracy of about 0.5 mbar. For the temperature monitoring, two systems are used. The electronics hut temperature is measured using a thermocouple sensor and associated digitizing electronics (Kane-May Digitherm Mk3) with an accuracy of better than $0.5^{o}C$, while the detector and atmospheric temperature monitors consist of a Dual Heathkit Digital Thermometer (ID-1309B/BE) with semiconductor transducers (accurate to within $0.5^{o}C$). Transducers for the meteorological data are housed in a screened enclosure. The electronics for each of these devices is interfaced to the rest of the array recording electronics by means of buffers.

Raw data from each density detector is in the form of a single voltage pulse which is transmitted to the central electronics hut. At this hut each pulse is shaped by a line receiver amplifier. This pulse is measured by a device known as PAJAMAS (Phil and Jim's Amazing Measurer of Air Showers) which consists of two independent parts, one performing pulse height measurements for particle density calculations and the other performing timing measurements on the fast timing

pulses. The density signal from each detector is fed into a sample and hold amplifier (Teledyne Philbrick 4853) which gives an output following the input until triggered at which time it holds the output constant. Triggering of the sample and hold amplifiers is timed for each detector to ensure that a pulse produced by a shower will be held at its peak. Errors due to jitter in the arrival time of the pulses caused by inclined showers is reduced to less than 5% by the pulse shaping mentioned previously which gives the pulses a very long decay time (about 1 μs time constant). From the sample and hold amplifiers, the signals go to a Datel DAS-16. This device contains an analogue multiplexer which presents the output of each sample and hold amplifier in turn to a 12 bit analogue to digital converter. Results of these conversions are temporarily stored in a shift register. Saturation of the sample and hold amplifiers limits the maximum density measurable to less than about 1000 particles per detector.

Fast timing signals from the fast photomultipliers go through discriminators (LeCroy 621L) to the timing half of PAJAMAS. Signals from A, B, D and E fast timing photomultipliers are delayed so that the timing signal from C detector always arrives first. This signal is then used to start an 8 channel time to digital converter (LeCroy 2228) which is stopped by the other fast timing signals. Hence the times of arrival of the shower front at A, B, D and E detectors relative to C detector are determined.

When an EAS is detected, a multiplexor is triggered,

and this device takes data from a digital clock which gives the local time (Australian Central Standard Time) of the event and also the temperatures and pressure (these are buffered through the clock electronics) mentioned previously. After recording this data on magnetic tape (via a P.I. 1387 7-Track Digital Incremental Tape Recorder), the multiplexor interrogates PAJAMAS for the density and fast timing data which is recorded in a second record block on the tape. A block diagram of the array electronics is shown in figure 2.2.

The triggering conditions, which have been constant since 1978, have been set (Crouch 1979) to ensure that any EAS fulfilling these conditions can be well analysed with a well determined collection area, and also that an unbiassed selection of EAS is recorded. To trigger the recording electronics , pulses from each of the fast timing detectors must be measured at a threshold of greater than two particles, thereby ensuring some redundancy, and hence increased accuracy in the determination of the shower arrival directions. Secondly, density detectors A and D are required to measure greater than 6 and 8 particles respectively. By using this minimum number of density detectors near the centre of the array, most density detectors are free to fluctuate upwards or downwards in density, and so shower selection involves rather little bias. Also, most EAS detected will have their cores within the area enclosed by the array, hence the maximum number of detectors will sample the shower.

At present, the array electronics are being upgraded,

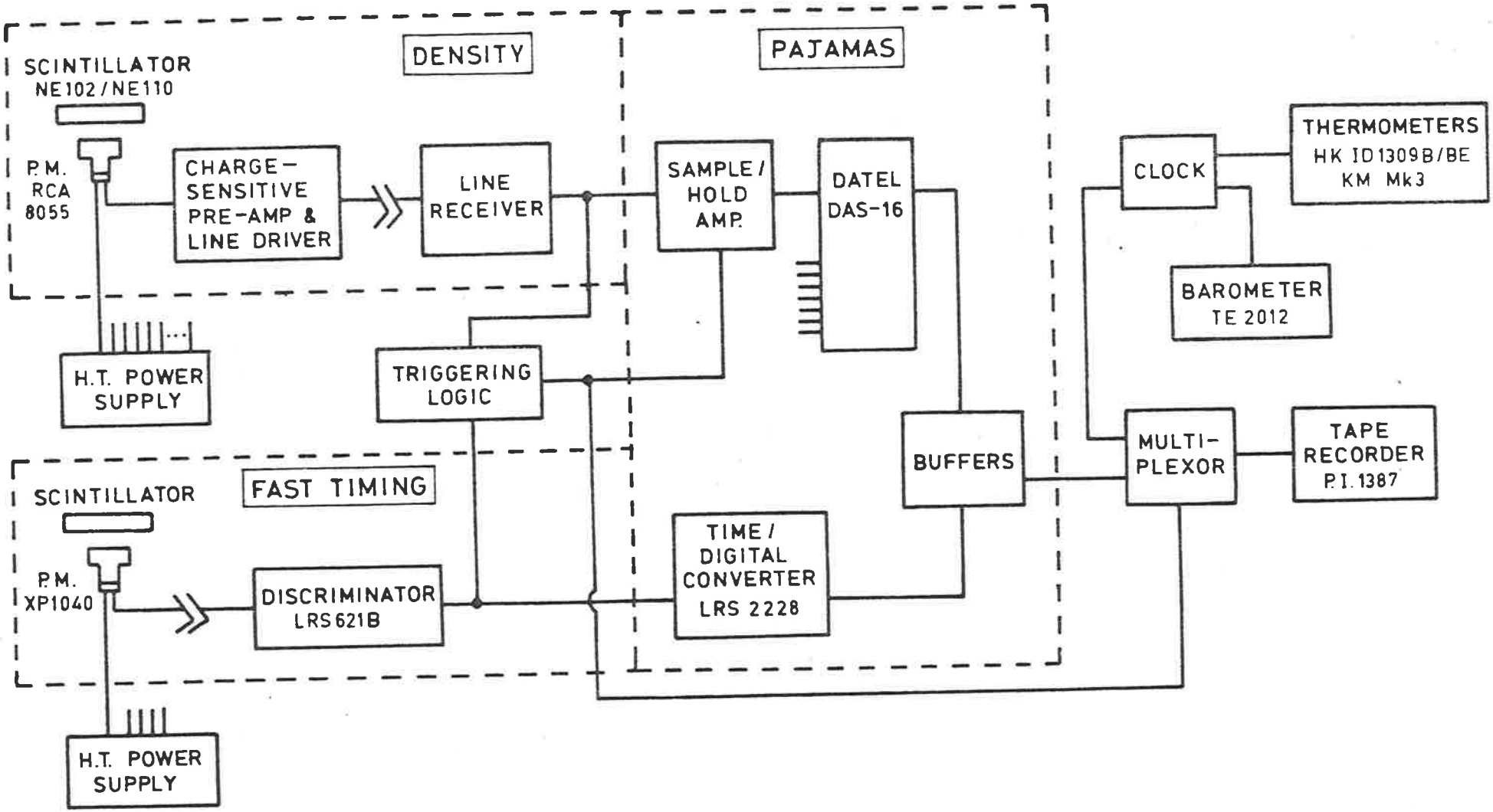

Figure 2.2 A schematic diagram of the Buckland Park detection and recording electronics

and it is planned to use a Nova 4S minicomputer to control a CAMAC system containing analogue to digital converters and time to digital converters for the data collection. The computer will also monitor the functioning of the array (e.g. singles rates in the density detectors) and do some preliminary real-time analysis, writing the results on floppy discs. The number of detectors is also being increased to allow accurate measurements on smaller showers. This system should be routinely operational by early 1983.

2.2 Calibration of the Array

2.2.1 Density Measurements

A scintillator responds to the passage through it of ionizing radiation by producing a light pulse proportional in amplitude to the energy deposited in it. For high energy particles, this is almost independent of the particle energy and also almost independent of the particle species (about 2 MeV/gm cm^{-2}, Hayakawa 1969). Therefore the light pulse energy produced by a scintillator is approximately proportional to the number of particles traversing it. This reasoning is the basis of density calibrations of the detectors.

Earlier it was shown that the most numerous component

of the secondary cosmic radiation at sea level is the uncorrelated muon flux. If an ungated pulse height spectrum from a scintillator is taken, its shape (a Landau distribution plus low energy noise) will be due to the passage through it of muons from all directions. When this spectrum is examined (for the 5 cm thick scintillators) a peak known as the single particle peak (SPP) due to the passage of a single ionizing particle (a muon) can be resolved. The voltage corresponding to this peak is used as the standard for density measurements.

Since density measurements are made in terms of 'equivalent single vertical muons', the mode (most probable pulse height) of the pulse height spectrum must be converted to this value. Measurements by Clay and Gregory (1978) have shown that gating the detector to receive only vertical particles reduced the pulse height by a factor of about 1.3. Also with about 5% variation, the ratio of mean to mode of the omni-directional pulse height spectrum was found to be about 1.3. Hence to a good approximation, for the thick scintillators, the SPP has been found to be a good measure of the energy deposited by an 'equivalent single vertical muon'. The ratio of the voltage measured in a detector to the voltage corresponding to the SPP is used to derive the detector particle density. This technique has the advantage of averaging the detector response over the whole sensitive area of the detector.

Unfortunately, for the thin (1 cm) scintillators, a SPP cannot be resolved from the noise in an ungated spectrum,

due to the reduction by a factor of 5 (the ratio of the scintillator thicknesses) of the energy deposited, and so, for calibration of these detectors, gating is employed. In this case, Crouch et al (1981) found the ratio of the mean to mode of the pulse height spectrum to be about 1.23. In practice, difficulties involving measurements made with thin scintillators have been resolved by noting that the ratio of thin scintillator to thick scintillator response for detectors placed side by side is about 1.11. This factor is used during data analysis to correct thin scintillator raw data to those that would have been given by the thick scintillators.

For setting threshold levels for the triggering detectors, the voltages for the number of particles are not set directly. Rather, from the pulse height spectrum, the rate of counts above the required level (n*SPP, where n is the number of particles required) is determined. The discriminator thresholds are then set to give this counting rate. An advantage of this method is that the triggering is then relatively independent of density calibrations and gradual variations in the detector are easily compensated for.

Observations of the SPP's from the detectors indicated, in general, only small (less than about 5%) and slow variations (over perhaps a month or more). This is near the resolution limit of the calibration technique. Catastrophic changes, which are fortunately rare, are easily detected in the computer analysis of the raw data from the array. A sample pulse height distribution from a detector is

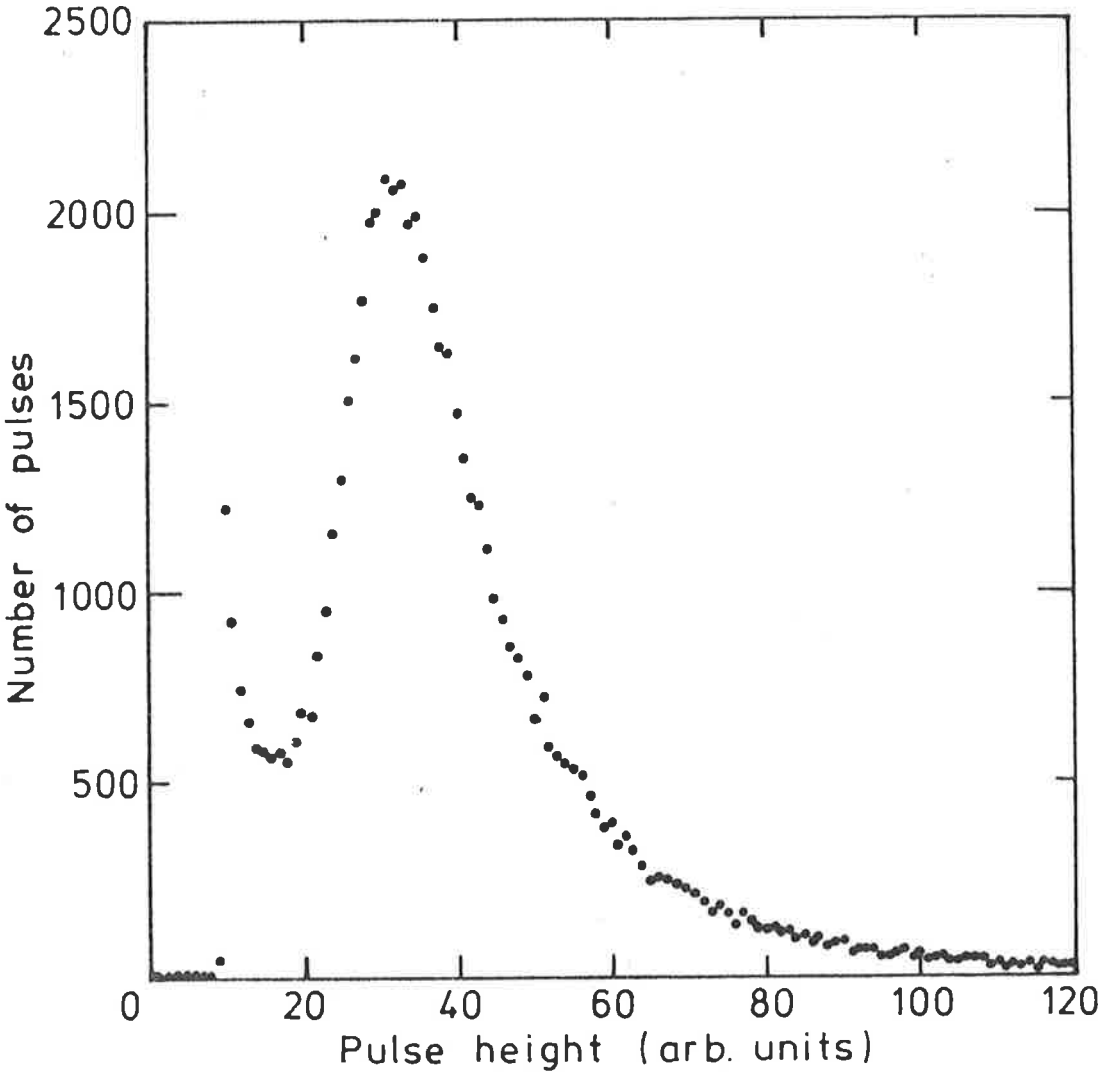

Figure 2.3 A sample pulse height spectrum from a 5 cm thick scintillator detector

shown in figure 2.3.

The recording and digitizing electronics are calibrated a number of times per year in terms of a standard reference pulse generator (BNC BH1) simulating the output pulses of the line receivers. This in turn is calibrated in terms of the multichannel analyser (Tracor Northern 1705) used to measure the pulse height spectra. Linearity of the electronics is good (figure 2.4) and again only small changes in the slope (less than about 2%) and offset (equivalent to less than about 2 particles) are observed. Sudden, larger changes, which are rare, are again relatively easy to detect and compensate for in the analysed data.

2.2.2 Timing Measurements

Calibrations of the timing part of the electronics are usually carried out whenever the density calibrations are checked. Using a switchable variable delay and a square pulse generator (Datapulse 100A), the time to digital converter is started and then each channel stopped separately to give the calibration curve for each channel. Again, the linearity of the device is very good (figure 2.5) and slope and offset variations are rarely greater than the resolution (including electronic jitter) of the system (about 4 ns).

Drifts in the triggering thresholds of the discriminators are a possible source of error due to the rise

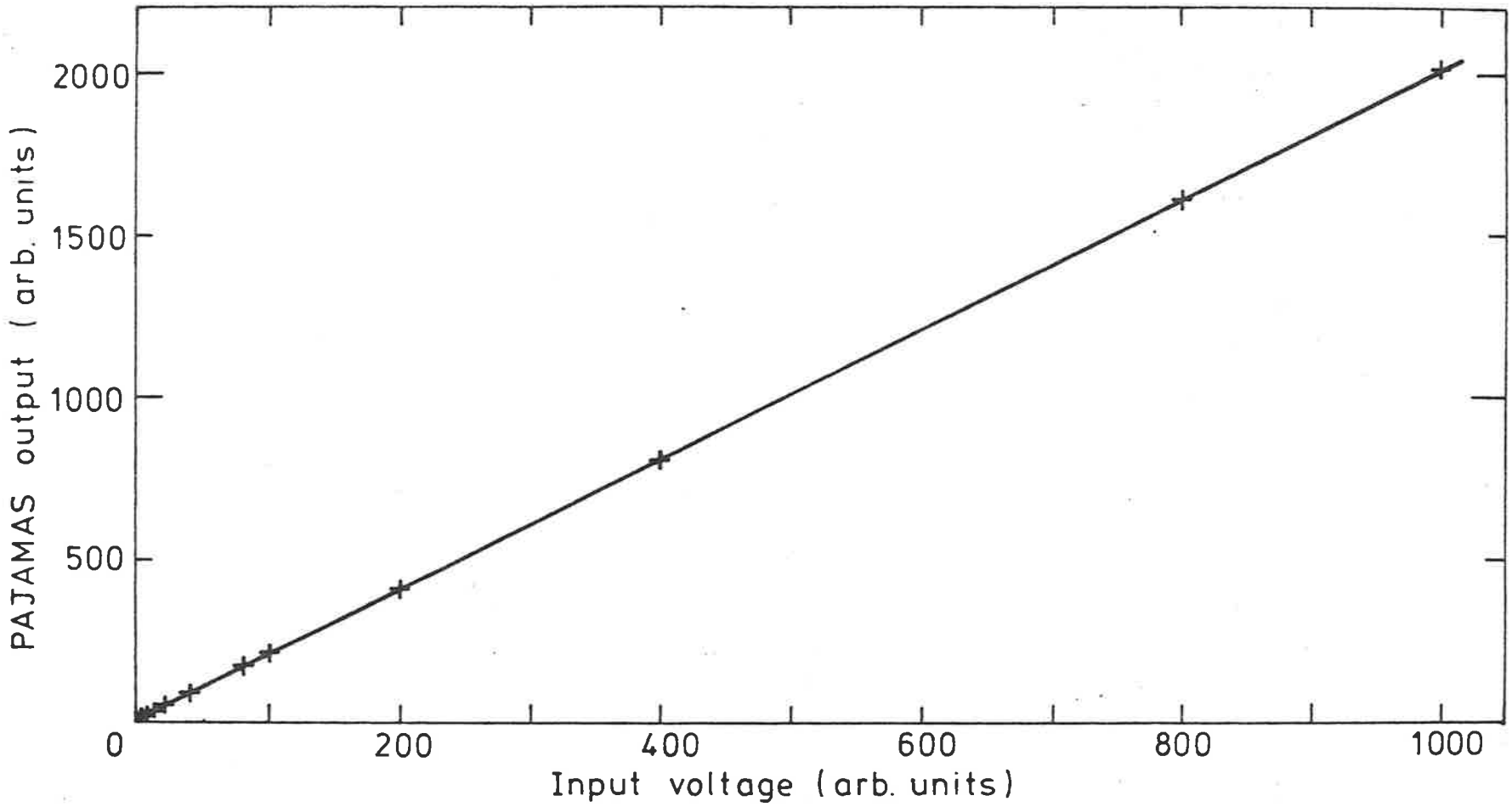

Figure 2.4 A sample PAJAMAS density calibration curve

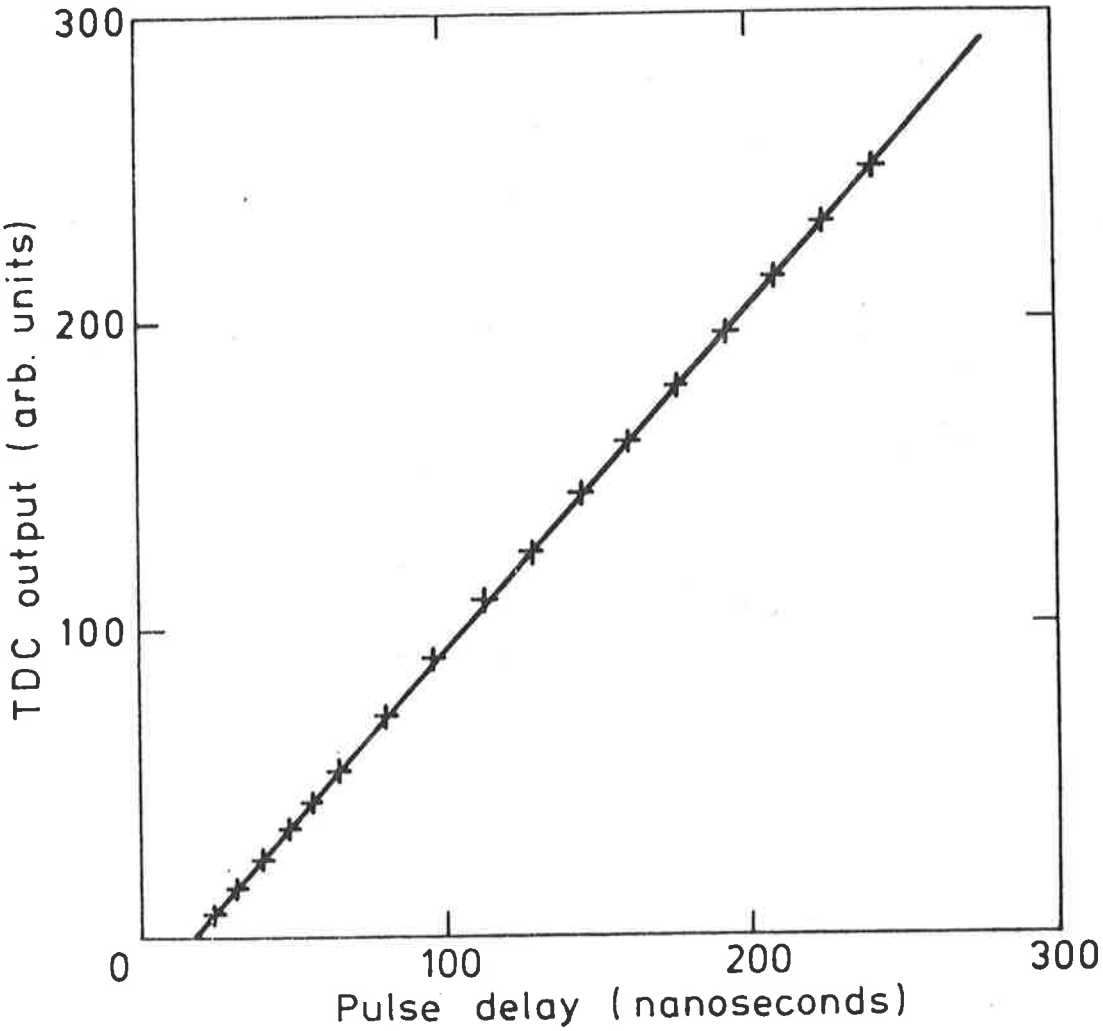

Figure 2.5 A sample TDC fast timing calibration curve

time of the photomultiplier tubes. A number of checks on timing drifts are possible. Because of the symmetry of the array fast timing square, detectors diagonally opposite (i.e. A and D or B and E) should have equal and opposite time delays with respect to C detector for any triggering EAS. Also, assuming a symmetrical flux of showers, the mean time delay between an outer fast timing detector (A, B, D or E) and the central fast timing detector (C) should be zero. This reasoning is used to set the zero delay and also allow for slow drifts in timing.

2.3 Analysis of the Raw Data

Data tapes written by the array electronics are collected periodically (about twice per week) from the field station and brought back to Adelaide for analysis on the University's Cyber 173 computer. Three separate programs are used in the analysis, these being somewhat mutated descendants of the programs brought with the rest of the original array from Penticton.

The first program reads the data from tape. At this stage a number of checks are performed on the data. As well as the parity bit written by the tape recorder, internal parity bits are also added by the array electronics, and both of these are checked for tape writing and reading errors. Data from each event is written as two different length records, the clock record containing the time and atmospheric

parameters of the shower, and the PAJAMAS record containing the fast timing and density raw data. The lengths of these records are checked. The characters read from the tape are also checked to see if they make sense (e.g. that the local time is later than that of the previous event).

After this program has been run, the second program applies the measured calibration curves to the raw data. This calculates the particle densities at each detector (in particles per square metre) and the delay times from the fast timing detectors (in nanoseconds).

Finally, in the third program, the data is analysed to produce the parameters of the shower i.e. its arrival direction in zenith and azimuth angles, its core location on the ground and its size (the total number of particles at ground level).

Shower arrival directions are calculated using a least squares fit to the detector times to produce the direction cosines of the shower (see Appendix 1). A plane shower front is used to approximate the actual curved shape of the shower front. This is quite a reasonable approximation since the radius of curvature of the shower front is expected to be of the order of a kilometre. Typical error values in shower directions are given by approximately $2.5*\sec(\theta)$ degrees where θ is the zenith angle. For showers with arrival directions less than 40^{o}, this corresponds to an uncertainty in the arrival direction of less than about 10^{-2} steradians.

The shower size and core position are determined by a gradient search technique developed by Crouch (1979), minimizing the χ^2 parameter (see Appendix 2). In this method, a trial core position is chosen using the weighted densities from detector A, and the outer detectors F, G, H, I, J and K. Using the empirical lateral distribution function of Greisen (1960) (from the work of Clark et al (1958) and Vernov et al (1960)) - the so-called 'Moscow/MIT' equation:

$$\rho(N_e,r)=a.N_e/r.\exp(-r/r_0) \qquad (2.1)$$

where $a= (2\pi r_0)^{-1}$, $r_0=60$ m

the program steps in the direction of the maximum decrease in the goodness-of-fit parameter until a minimum is found, thereby determining the core position and shower size.

Monte Carlo simulations on the array (Crouch 1979) have shown that for showers whose sizes and core locations give them a high triggering probability for the array, errors in these parameters are generally less than 10% and 10 metres respectively and in some cases (depending on location and size) substantially less.

For most events, this analysis produces satisfactory shower parameter determination, however local minima in the goodness-of-fit parameter surface can trap the search and lead to erroneous results. To overcome this problem a program package developed in CERN (James and Roos 1975) has been used

to reanalyze the data. This package, MINUIT, can utilize a number of options in the minimization of the goodness-of-fit parameter and has been found most satisfactory in its results. For showers which are well analysed by the gradient search technique there is little difference between the results of the two techniques. The difference in core locations is generally less than about 2 metres, for well analysed showers. However, while the gradient search procedure fails in about 3% of events to find a good minimum, the failure rate for the MINUIT package is much less than 1%.

Another advantage of the MINUIT package is the ease with which it can be adapted to fit a larger number of free parameters. For this reason as well, it has been used to reanalyse the data using the NKG function with varying age parameter and Moliere unit (depending on atmospheric conditions see Cocconi 1961). A comparison of shower sizes determined using equation 2.1 with the gradient search routine and the NKG function with MINUIT is shown in figure 2.6. It can be seen from this that the NKG sizes are on average about 10% larger than the Moscow/MIT sizes. The difference is attributable to densities measured at large core distances flattening the variable NKG lateral distribution and so increasing the calculated size. Note that events which show large differences between their calculated sizes using both methods, invariably have extreme ages for the best NKG fit.

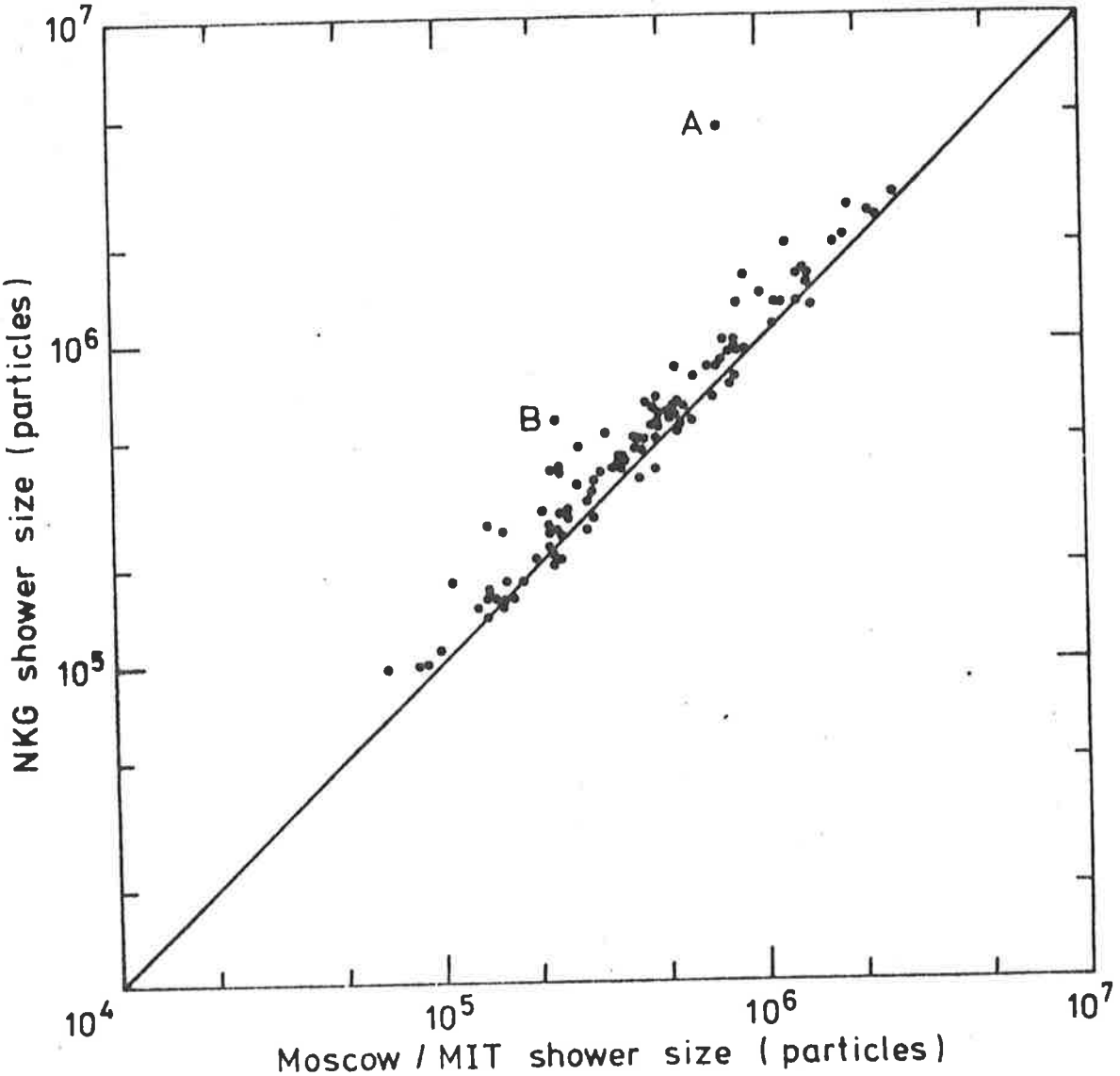

Figure 2.6 A comparison of shower sizes assigned by the Moscow/MIT and NKG functions. Showers A and B were assigned very young and very old ages respectively by the NKG function.

2.4 Behavior of the Array

In this section, the behavioral characteristics of the Buckland Park Array with respect to detected EAS will be described. These characteristics can be summarized by four distributions: the shower size distribution, the core position distribution, the zenith angle distribution and the azimuth angle distribution. Attempts will be made to give at least qualitative explanations for the shapes of these distributions.

2.4.1 The Shower Size Distribution

The size range of EAS collected by the Buckland Park Array is determined by the triggering levels (i.e. the number of particles required) and the geometrical arrangement and distances between the triggering detectors. Since the array is used specifically for studies of the cosmic ray flux near the spectrum knee, it is desirable to have a sharp cut-off at small shower sizes so that the much more numerous and unwanted low energy flux is not recorded. This requirement has been met very satisfactorily by the conditions described earlier and the results are shown in figure 2.7. It can be seen that the cut-off occurs at size about 10^5 particles and useful numbers of events are collected up to sizes of near 10^7 particles - a dynamic range of about two decades.

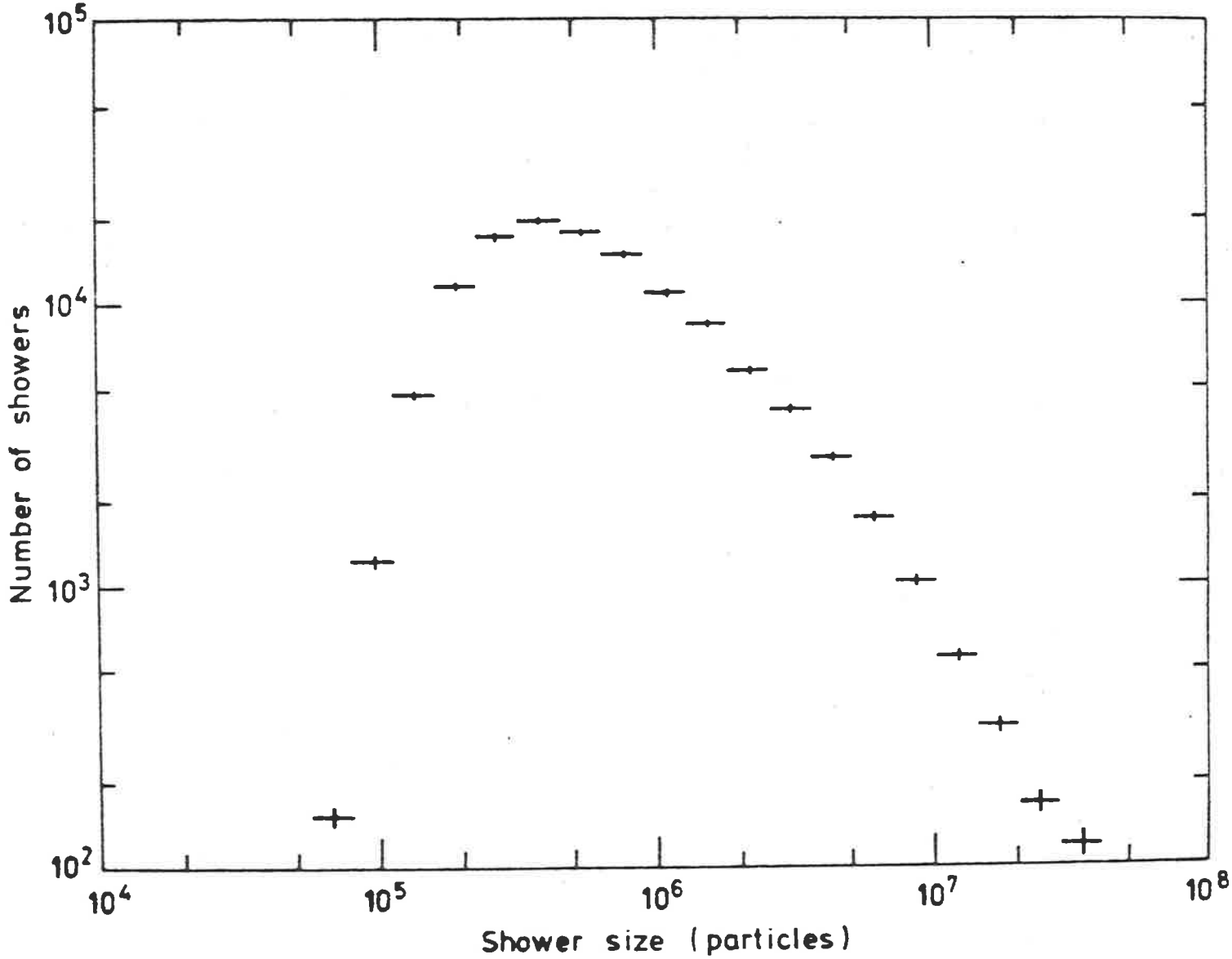

Figure 2.7 The number spectrum of detected showers

For restricted areas inside the array, the triggering probability should rise asymptotically with size to 100% (due to statistical density fluctuations). This can be used in the accurate determination of the EAS size spectrum and related to the primary cosmic ray energy flux. In figure 2.8a the number spectrum of shower sizes is shown for a sample from a restricted area (a circle with radius 25 metres). Figure 2.8b shows the corresponding triggering probabilities as a function of shower size. Once the triggering probability approaches 100%, the size distribution detected should reflect the true EAS size spectrum.

2.4.2 The Core Position Distribution

Core positions of the detected EAS are, as seen in the previous section, determined by the shower size distribution and the triggering conditions. Nevertheless, they can be used by themselves as a check on the operation of the array.

Most obviously, since the array is symmetrical with respect to its north-south axis, the core distribution of detected showers should also be symmetrical with respect to their x-coordinates. In figure 2.9, the distribution of x-coordinates is plotted. A high degree of symmetry can be seen, however a slight excess of showers (0.8%) detected on the eastern side of the array is apparent. Over an extended period, the array electronics shows slow variations, and changes in the detector gains or triggering discrimination

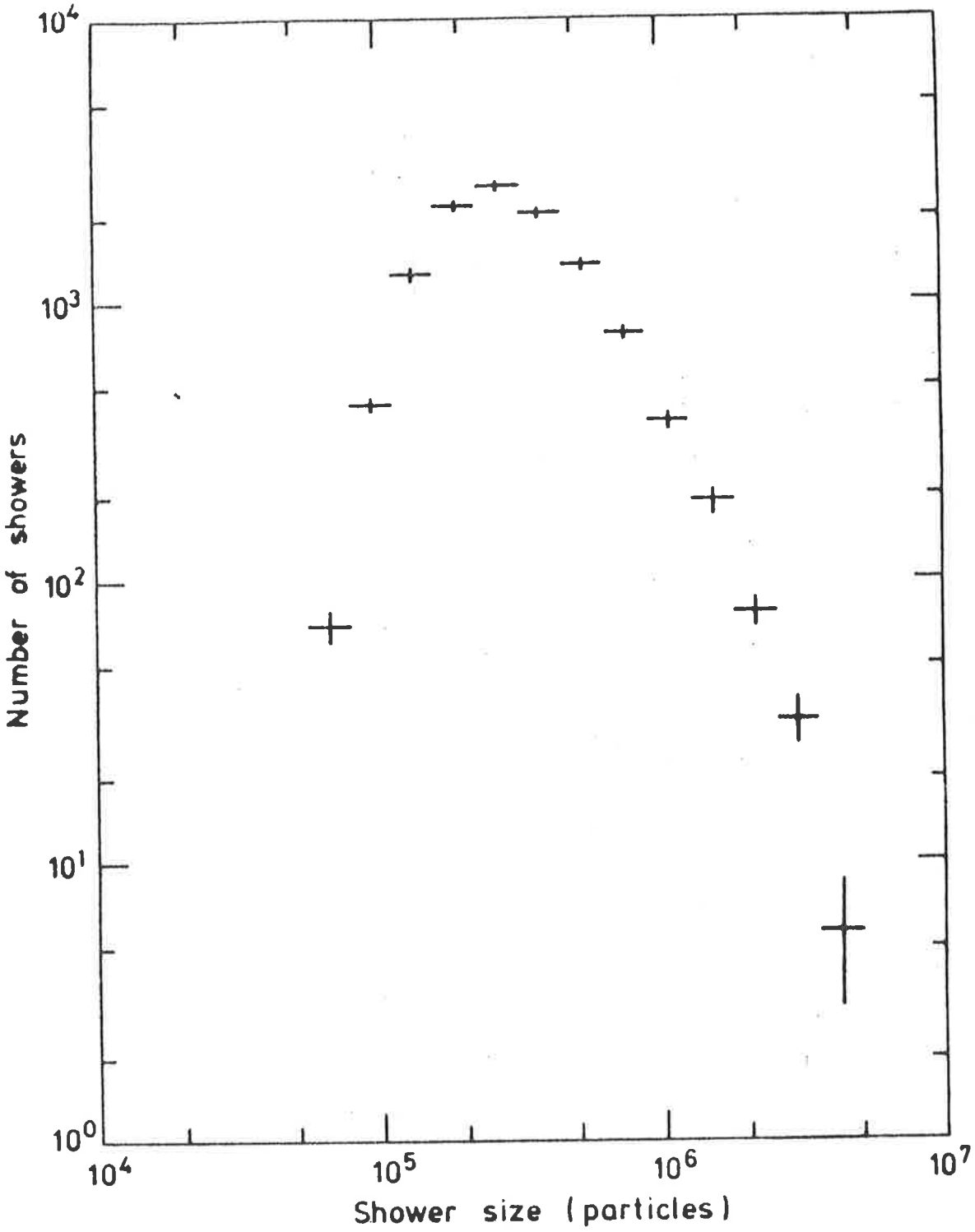

Figure 2.8a The number spectrum of showers with core locations within 25 m of the array centre.

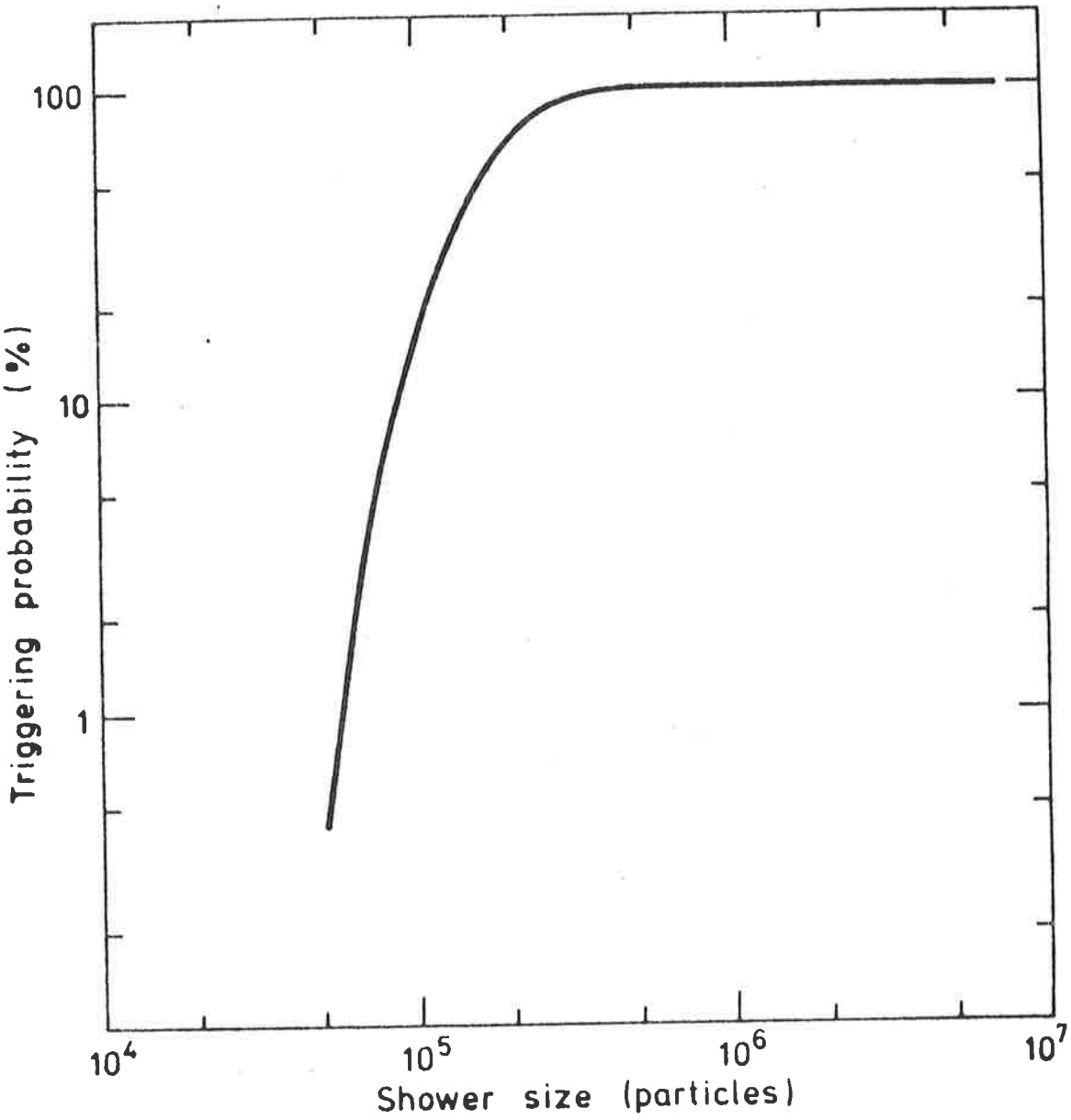

Figure 2.8b The triggering probability of showers with core locations within 25 m of the array centre

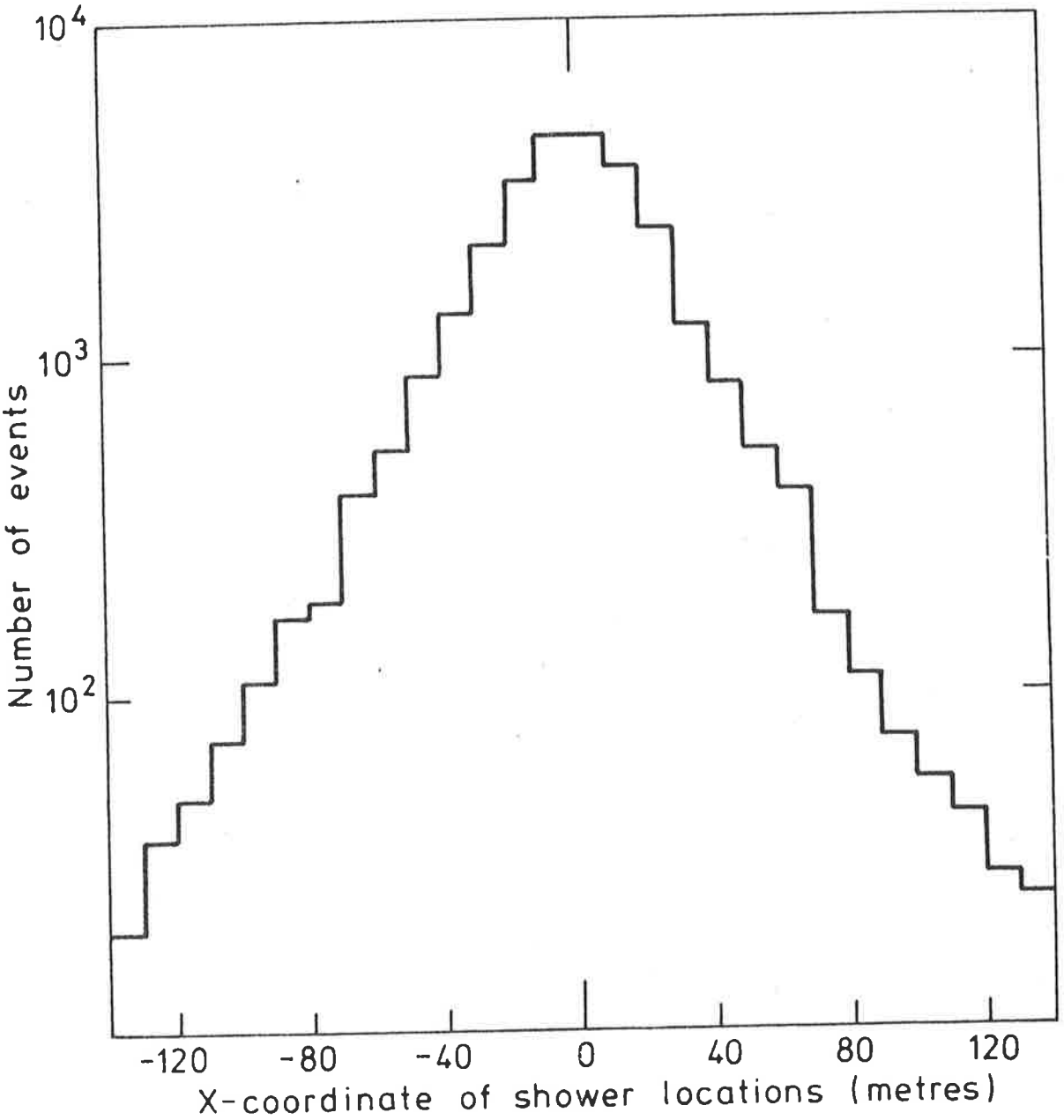

Figure 2.9 The distribution of x-coordinates of shower core locations

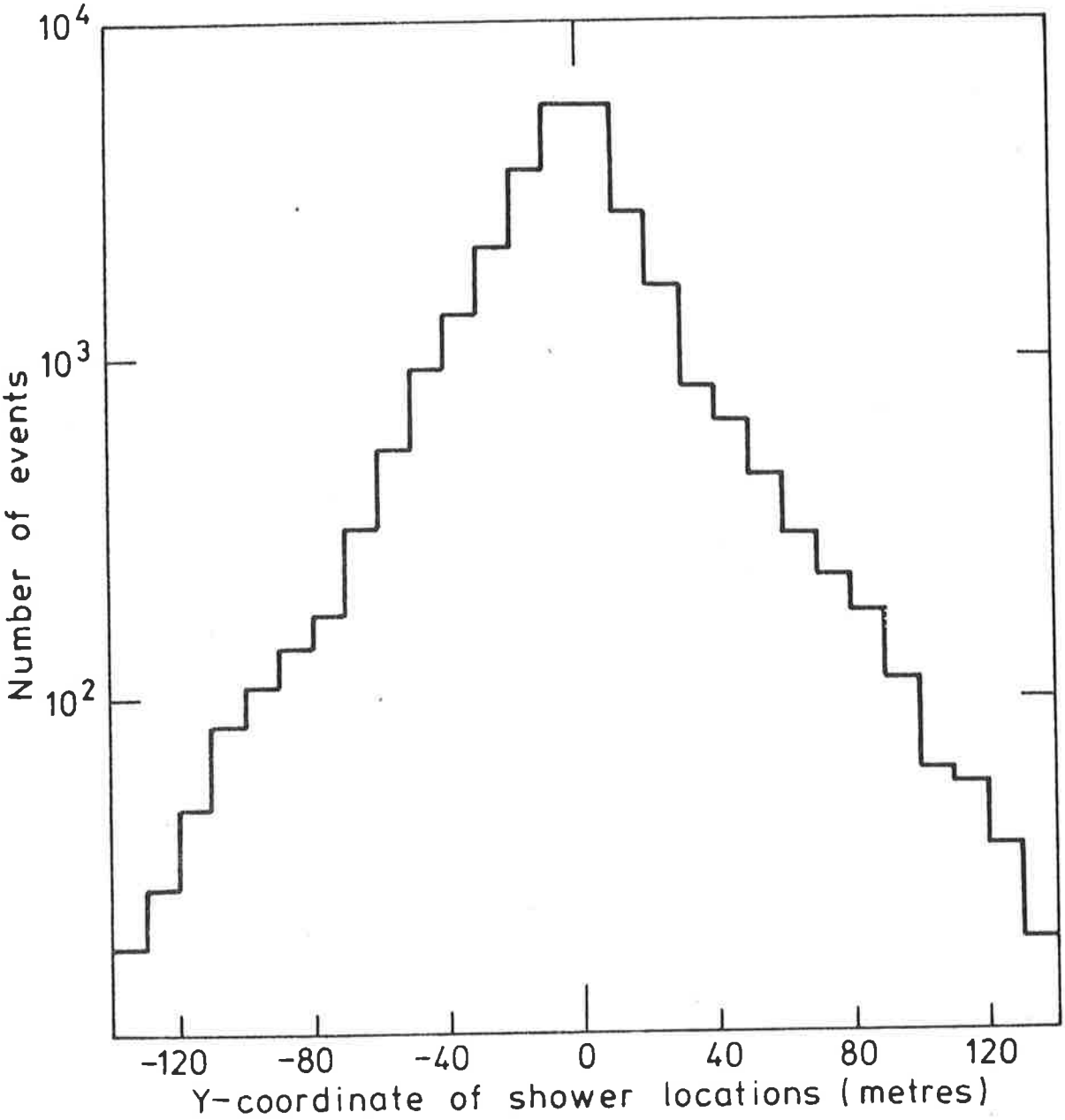

Figure 2.10 The distribution of y-coordinates of shower core locations

levels obviously change the triggering conditions. The slight asymmetry can be attributed to this problem.

Since there is no north-south symmetry in the array corresponding to the east-west symmetry, no similar test on the array performance can easily be made. Qualitatively however, it can be seen from the triggering conditions that the shower detection should be biassed towards the south of the array and this may be seen in figure 2.10, there being an excess of nearly 10% observed to the south.

For making quantitative measurements on the EAS flux, it is important to know the way that the triggering profile changes as a function of core position. This information may be obtained from Monte Carlo simulations of showers incident on the array. Results of these for three shower sizes are shown in figure 2.11. The most important characteristics of these data are the triggering centroid which is found to be at coordinates (0,-5), and the relatively large region of 100% triggering (asymptotically) compared to the sharp fall-off of triggering probability away from this area.

2.4.3 The Zenith Angle Distribution

Most EAS detected by the array are well past their maximum development, therefore the factor determining the zenith angle distribution of detected showers is the way that the showers are attenuated by the atmosphere. At low zenith

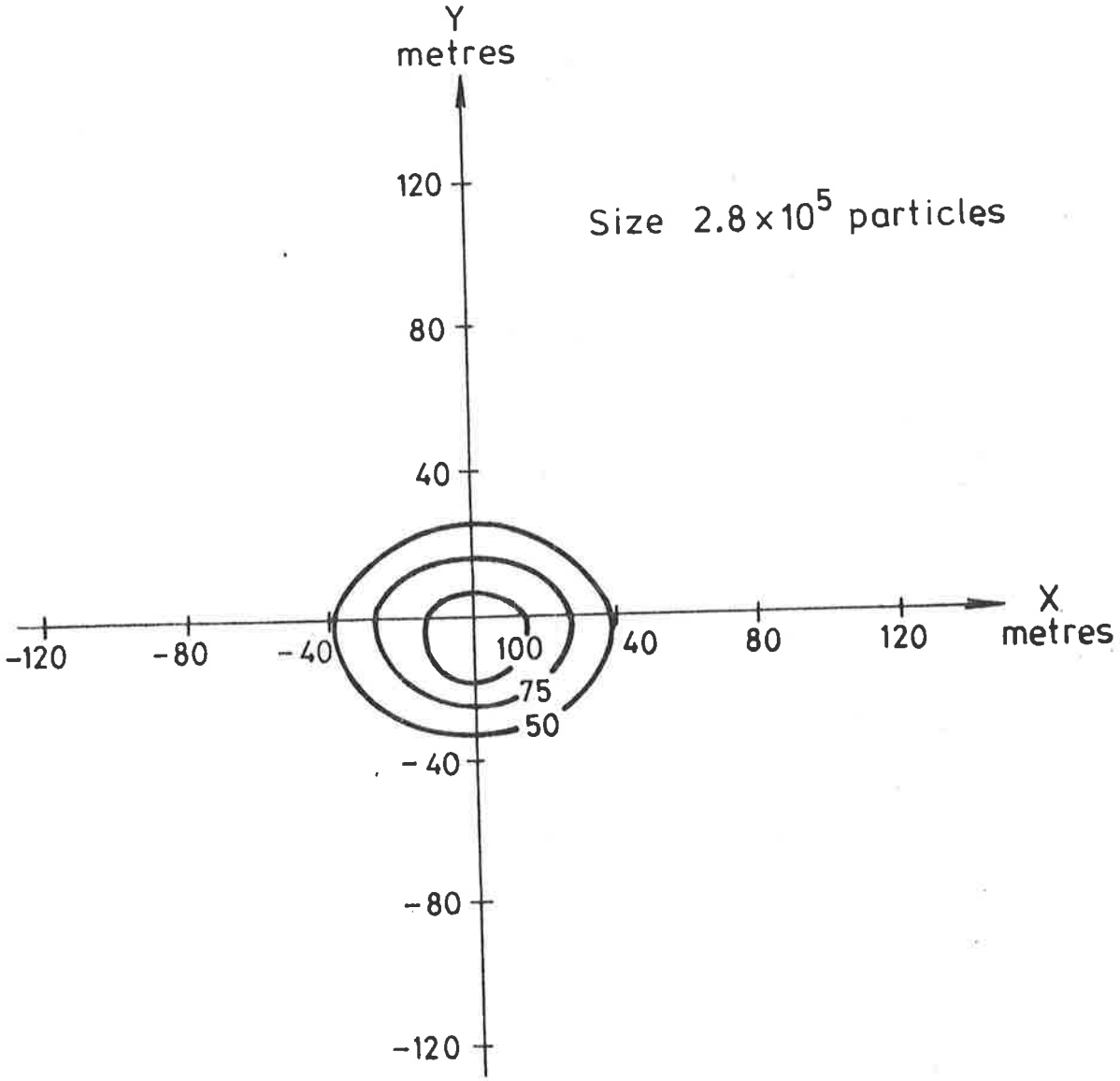

Figure 2.11a Triggering probability percentiles as a function of core position for showers of size $2.8*10^5$ parts.

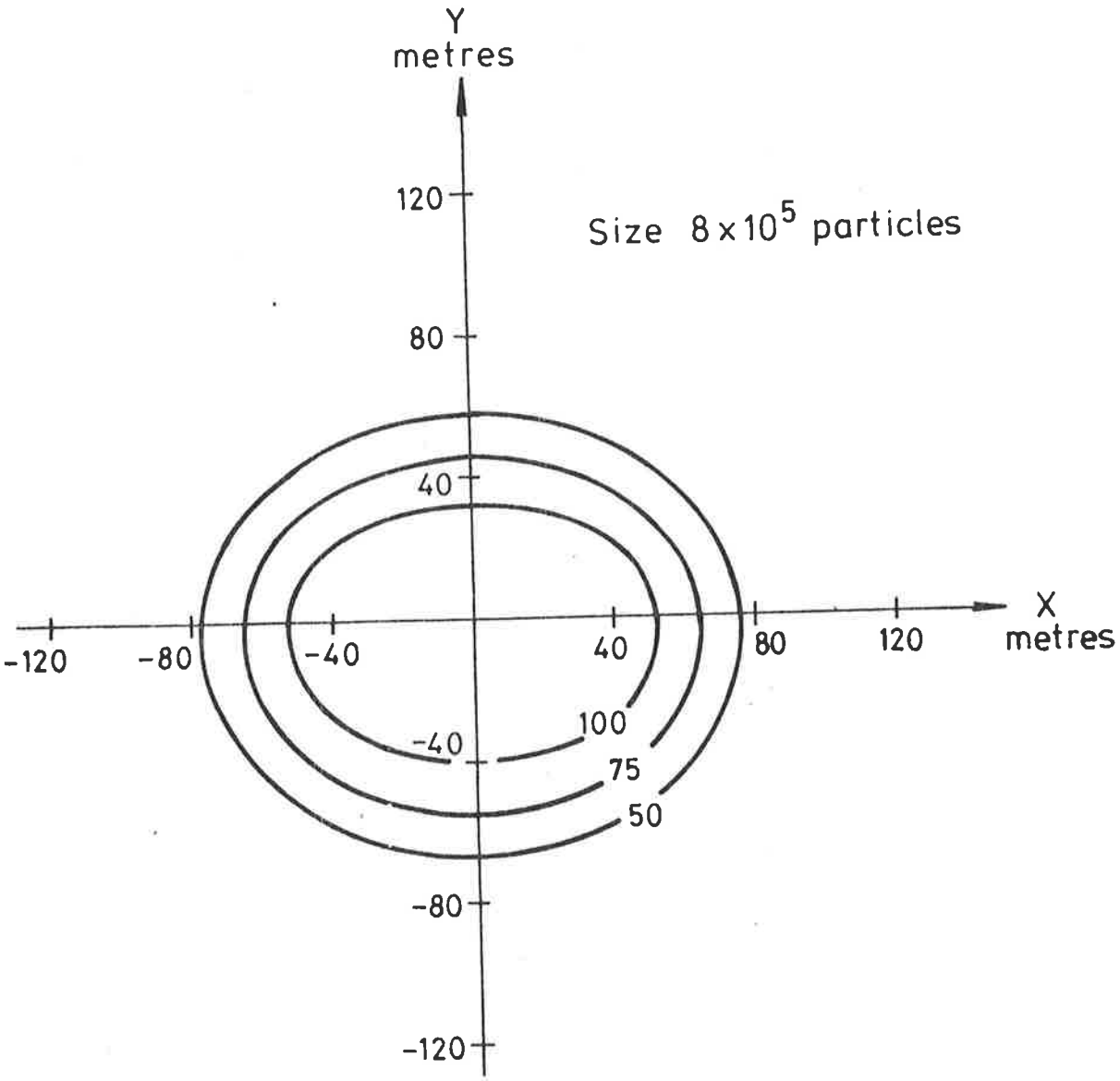

Figure 2.11b Triggering probability percentiles as a function of core position for showers of size $8*10^5$ parts.

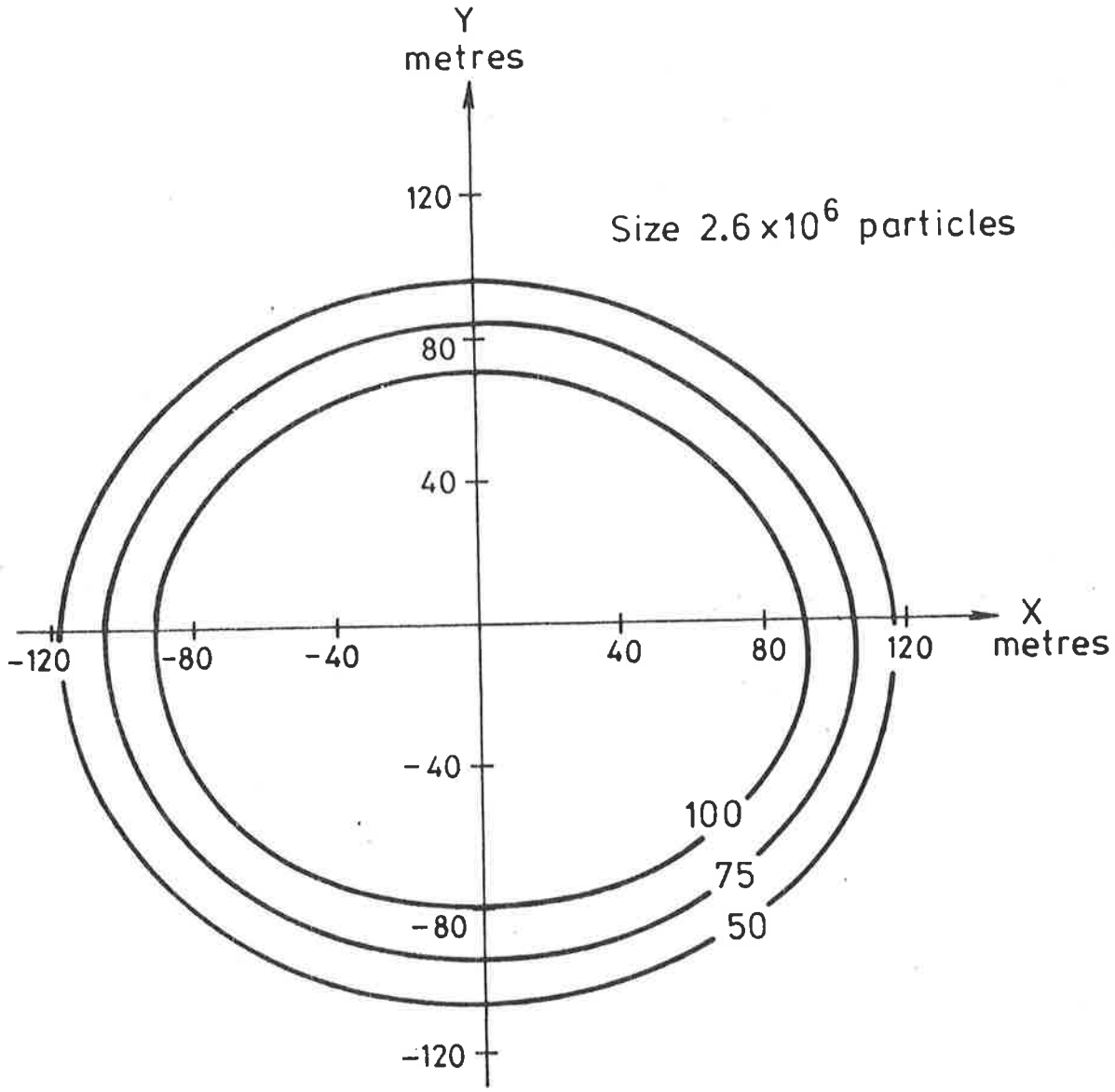

Figure 2.11c Triggering probability percentiles as a function of core position for showers of size $2.6*10^6$ parts.

angles, this effect is small and so the number of showers detected from these angles will increase with the solid angle of the sky viewed (figure 2.12). However, at zenith angles greater than about 20^{o} the changing thickness of the atmosphere which the EAS traverse becomes important.

For showers with size at maximum, N_{max}, the size, N_e, measured at sea level from zenith angle, θ, goes as:

$$N_e(\theta)=N_{max}.\exp(h.\sec\theta/\lambda) \qquad (2.2)$$

where h is the depth of the atmosphere (in gm cm^{-2}) and λ is known as the shower size attenuation length. Assuming that the primary cosmic rays are incident isotropically on the top of the atmosphere (with respect to the array zenith angle), the actual zenith angle distribution will be determined by the primary energy spectrum of the primary particles and also by the way the shower develops i.e. the atmospheric depth required for maximum to be reached. The latter datum is not known with certainty, and therefore a solution to the zenith angle distribution shape at large angles will not be attempted.

2.4.4 The Azimuth Angle Distribution

In a similar way to the distribution of detected EAS core positions, the azimuth angle distribution is determined by the triggering conditions of the array. Figure 2.13 shows

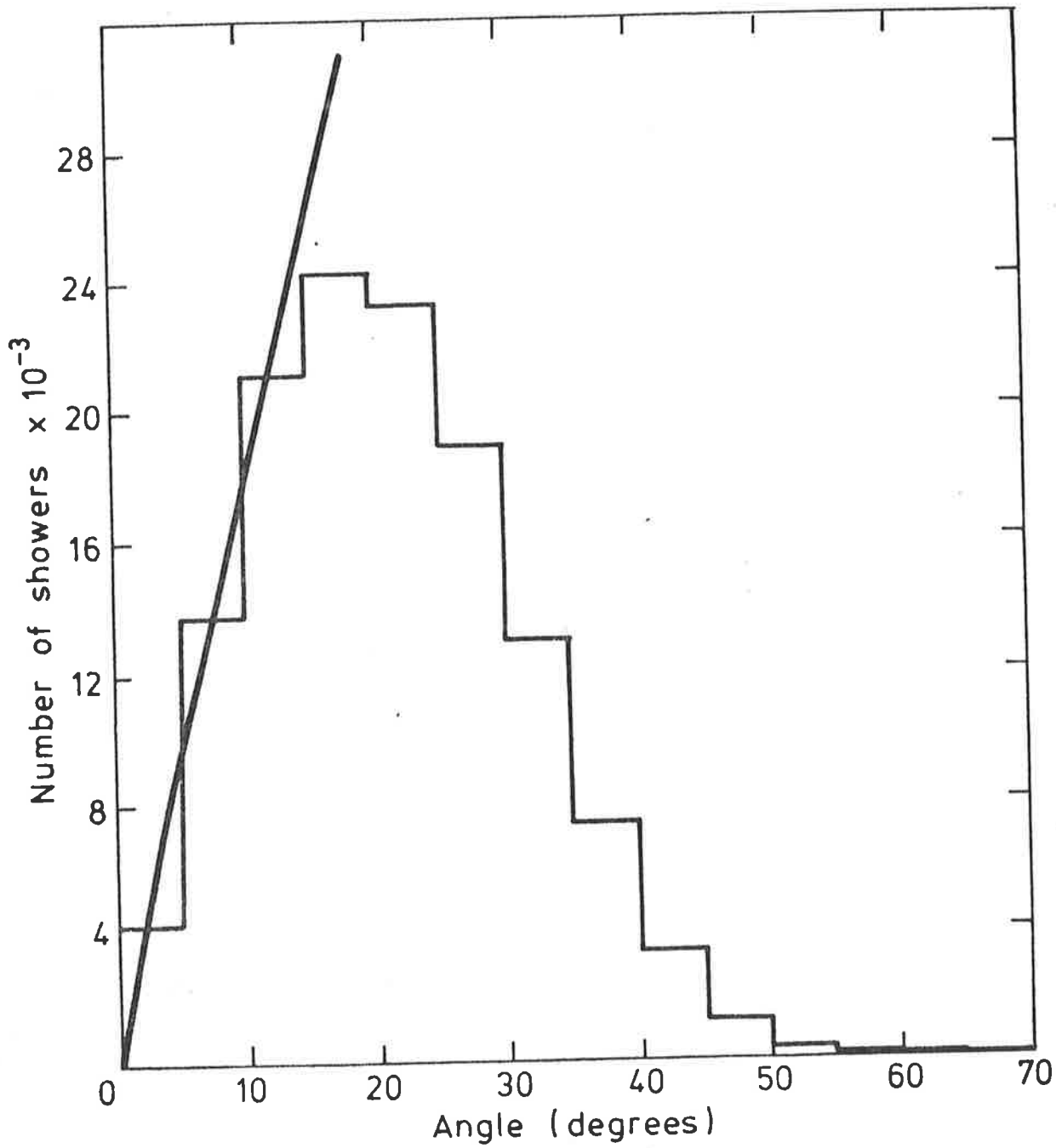

Figure 2.12 The array zenith angle distribution - the solid line indicates the increasing solid angle.

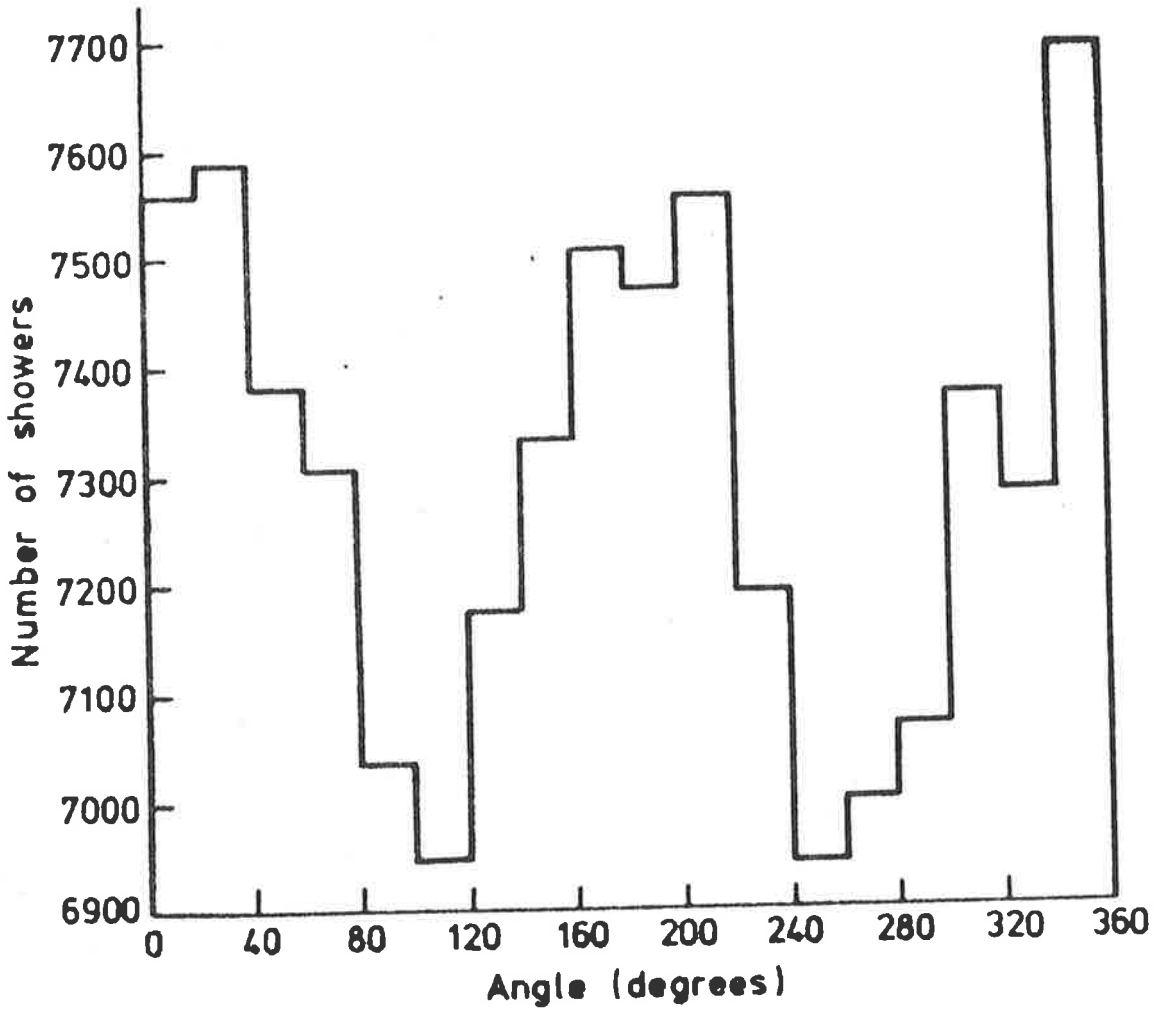

Figure 2.13 The array azimuth angle distribution

this distribution. The most obvious feature of this distribution is the modulation by a relatively large second harmonic. Details of the Fourier analysis (up to the fourth harmonic) of this distribution are shown in the Table 2.1 below. In the fourth column, the probabilities that random distributions could give rise to the measured amplitudes are shown.

Table 2.1: Fourier analysis of the azimuth distribution

Harmonic	Amplitude(%)	Phase(deg)	Probability(%)
1	1.3	23	0.4
2	4.0	12	$<10^{-10}$
3	0.6	195	37
4	0.4	170	57

The low significance of the third and fourth harmonics indicates that the distribution is well described in terms of the first and second harmonics. This is further confirmed by a check on the most obvious lines of symmetry (north-south and east-west). Comparing the number of showers arriving from northerly directions with that of southerly directions, it is found that there is an excess from the north of about 2%. Although this is quite close to symmetrical, when the data are statistically tested, it is found that the probability of a symmetrical distribution producing this difference is less than 1%. Checking the east-west symmetry in the same way, the flux difference is only 0.4% and this difference is rather likely to arise from random fluctuations.

The explanation for the large second harmonic lies in the arrangement of the two main triggering detectors A and D, i.e. the north-south alignment. Showers incident on the array from northerly and southerly directions reduce, by projection, the distance between these detectors and hence are more likely to trigger the array than showers from the east and west which see no such reduction.

Unfortunately, no such simple explanation offers itself for the first harmonic. Clay and Gerhardy (1982b) have shown that the north-south asymmetry can be produced by errors in the timing calibrations which are only of the size of the timing resolution. These may act to shift the effective zenith and thereby produce an artificial azimuth asymmetry.

CHAPTER THREE

THE SEA LEVEL SPECTRUM

In this chapter, results of spectral measurements on the sea level cosmic ray flux are given.

3.1 The Sea Level Density Spectrum

3.1.1 Introduction

Because of their low flux and extreme energies, the medium energy cosmic rays are almost inaccessible in terms of direct measurements. Therefore ground level observations of the secondary particles (EAS) must be employed to deduce information about their spectrum. Unfortunately, this process of deduction generally involves a number of relatively unproven assumptions about shower development, making the final results uncertain. A way of avoiding much of this process explicitly is by making measurements of the density spectrum defined by the rate of detection of secondary particle densities in a detector. Determinations of this spectrum require, in the production stage, no assumptions at all about either the form of the primary energy spectrum (to

at least a first approximation), or about the way in which secondary particles are produced and scatter out about the primary particle trajectory. The trade-off for the ease of measurement of this spectrum is the difficulty in the interpretation of the result.

As an approximation, the density spectrum may be interpreted as follows (after the work of Allan and Davies 1979). The shower size, $N_e(r)$ required to produce particle density, ρ, at a distance, r, from the shower core is given by:

$$N_e(r)=\rho/f(r) \qquad (3.1)$$

where f(r) is some appropriate lateral structure function. If the integral size spectrum, the rate of detection of showers exceeding some threshold size, is given by:

$$K(N_e)=K_0.(N_e)^{-\gamma} \qquad (3.2)$$

or $$K(\rho,f)=K_0.(\rho/f(r))^{-\gamma}$$

then the integral density spectrum is given by:

$$H(\rho)=\int_0^\infty K(\rho,f).2\pi r.dr$$

i.e. $$H(\rho)=K_0\rho^{-\gamma}\int_0^\infty 2\pi r.(f(r))^{\gamma}.dr \qquad (3.3)$$

$$=H_0.\rho^{-\gamma} \qquad (3.4)$$

where H_0 depends on the normalization of the lateral

structure function. The important point to note is that for this straightforward case, the integral density spectrum is characterized by the same power law index as the integral size spectrum. Unfortunately, implicit in this derivation is the assumption that the lateral structure function at all core distances is independent of the shower size. Nonetheless, if this shower size dependence is weak or can be compensated for, the density spectrum technique offers an uncomplicated way of examining the size spectrum index in a way which is almost independent of shower development models.

If the shower size spectrum can then be related to the primary energy spectrum , the detailed form of these spectra are accessible from experiments involving relatively unprocessed data. This is especially significant for studies near the spectral 'knee', which corresponds to a primary energy of just above 10^{15} eV or a sea level shower size about $5*10^{5}$ particles.

3.1.2 Previous Experiments

Studies of the cosmic ray density spectrum have been conducted for over forty years, often, unfortunately producing somewhat contradictory results, depending on detector types and arrangements, and especially the atmospheric depth at which the experiments were carried out. Assuming the power law form of the density spectrum, it was hoped that measurements of the variation of the spectrum with atmospheric

depth would give direct information on the primary spectrum and shower development. However the interpretation of these data has proved very difficult (McCaughan 1982a,b,c).

The density spectrum was first studied as an adjunct to experiments on the lateral spread of shower particles (e.g. Auger et al 1939, Clay 1942), however when the early experiments were found to be in conflict (Cocconi et al 1946) many experiments followed in attempts to produce definitive results. Analyses of the raw data from these experiments relied on the following assumptions:

(i) the density spectrum was described by one or more inverse power laws;

(ii) the distribution of particles in the shower over the size of the detectors was random;

(iii) the mean particle density for each event was constant across the experimental apparatus.

The early experiments employed a statistical approach (adapted for cosmic ray experiments by Auger et al 1939) to the problem of density measurements. In these experiments, trays of Geiger-Muller counters, spaced by of the order of 5 metres, were used as the detectors. Coincidences between individual counters and also the trays of counters were recorded. The density spectrum was then evaluated from these data by two alternative techniques. Firstly by comparing the rates of coincidences of a number of detectors, the average 'local' shower density was determined for a given set of

coincidence requirements. This density, derived statistically from the above assumptions was given by:

$$\rho = \ln(1/(1-C_n/C_{n-1}))/A \qquad (3.4)$$

where A was the effective detector area and C_n was the rate of n-fold detector coincidences. Knowing the rate of coincidences, the density spectrum was constructed from a number of different coincidence and detector arrangements. Careful analysis by Broadbent et al (1950) showed that assumption (iii) was fallacious, introducing errors into the results obtained by the technique. However, the magnitude of these errors for the power law index was less than 10% (Prescott 1956).

Alternatively, when the rate of coincidences of a given number of detectors was measured as a function of the detector area, the power law index of the density spectrum was given by:

$$\gamma = d(\ln C_n)/d(\ln A) \qquad (3.5)$$

This technique does not require assumption (iii), but still assumes that the lateral distribution is not a function of shower size and hence of particle density. Since this method required less assumptions, it was most often applied to counter experiments.

More recent experiments to determine the spectrum have

generally employed more direct methods to measure the particle density. These include ionization chambers (Prescott 1956), proportional counters (Norman 1956), cloud chambers (Reid et al 1962) and scintillators (Katsumata 1964). As well as the actual density detectors for these experiments, other particle detectors were used in coincidence to trigger the recording device so that only densities from showers were recorded. A common feature of these experiments was the separation distances of the detectors - usually only a few metres. This meant that densities were generally measured within a few metres of the shower core.

A compilation of results from a number of sea level determinations of the power law index is shown in figure 3.1. It can be seen that these results indicate a sharp change in the index from about 1.5 to nearly 2.4 at near 1000 particles m^{-2}. Although this change is clear in the compilation, occasionally individual experiments (e.g. Hara et al 1979b) measure a constant index over a wide density range. Unfortunately, the index above the change is perhaps larger than that expected from size spectrum measurements. Also, at the low density end of the spectrum, a slowly increasing index with density has been proposed (Greisen 1956), whereas the primary energy spectrum and size spectrum in the corresponding regions are usually fitted by a single power law. These interpretation problems stem from the experimental arrangement mentioned previously, i.e. the measurement of the density close to the shower core.

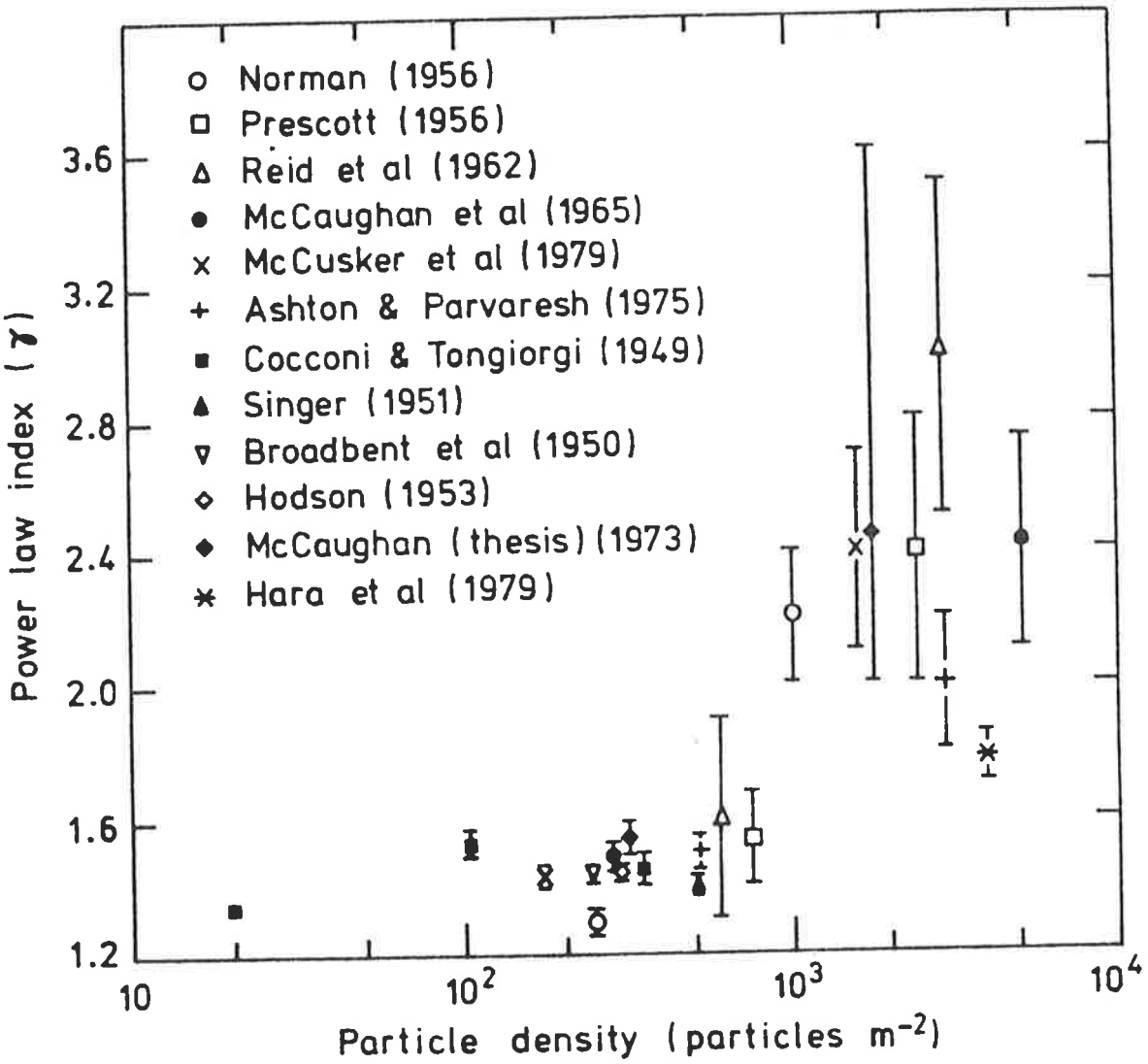

Figure 3.1 Compilation of the power law index results of density spectrum experiments.

Near the EAS core, a number of difficulties are encountered. Firstly the particle density is changing rapidly with core distance. Secondly, the presence of the nuclear-active particles of the shower core near the detectors may produce anomalous changes in the lateral distribution of the electromagnetic component. In fact, the lateral distribution of particles near the EAS core is not well known. Thirdly, the nuclear-active particles may produce bursts of particles in the material above the detectors, thereby leading to anomalous density measurements. McCaughan (1982a) has critisized the results of these density spectrum experiments mainly on the basis of core effects, however other efforts to reconcile the size and density spectra (Ashton and Parvaresh 1975, Khristiansen et al 1979) have invoked a varying lateral structure function. These efforts have had, at best, limited success.

Recently McCaughan (1982a,b) has proposed an interesting interpretation of the results of the density spectrum. If the spectrum is simulated, for successful fitting, it is required that a parameter, in this case the lateral age parameter in the NKG function, varies in a way that cannot be interpreted in terms of a change in the primary spectrum, but instead must reflect a change in the nature of the nuclear interactions at the energy corresponding to the spectral knee. Other evidence, for example the existence of 'Centauro' events may support this interpretation. Hillas (1981b), however has used interpolations between the sea level and mountain level density spectra for the same experiments to

deduce a very short absorption length for the shower cores. He proposes from this that less than 2% of the primaries are protons - thereby implying a rapid change in the primary mass composition near the spectral knee.

3.1.3 The Buckland Park Array Density Spectrum Experiment

In 1979, Allan and Davies suggested that to avoid the problem of density measurements near the core, relatively widely spaced detectors could be used to measure the density spectrum. If the variations in the lateral distribution as a function of shower size are not too large, then the density spectrum power index measured should accurately reflect the size spectrum. Equivalently, these measurements could be used as a check on the self-consistency of the lateral structure function and the measured size spectrum.

Before actual measurements of the array density spectrum are described, the equation 3.4 requires further examination. Allan and Davies (1979) have shown that appropriate limits for the integral in equation 3.3 are actually some minimum distance r_0 and ∞. This is due to the fact that the detectors are not infinitesimal in size, so that the density measured is actually averaged over the detector area and not a point density. Moreover, the requirement for shower detection is - densities greater than some threshold in coincidence in a number of spaced detectors. The constant, r_0, is then related to the spacing and arrangement of the

array. It is clear then, that the 'constant', H_0, is actually a function of r_0 and γ (as well as the shape of the lateral structure function). Calculations by Wenneberg (1982) show that although at spacings (of two detectors, r_0) less than 10 metres, H_0 is strongly dependent on γ, at r_0 greater than this, the dependence is rather weak. If variations in the lateral distribution as a function of shower size at the detector distance from the shower core are small, then the power law index of the density spectrum is a useful measure of the size spectrum in the region of the 'knee' in the spectrum. Figure 3.2 shows the shape of the NKG structure function with respect to core distance for a number of different shower age values. It can be seen that although there are variations, at distances greater than about 20 metres they are not large. However, the lateral distribution shows large variations within 10 metres of the core. This indicates the main reason for the variations in the density spectrum measurements for experiments with closely spaced detectors.

The array density spectrum is defined in the following way. An array of detectors can be constructed to detect EAS, with the rate of shower detection determined by the threshold (in terms of the particle density at the detector locations) required to trigger the system. If the particle density thresholds for each detector are then changed by the same ratio, then a new shower detection rate will be produced. The array density spectrum is defined by the dependence of the rate of detection of EAS on the relative threshold levels.

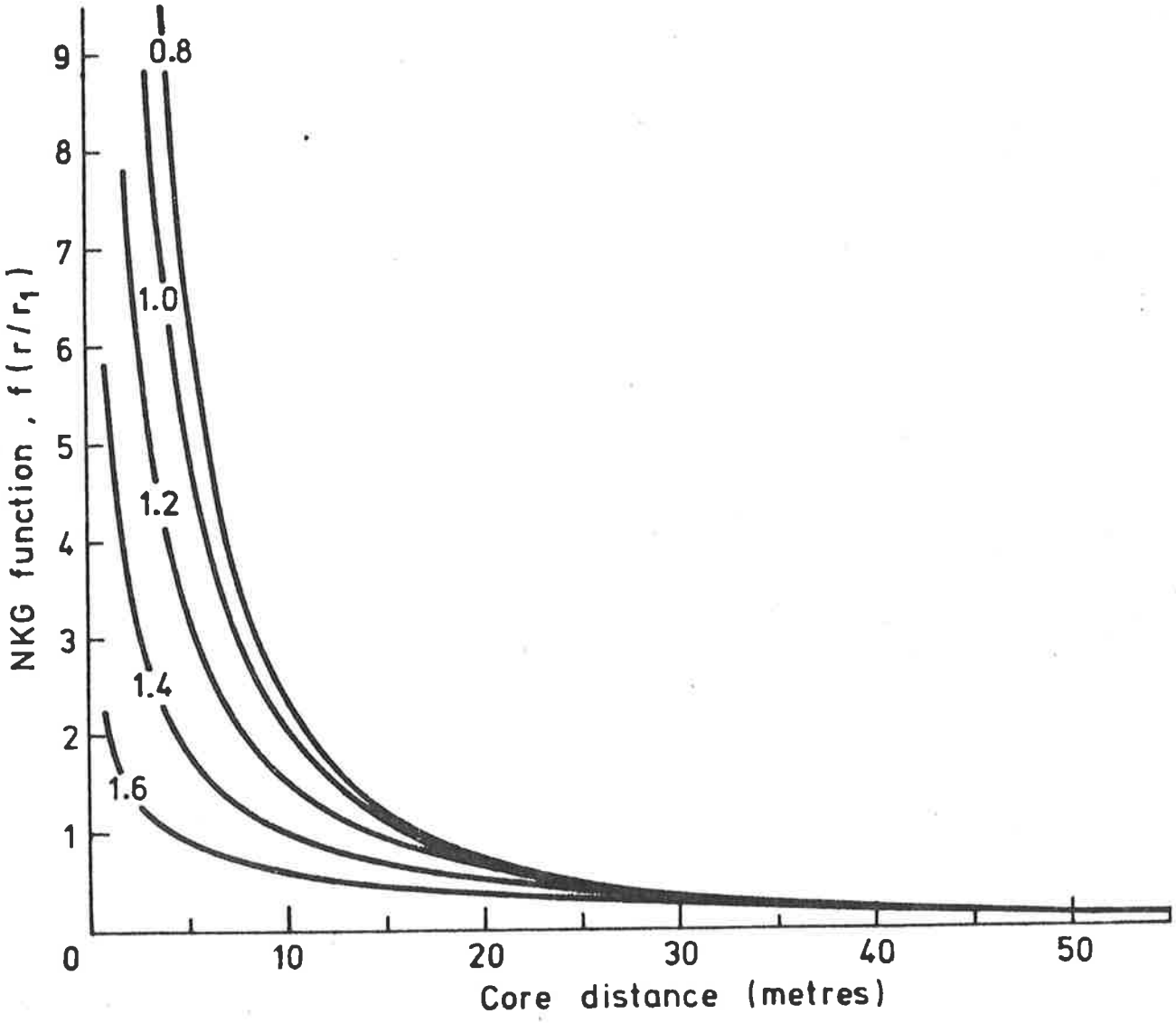

Figure 3.2 The shape of the NKG function for various ages as a function of core distance.

This definition highlights the difference between the 'local' density spectrum requiring basically one detector (measured in the experiments described earlier) at usually rather small shower core distances, and the 'array' density spectrum for which measurements are generally conducted some distance from the shower core.

There are two alternative ways of performing this experiment. In the first case, the electronic discrimination levels on the outputs of the individual detectors are fixed and then the density threshold is varied by physically changing the effective size of the detector. Care must be taken in this method to allow for variations in the detector efficiency as a function of detector size. This method was chosen by Allan and Davies (1979) for their investigation. Since the Buckland Park array is a permanent installation and the detector sizes fixed, this is not a suitable technique for the equipment. Alternatively, an array of detectors can be set up to record EAS in the normal way - by detecting coincidence levels above a given particle density threshold in the detectors. By recording all particle densities above this triggering level for the array, the data can later be checked at higher density thresholds in coincidence to find the rates of shower detection corresponding to the higher densities. This method does not interfere with the normal continuous running of an array and was therefore chosen for the Buckland Park density spectrum experiment.

To obtain reasonable particle numbers in the

detectors, the central part of the Buckland Park array, which includes the fast timing array was used in the experiment (figure 3.3). Shower detection was determined by these detectors with triggering requirements being greater than 2 particles m^{-2} in each of the fast timing detectors and also greater than 6 particles m^{-2} in A density detector and greater than 8 particles m^{-2} in D density detector. Apart from statistical fluctuations in the local particle densities, the latter condition is sufficient to ensure that the threshold levels in the former condition are satisfied. In the initial experiment (Clay and Gerhardy 1980), density detectors A and D were chosen. With a separation of about 42 metres, the minimum threshold (i.e. 6 particles m^{-2} in A and 8 particles m^{-2}) corresponds to a most probable shower size of near 10^5 particles (see figure 2.8). Later, other detectors with smaller separations were used to extend the spectrum to include densities from smaller shower sizes (Clay et al 1981a). These other pairs of density detectors were D and E detectors (separated by 30 metres) and B and C detectors (separated by 21 metres). For the parts of the experiment using the smaller separations, the triggering requirements for the array were temporarily set to only 2 particles m^{-2} in each of the density detectors A, B, C, D and E.

To determine the array density spectrum, the data from these pairs of detectors were compared with artificial computed thresholds which were increased by multiples of $\sqrt{2}$. Hence, for example, the thresholds considered for density detectors A and D respectively were: 6 and 8 particles m^{-2},

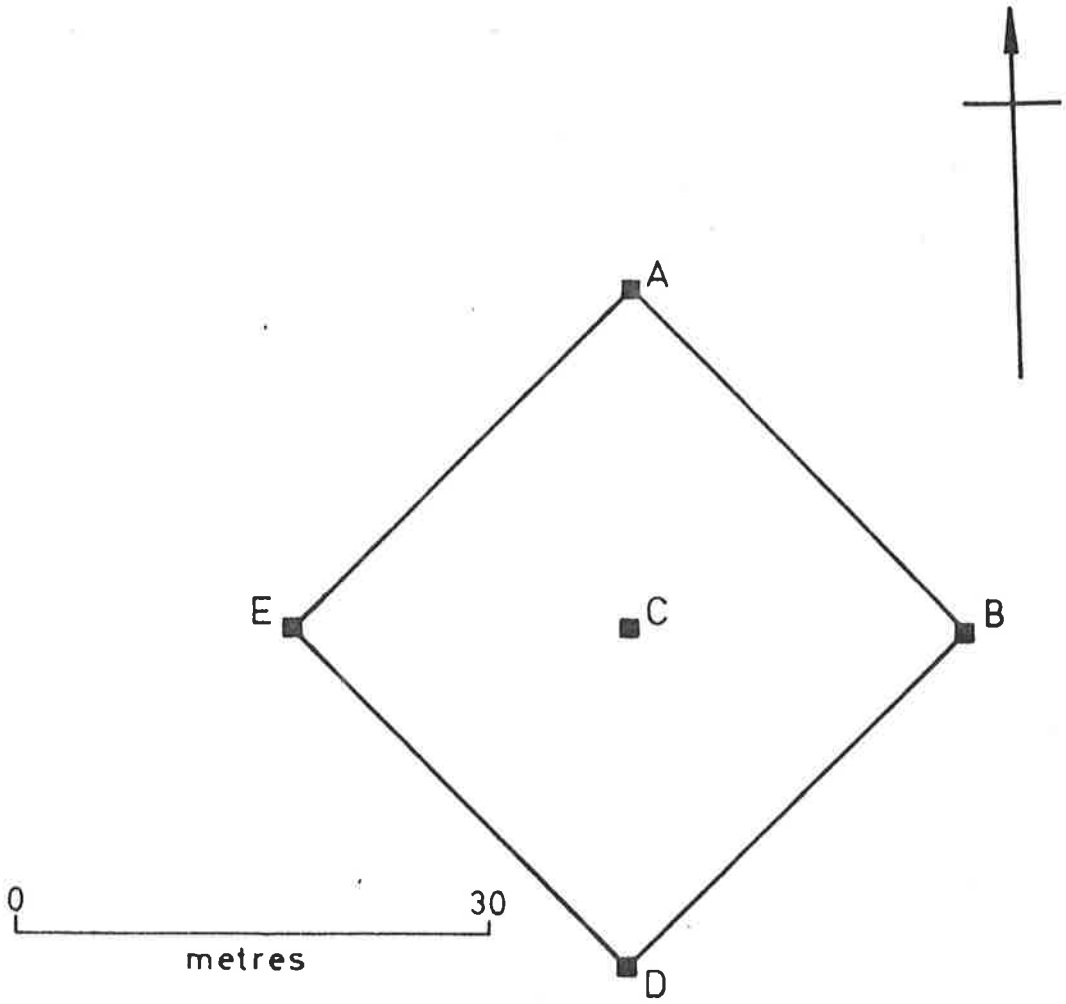

Figure 3.3 The fast timing array - used in the density spectrum experiments.

$6\sqrt{2}$ and $8\sqrt{2}$ particles m^{-2}, 12 and 16 particles m^{-2} and so on. Simply counting the number of showers to trigger each of these artificial thresholds then gave the array density spectrum. This spectrum is shown for detectors A and D in figure 3.4.

Spectra from the various pairs of detectors were combined using the results of the normal analysis of the raw data recorded by the array. For the detector pairs, size spectra for given density thresholds were determined and from these the most probable shower sizes for these thresholds were evaluated. By finding the thresholds for each detector pair which corresponded to the same most probable shower size, the density spectra could be combined.

The most interesting parameter of the density spectrum is the power law index which, as shown earlier, should be directly comparable with results obtained from size spectrum experiments. Therefore, values of the index for each of the density spectra in intervals of $\sqrt{2}$ in threshold were evaluated and are plotted in figure 3.5 as a function of most probable shower size.

Over the range of shower sizes from about $4*10^5$ particles to at least 10^7 particles, the spectral index appears to be approximately constant with a mean value of near 1.9. Below $4*10^5$ particles, the index appears to decrease fairly sharply, however in the lowest size bins for each detector pair, particle statistical limits become important.

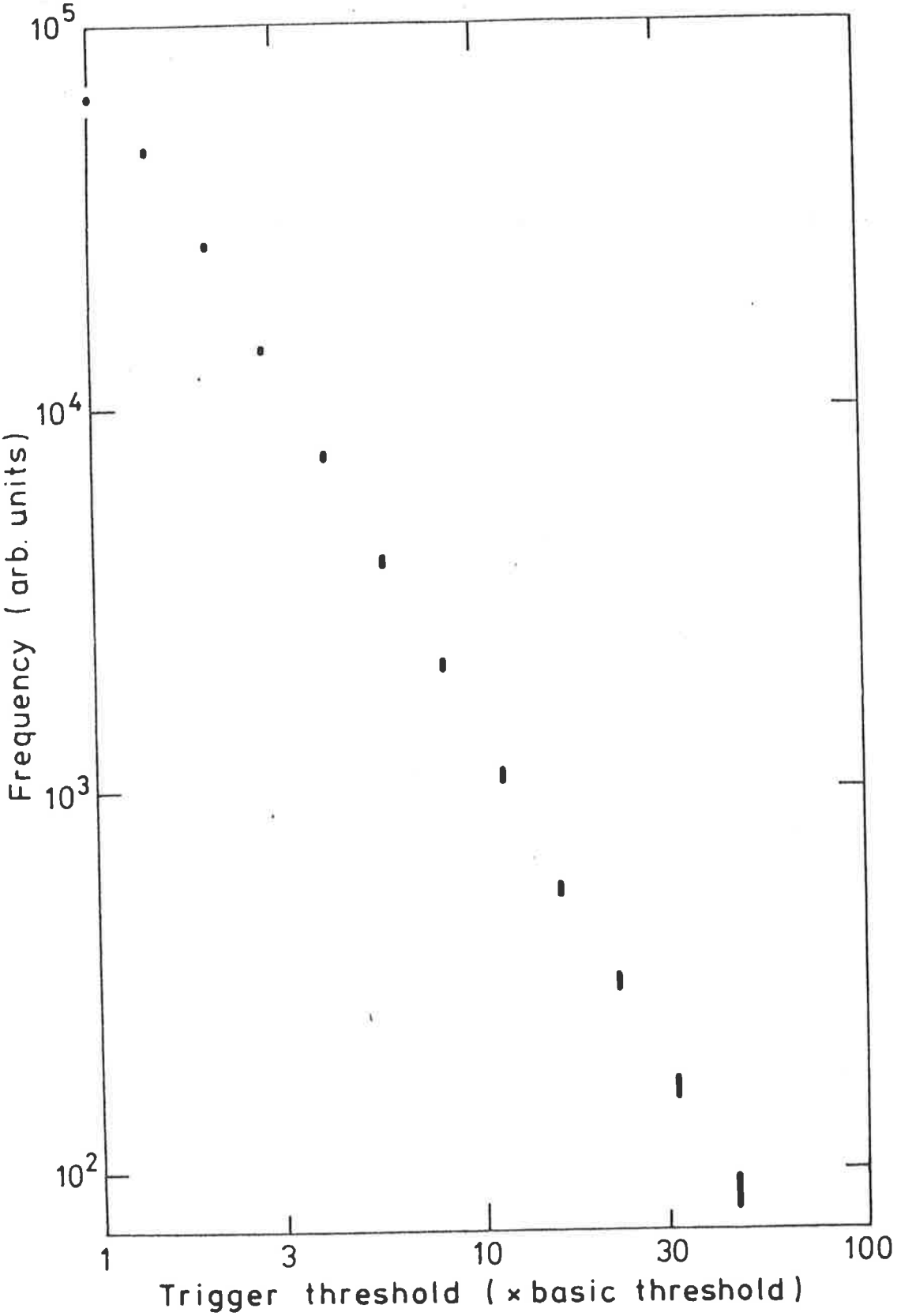

Figure 3.4 The density spectrum from A and D detectors

For example, in the case of A and D detectors , the lowest threshold used in figure 3.5 is $\sqrt{2}$ times the minimum requirement for the array (since upward density fluctuations at below the minimum requirement make the corresponding rate uncertain). However, densities of 2 particles m^{-2} are also required in detectors B, C and E, so that events may not trigger the array at this level if the densities at B, C and E detectors fluctuate downwards from about 10 particles m^{-2} to less than 2 particles m^{-2}. There is a small but finite probability of this occurrence which would produce a corresponding error in the spectral index. Similar problems occur with the other detector pairs in their lower size bins.

To try to overcome this problem, for a short time the array triggering thresholds were reduced to 2 particles m^{-2} in A and D and a threshold corresponding to 1.5 particles m^{-2} in C detector only. Detectors A and D were again used for the density spectrum measurements. In this way, the problem of particle statistics in the bins corresponding to the lower sizes in the other experiments was minimized. Due to the much smaller number of events collected, the index measurements from these data are relatively imprecise, although they still show the decrease in the index at low sizes measured by the other detector pairs. Results from this experiment are also shown in figure 3.5. The substantial agreement between the results of this experiment and the others indicate that it is likely that threshold effects on all the experiments are not significant for the shower sizes used. A check on this is given by the shapes of the shower

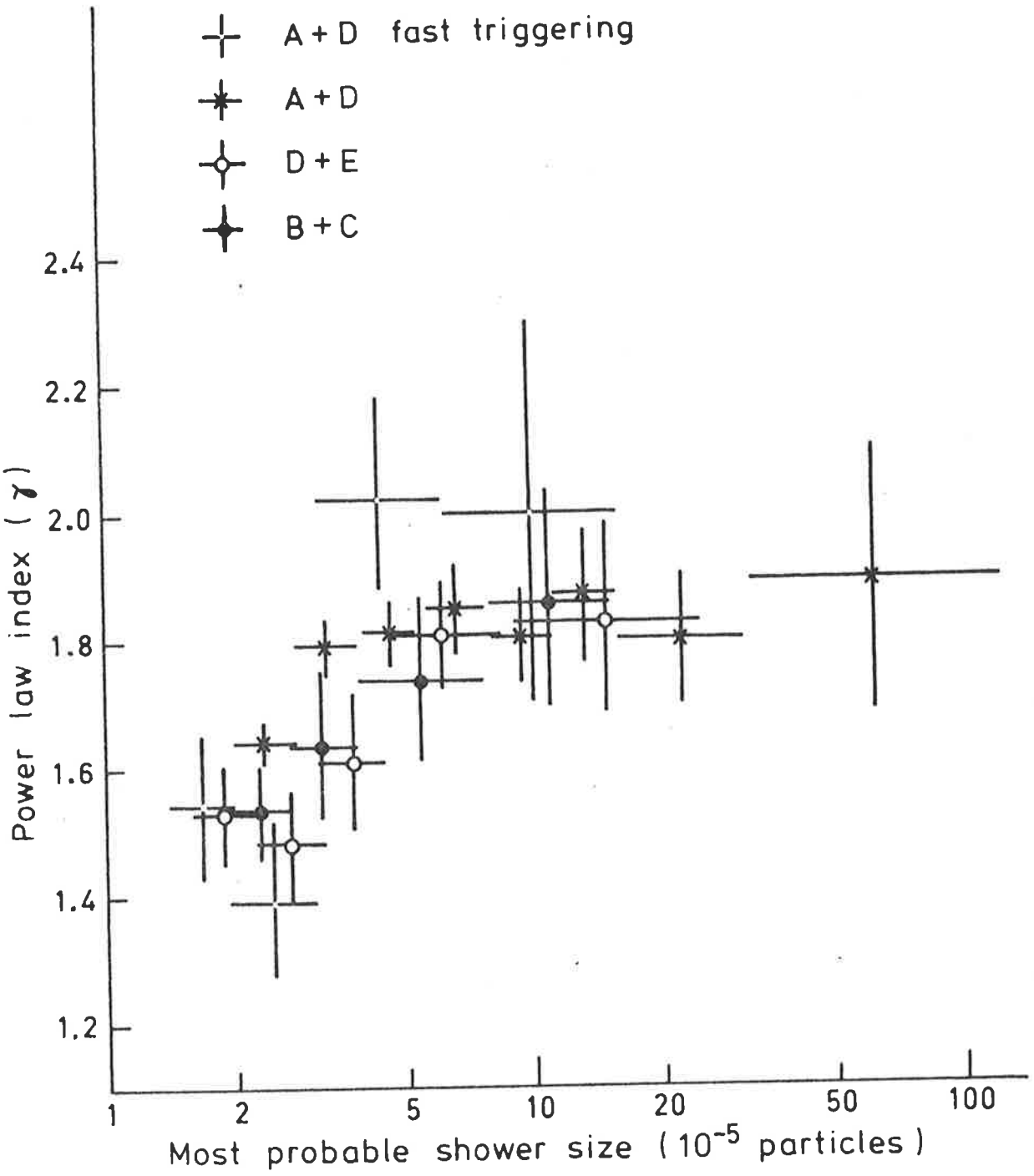

Figure 3.5 The power law indices as a function of most probable shower size from the density spectrum experiments.

size distributions for the two different triggering systems at the threshold values of 12 and 16 particles m^{-2} in A and D detectors respectively. These are in good agreement as seen in figure 3.6.

It has been shown (Allan and Davies 1979) that the shape of the observed shower size distribution is dependent on the spectral index. Therefore as a check on the constancy of the index above shower size of about $4*10^5$ particles , the size distribution was determined for the normal array triggering with an additional artificial threshold of 60 particles m^{-2} in A detector and 80 particles m^{-2} in D detector. Scaled down by a factor of 5 in size, this distribution is also shown in figure 3.6. It can be seen that the distributions are in excellent agreement. This result gives further support for the proposition of a constant spectral index between shower sizes of $4*10^5$ particles and 10^7 particles.

3.1.4 Comparable Experiments

The experiment of Allan and Davies (1979) used an array of six scintillator detectors arranged in pairs at the vertices of an equilateral triangle having a circumcircle of radius 12 metres. Each of the detectors could be varied in area from a maximum of 1 m^2 down to approximately 0.01 m^2. Data was then collected using basically the counter technique of, for example, Cocconi et al (1946). Coincidence rates,

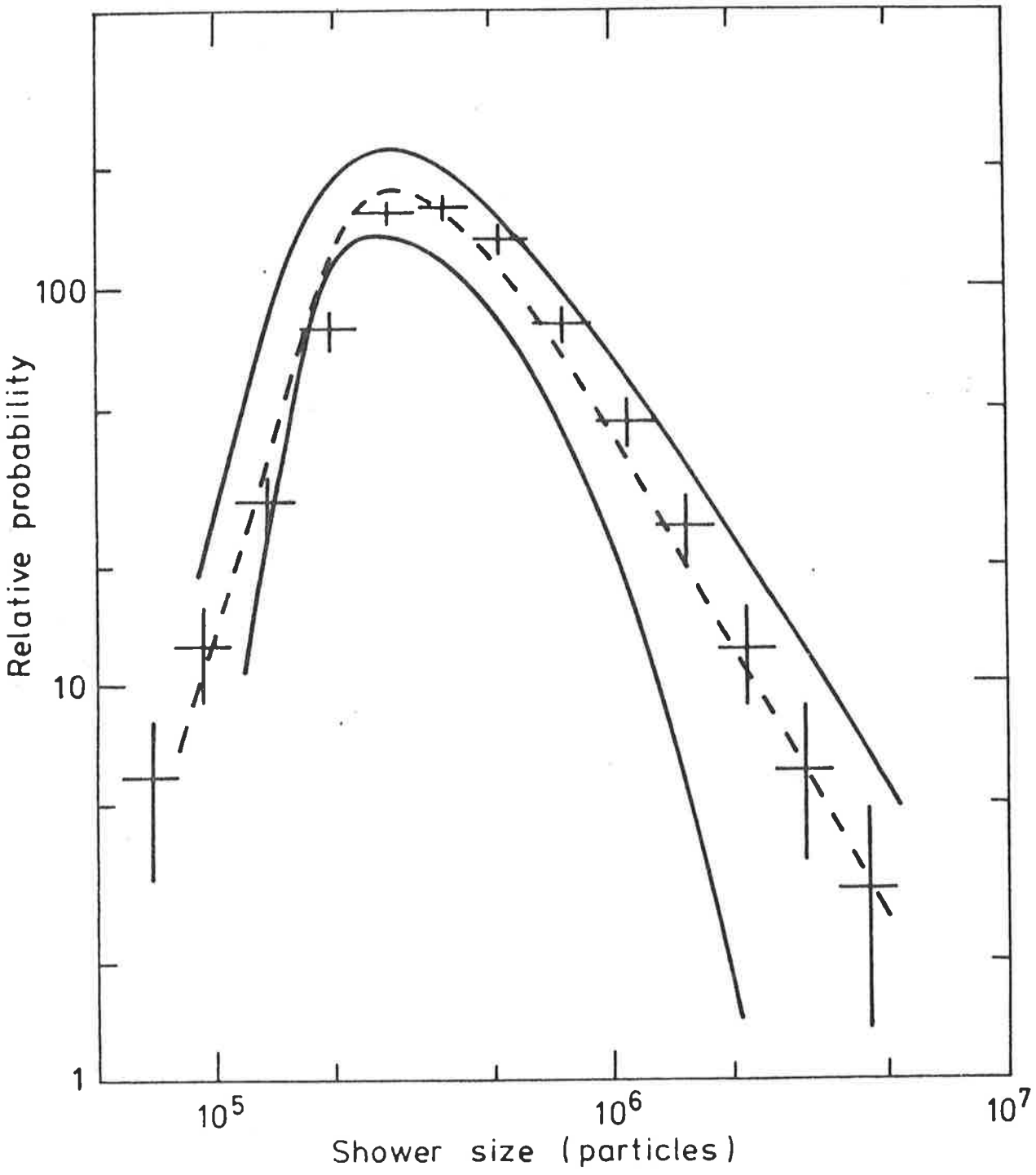

Figure 3.6 Shower size spectra under different threshold conditions:
error bars - full experiment with threshold of 12 particles in A and 16 particles in D.
area bounded by curves - full experiment with threshold of 60 particles in A and 80 particles in D (shower sizes reduced by a factor of 5).
dashed line - fit of data from short experiment with low thresholds, the artificial threshold imposed here is 12 particles in A and 16 particles in D

determined by some arbitrary electronic threshold at the equivalent of 1 particle of the two sets of three detectors as well as for all six detectors were counted. Comparison of the rates from the two sets of three detectors provided a check on the correct operation of the array, and comparison of the three-fold to six-fold coincidence rates provided an estimate of the spectral index using a simple rearrangement of equation 3.5. (For this experiment, a six-fold coincidence was considered to be a three-fold coincidence of detectors with double the effective area.) The particle density was assumed to be given by the reciprocal of the area (e.g. see Greisen 1956). By varying the detector areas an array density spectrum was built up.

Preliminary results of this experiment gave a spectral index of about 1.3, at a density of 0.7 particles m^2, which from their calculations corresponded to a median shower size of near $7*10^3$ particles. Further unpublished results (Allan priv. comm. 1981) indicated no sharp kink in the spectrum, but rather suggested a gradual increase in the index. However, Allan has suggested that the change in the detector sensitive area as the detector size was changed may have introduced some problems in the calculations.

An experiment using two of the Buckland Park detectors (B and C), but an independent triggering and recording system was run by Clay (reported in Clay et al 1981a). In this experiment, the only triggering requirement was a coincidence between the two detectors at a threshold density of greater

than 1.5 particles m^{-2}. This system enabled the recording of large numbers of events - about 3000 events per day, as compared to about 150 - 200 events per day for the Buckland Park array in its normal triggering mode. On detecting a coincidence, the particle density for each detector was calculated from the measured pulse height spectrum for the detector. The array density spectrum was then constructed by the usual technique of imposing artificial thresholds and counting the shower rate for each threshold. Simulations by Dawson (1980) were used to determine the most probable shower size corresponding to each density threshold. Results of this experiment are shown in figure 3.7. It is clear that they are in very good agreement with the results presented in the previous section.

To try to resolve the difference between the experiments of Allan and Davies (1979), Clay and Gerhardy (1980) and Clay et al (1981), an experiment using both the technique of varying areas and also that of varying thresholds was developed by Clay et al (1982). By comparing the techniques in this way, the biasses introduced by each method could be accounted for. The experimental arrangement used two scintillator detectors with initial areas of 1 m^2 each, at a separation of 16 metres. The minimum threshold for each detector was set 'well below' the 1 particle m^{-2} level and the data train investigated for coincidences. Again the spectrum was determined by the imposition of artificial thresholds and counting the coincidence rate.

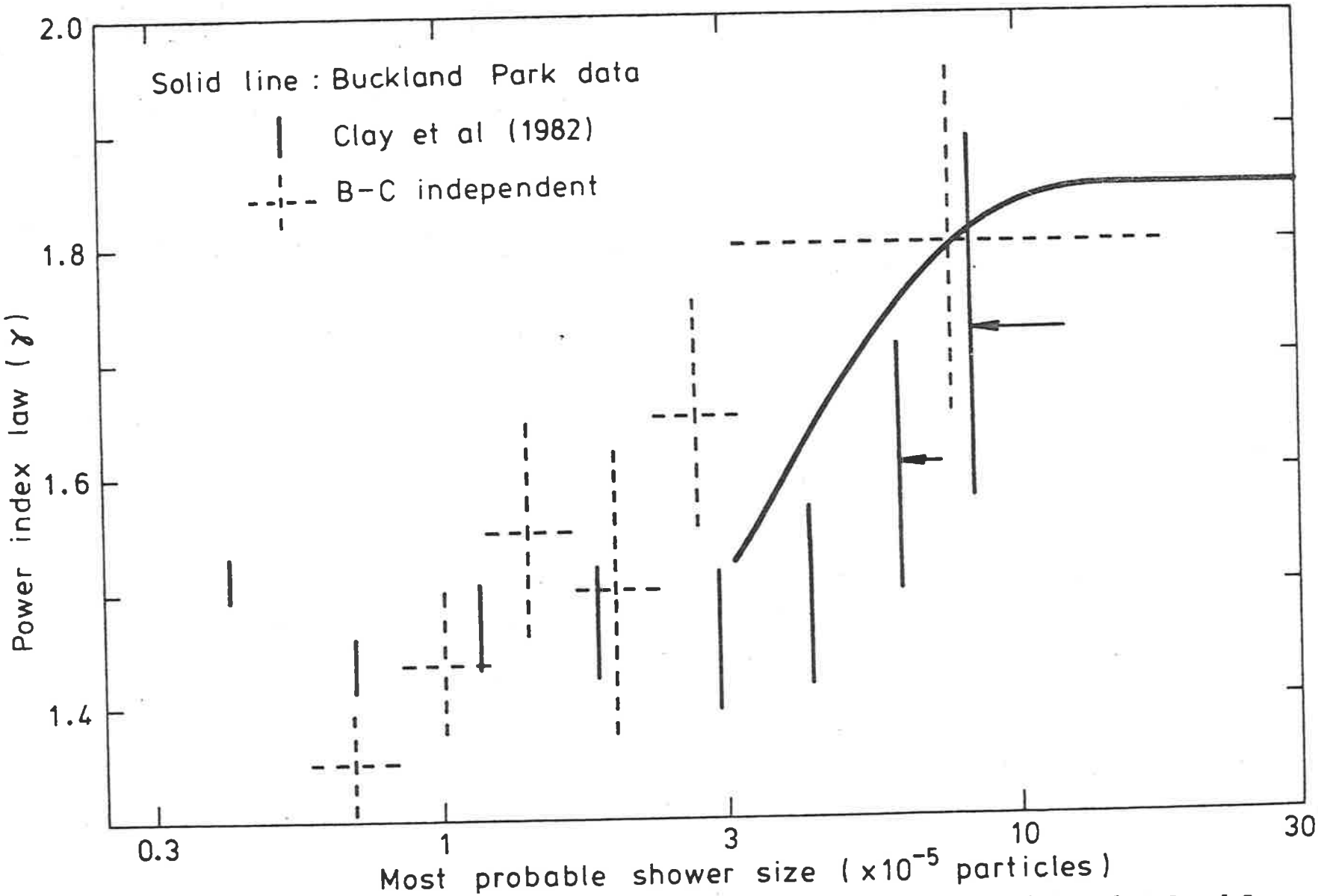

Figure 3.7 Comparison of Buckland Park results with those of Clay et al (1982b) and independent B and C experiment of Clay.

After this spectrum had been determined, the scintillators were then progressively halved in size down to 0.125 of the m^2 with spectra determined for each detector size in the same way as the original. These spectra were expected to be identical except for a factor of 2 change in density for each different detector size. Differences in the spectra enabled systematic biasses to be removed. The final density spectrum was then calibrated in terms of most probable shower sizes using Monte Carlo simulations. The results of this experiment are also shown in figure 3.7 along with a summary of the Buckland Park results. It can be seen that there is support for the proposition of a change in the spectral index from about 1.45 to 1.85 although the shower sizes at which the kinks occur are at slight variance. This may be due to differences in the particle lateral distributions used in calibrating the spectra from each experiment.

3.2 The Size Spectrum

3.2.1 Introduction

The cosmic ray size spectrum is of interest not only because of its relationship to the primary particle energy spectrum, but also since observations of the way the size spectrum varies as a function of atmospheric depth can provide information about the particle interaction characteristics at

energies inaccessable to man-made particle accelerators. This spectrum (shower flux as a function of size) is defined in its integral form, by the number of showers detected greater than a given size per unit time, in unit area, from unit solid angle, or mathematically by:

$$J(>N_0)=\int_{N_0}^{\infty}(n(N).dN/(dt.dS.d\Omega) \qquad (3.6)$$

where n(N) is the number of showers in the size range between N and N+dN and t, S and Ω are time, area and solid angle respectively.

To a first approximation, the shower size spectrum is presumed to follow one or more inverse power laws characterized by the power law index, , i.e.

$$J(>N)=J_0.N^{-\gamma} \qquad (3.7)$$

and may depend in some way on the shower size. On the basis of the early density spectrum data, Greisen (1960) proposed a size spectrum where the inverse power law index increased logarithmically as a function of shower size between 10^3 particles and greater than 10^9 particles. Data from the previous section however, indicates a spectrum with relatively constant index between at least 10^4 and 10^5 particles with a rapid change at about $3*10^5$ particles to a relatively constant index up to at least 10^7 particles.

Although measurements of the size spectrum rely

implicitly on the form of the lateral distribution used, its accurate determination also relies heavily on a number of other parameters of the detector system. Probably the most important of these is the effective collecting area. Any array of detectors will show, over its arrangement, variations in its detection efficiency for showers. This will be a function of the shower size. The determination of the flux relies on the accurate knowledge of this collection efficiency function. Other factors which must also be taken into account are the recording dead-times for the detectors and the acceptance angle and angular resolution of the array.

3.2.2 The Buckland Park Size Spectrum

The EAS size spectrum was compiled using the raw data collected by the Buckland Park EAS Array as described in Chapter 2. For each detected event, the collected and recorded data are:

(i) the particles at nominally 12 density detectors (depending on breakdowns etc.)

(ii) the relative arrival times of the shower front at 5 fast timing detectors;

(iii) the local time;

(iv) the local barometric pressure, atmospheric temperature, a sample detector temperature and the temperature of the recording electronics.

These raw data are analysed to give the arrival

directions, shower core location on the ground, and shower size. Routinely, the shower size is determined using the lateral distribution given in equation 2.1, however to allow for variations in the structure of the showers, the NKG function (equation 1.5) with a variable lateral age parameter has also been used.

Since the showers detected by the Buckland Park array are well past the shower size maximum, the shower size measured is reduced as the amount of atmosphere traversed increases. Hence, showers detected with large zenith angles will be smaller than equivalent vertical showers. The rate of size change with atmospheric thickness past shower maximum is characterized by a thickness known as the shower size attenuation length. Events utilized in the measured spectra have been adjusted in size to equivalent vertical showers using the measured attenuation length (185 g cm^{-2}, see Chapter 4).

Integral vertical shower size spectra determined by both these lateral distribution functions and drawn from about $1.2*10^5$ events are shown in figure 3.8. To avoid the problem of variation in detection efficiency, areas of the array which had close to 100% triggering probabilities for given shower sizes were determined, and only events whose size and core locations obeyed these criteria were accepted for the construction of the spectrum. These regions, determined by simulations, were taken to be circular, with the centre 5 metres south of C detector. Details of the radii and minimum

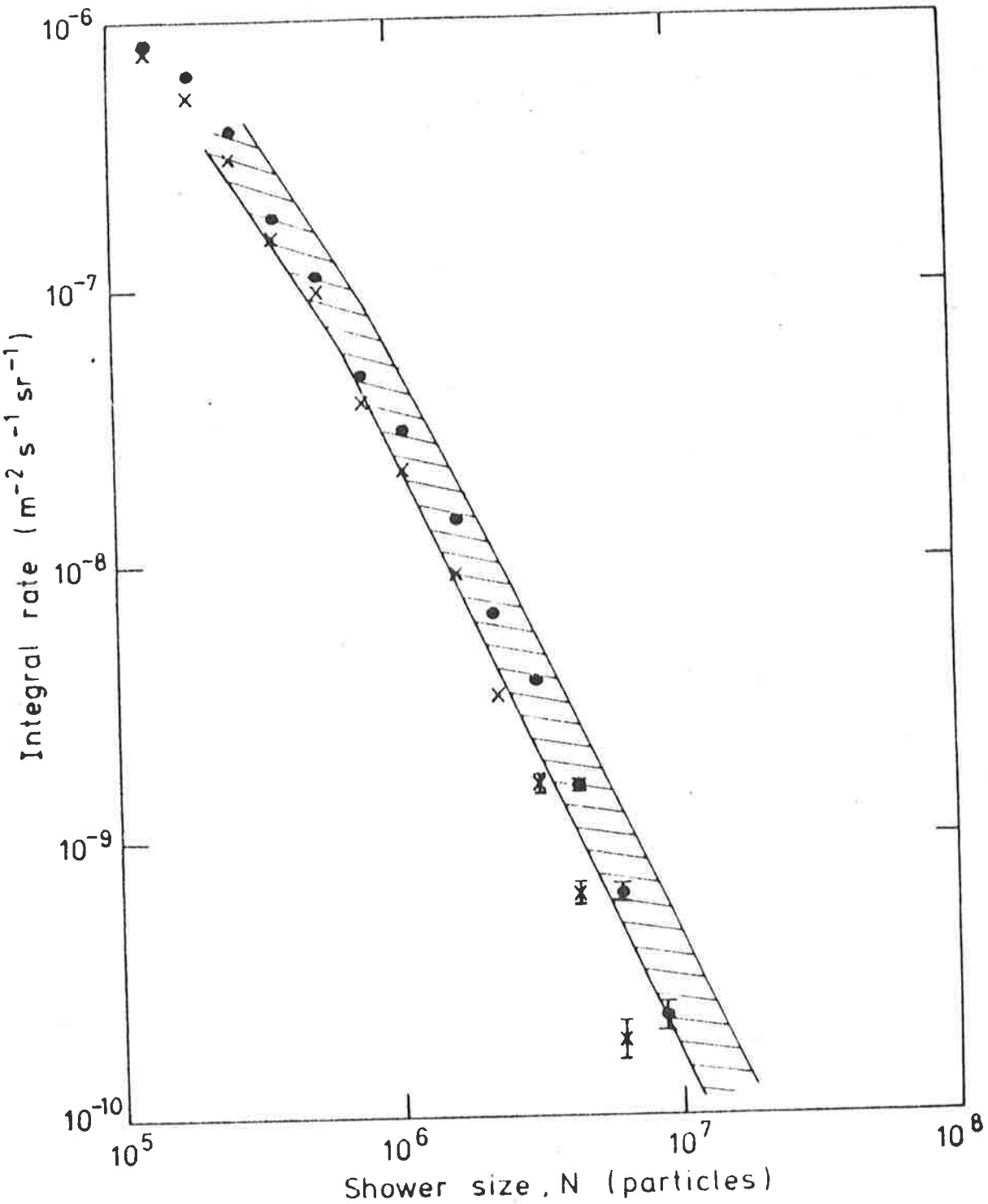

Figure 3.8 The Buckland Park vertical integral size spectra - filled circles - using the NKG function, crosses - using the Moscow/MIT function, shaded area - indicates the region covered in the compilation of Hillas (1980)

shower sizes for these regions are given in table 3.1 below.

Table 3.1: 100% triggering radii and sizes for the array.

Minimum Shower Size (particles)	Radius (metres)
$<4.6*10^5$	10
$4.6*10^5$	20
$9.1*10^5$	40
$2.6*10^6$	60

Two points have been plotted at sizes below $2*10^5$ particles. At this shower size, statistical fluctuations in particle densities in the triggering detectors should no longer significantly affect the rate of detection, however the two lower points may be biassed. Showers which were not well fitted by the analysis (i.e. which had reduced chi-squared greater than 5) were not used in the construction of the spectrum. Also, only showers with zenith angles less than 20^o were accepted. These limits for acceptable events reduced the number of showers used to about $1.7*10^4$ for the NKG analysed data and $1.3*10^4$ for the Moscow/MIT analysed data. The effective exposure time of the array was determined by summing the running times and subtracting dead times - including those due to poor analysis.

Since analysis using the NKG function allows for variations in the lateral structure of the shower, it is expected that this analysis would give the best estimate of

shower sizes. It can be seen however, (figure 3.8) that there is reasonable agreement between the size spectrum derived with the NKG function and that determined from shower analysis using the fixed lateral distribution function. Differences in the spectra are due to the poor fitting of some events to the Moscow/MIT function causing events to be rejected or placed outside the limits and thereby decreasing the measured flux - this is particularly important for the larger showers. These spectra then indicate that the way particles are distributed over the lateral extent of the shower is a function of shower size, or equivalently, that the way EAS develop in the atmosphere is a function of the energy of the primary particle which initiated the shower. (This interpretation assumes a unique relationship between primary particle energy and the shower size at any given depth in the atmosphere.) Qualitatively, this result is expected from variations with energy of the nuclear interactions as given by the various nuclear interaction models (e.g. see Linsley and Watson 1981a).

An interesting feature of the integral size spectrum is the change in the power law index which occurs near a shower size of $4*10^5$ particles (shown in figure 3.9). Below this size, the index is less than 1.5, and above it it near 2.0 to at least a shower size of 10^7 particles. This is in excellent agreement with the results of the array density spectrum experiment. It is not clear however, that the index change is a sharp change between two relatively pure power laws (which is the shape generally given to the shower size

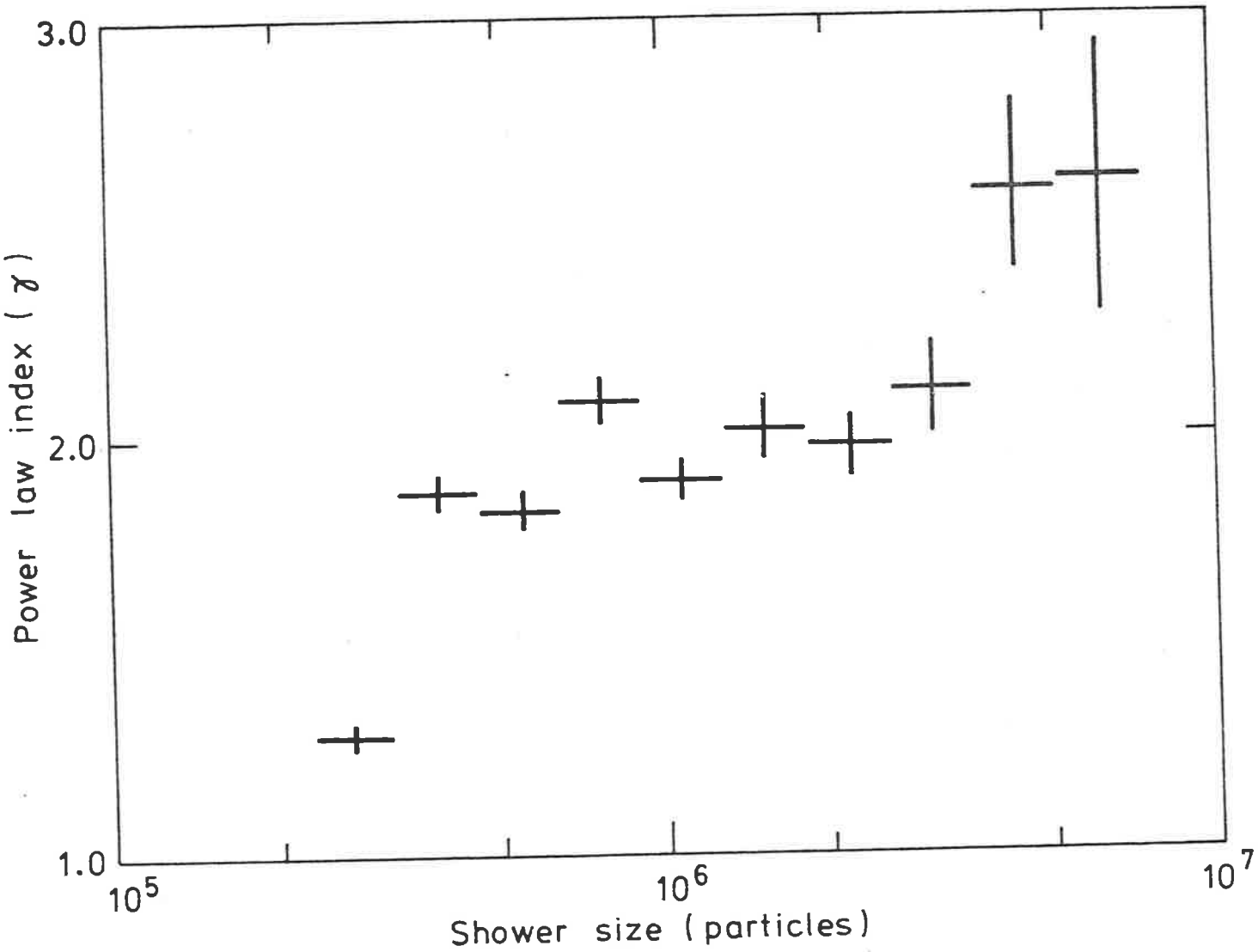

Figure 3.9 Power law indices from the Buckland Park vertical size spectrum.

spectrum (e.g. Efimov et al 1962, Hara et al 1979b)). In fact, the Buckland Park data can be interpreted to indicate that the integral size spectrum is fitted by inverse power laws with progressively increasing indices between shower sizes of about 10^5 particles and 10^7 particles, where the index may be larger than 2.4.

Included in figure 3.8 is a summary of results of sea level size spectrum measurements from the compilation of Hillas (1980), indicating the spread of these results. It is clear that the Buckland Park results are in general agreement with these data. In table 3.2, the Buckland Park results are compared with those of the Akeno array (Hara et al 1979b).

For consistency with the Akeno shower sizes, adjustments must be made to the Buckland Park shower sizes because of different calibration results and analysis procedures (Clay and Gerhardy 1982a). In their calibration procedures , the Akeno group find an 11% difference between the mode of the pulse height distribution for all particles passing through the detectors and the mean response of the detectors to vertical particles. By comparison, as shown in Chapter 2, these two parameters are found to be equal at Buckland Park. Secondly, the lateral structure function used in shower analysis at Akeno is an NKG function modified by an extra factor (Hara et al 1979a). This factor has been shown (Gerhardy et al 1981) to increase the measured size by about 20% while leaving the other shower parameters (age, core location) unchanged. These two factors cause a systematic

TABLE 3.2

INTEGRAL RATE $m^{-2} s^{-1} sr^{-1}$	BUCKLAND PARK SIZE (Particles $\div 10^5$)	AKENO SIZE (particles $\div 10^5$)	BUCKLAND PARK (Akeno Size) (particles $\div 10^5$)	PRIMARY Energy (eV)
10^{-7}	6.44 ± .10	7.3 ± 1.1	7.0 ± .1	7.5×10^{15}
$10^{-7 \cdot 5}$	12.13 ± .15	13.2 ± 1.2	13.1 ± .2	
10^{-8}	21.93 ± .40	23.8 ± 1.0	23.7 ± .4	1.9×10^{16}
$10^{-8 \cdot 5}$	38.7 ± .6	42 ± 4	41.8 ± .7	
10^{-9}	64 ± 1	78 ± 10	69 ± 1	6.5×10^{16}

difference between the shower sizes determined by the Buckland Park and Akeno arrays. However, when the Buckland Park shower sizes have been suitably modified, the results agree very well. Also shown in table 3.2 are the primary energies derived by Protheroe (1977) which correspond to these integral intensities. The factor of 10^{10} between shower size and primary energy near shower sizes of 10^{6} particles which was given in Chapter 1 can be seen to be a fairly good approximation.

CHAPTER FOUR

SHOWER DEVELOPMENT AND ATMOSPHERIC EFFECTS

Extensive air shower experiments use the atmosphere as a large crude ionization calorimeter for the detection and measurement of the primary cosmic ray particles. For a complete description of the primaries, it is necessary to know details of the shower development in the atmosphere. Sea level studies can be used to determine some of the air shower properties particularly for the shower development past shower size maximum. Studies of the longitudinal shower development and atmospheric effects on the shower flux carried out at Buckland Park are described in this chapter.

4.1 Longitudinal Shower Development

4.1.1 Introduction

Studies of the development of EAS in the atmosphere have been carried out using direct observations of the showers high in the atmosphere with aeroplane (Antonov et al 1971) and balloon borne (Antonov et al 1977) equipment. However, due to the relatively poor statistics of the collected data and the difficulty in obtaining accurate shower parameters for the

collected data (because of size limitations on the equipment), the results of these experiments are difficult to interpret and have been somewhat controversial. Ground based experiments on the other hand, although still having analysis difficulties, are not limited by the problem of poor collection statistics.

The technique used by the ground based experiments relies implicitly on the zenith angle resolution of the equipment. Size spectra of EAS are measured at different zenith angles and hence at different atmospheric depths. If it can be assumed that showers which are detected at the same rate come from the same subset of primary particles, then by taking constant intensity cuts in the size spectra from various zenith angles, it is possible to build up data on the average shower development as a function of intensity. This data is essential for checking the models which relate EAS size at any stage of development to the energy and mass composition of the particle which initiated the shower. Clearly this technique can only give information on the shower development at atmospheric depths greater than the vertical depth of the observatory. Complete descriptions of shower development for a range of primary energies then require the use of this method at a number of different atmospheric depths and the compilation of shower development curves from these data. Since these curves should be continuous, this technique also provides a valuable check on analysis and allows intercalibration between various observatories.

4.1.2 The Buckland Park Development Curves

Using the technique of constant intensity cuts, shower development curves were derived (Clay and Gerhardy 1981a) from the raw data collected by the Buckland Park EAS Array and analysed using the NKG lateral structure function. Since Buckland Park is a sea level installation, these development curves do not cover the important region near shower size maximum, but extend over a range of atmospheric depths from about 1000 g cm^{-2} to over 1400 g cm^{-2}. These results are however, an important test on the data obtained from high altitude observatories where the longitudinal development near shower size maximum can be observed.

The Buckland Park data (shower sizes, core locations, and arrival directions) were sorted into size intervals, each a factor of 2 wide above a threshold of $2.3*10^5$ particles. In this case, the data were also sorted by arrival direction, being placed in zenith angle intervals 4^o wide, from the zenith out to 48^o. Showers used were again restricted to well analysed showers and those detected with close to 100% efficiency to ensure that the effective collecting area was known. For each zenith angle interval, an integral size spectrum was then constructed by normalization with the collecting area (which is also a function of zenith angle), effective array exposure time, and the appropriate solid angle viewed. To improve collection statistics at low zenith angles, the data from the first three zenith angle bins were

combined (0^o - 12^o). About $1.6*10^4$ events were retained for these size spectra (shown in figure 4.1). The longitudinal development results were produced by sampling the size spectra from each zenith angle at integral intensities of 10^{-7}, $10^{-7.5}$, 10^{-8}, $10^{-8.5}$, and 10^{-9} $m^{-2}s^{-1}sr^{-1}$ and plotting as a function of zenith angle. These results are displayed in figure 4.2. On the abscissa, the zenith angles have been converted to the corresponding mean atmospheric depth traversed by the showers.

4.1.3 Other Results

To make the development curves more complete (and also for comparison), the results of a number of similar experiments at smaller atmospheric depths have also been plotted in figure 4.2. Amongst these, the results from Mt Chacaltaya (La Pointe et al 1968) are of particular interest since Mt Chacaltaya (at a height of 5200 metres above sea level corresponding to an atmospheric depth of 530 g cm^{-2}) is expected to be, on average, near the atmospheric depth of maximum shower development for primary particles with energies above 10^{14} eV. Unfortunately, these results have been the subject of some debate since they are systematically in poor agreement with results from experiments conducted lower in the atmosphere. However, Hillas (1979) showed that these results could be brought into agreement if the shower sizes derived in the Mt. Chacaltaya data were reduced by a factor of 1.5, and they are shown with this reduction in figure 4.2. The solid

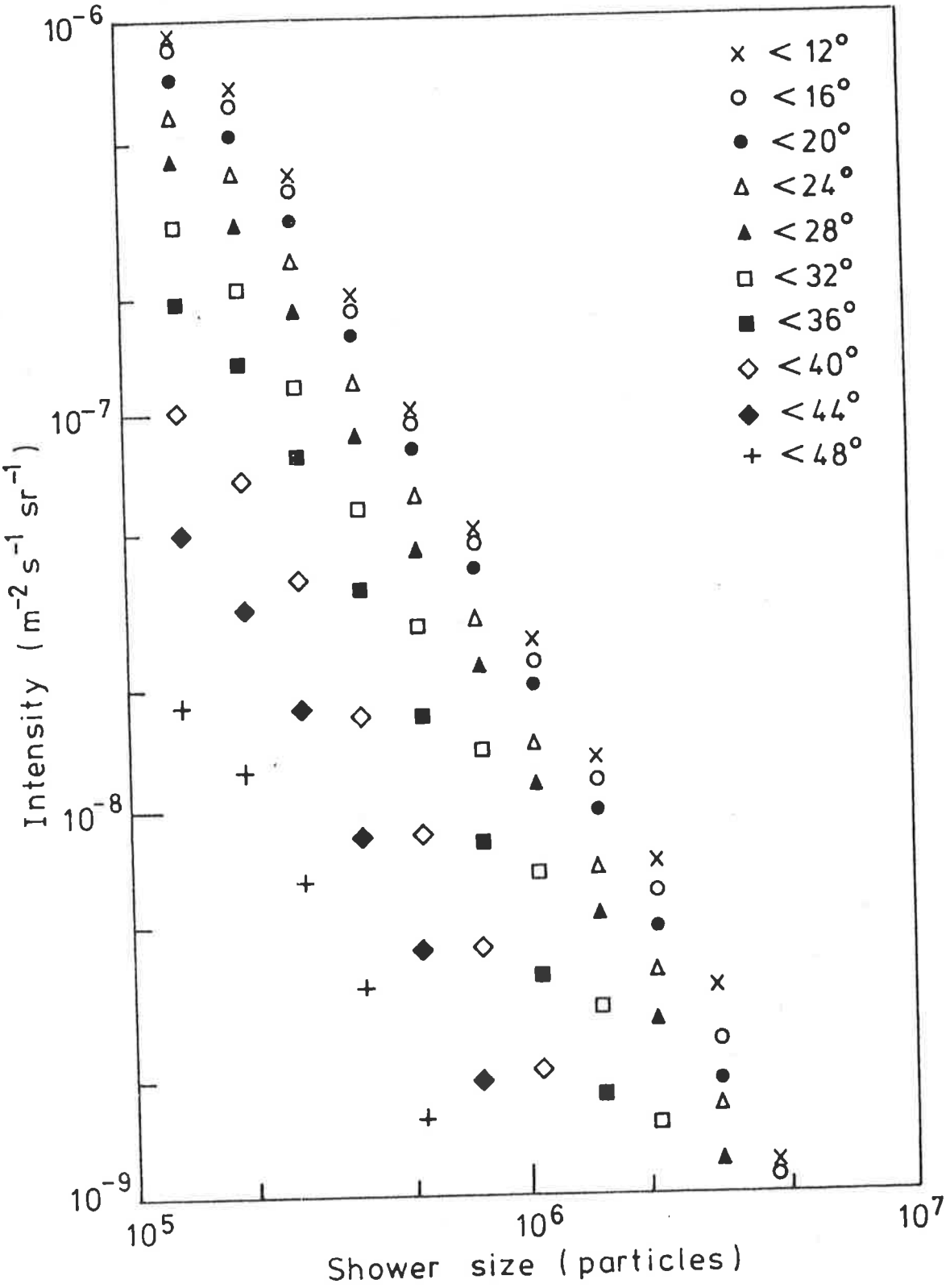

Figure 4.1 Buckland Park size spectra as a function of zenith angle.

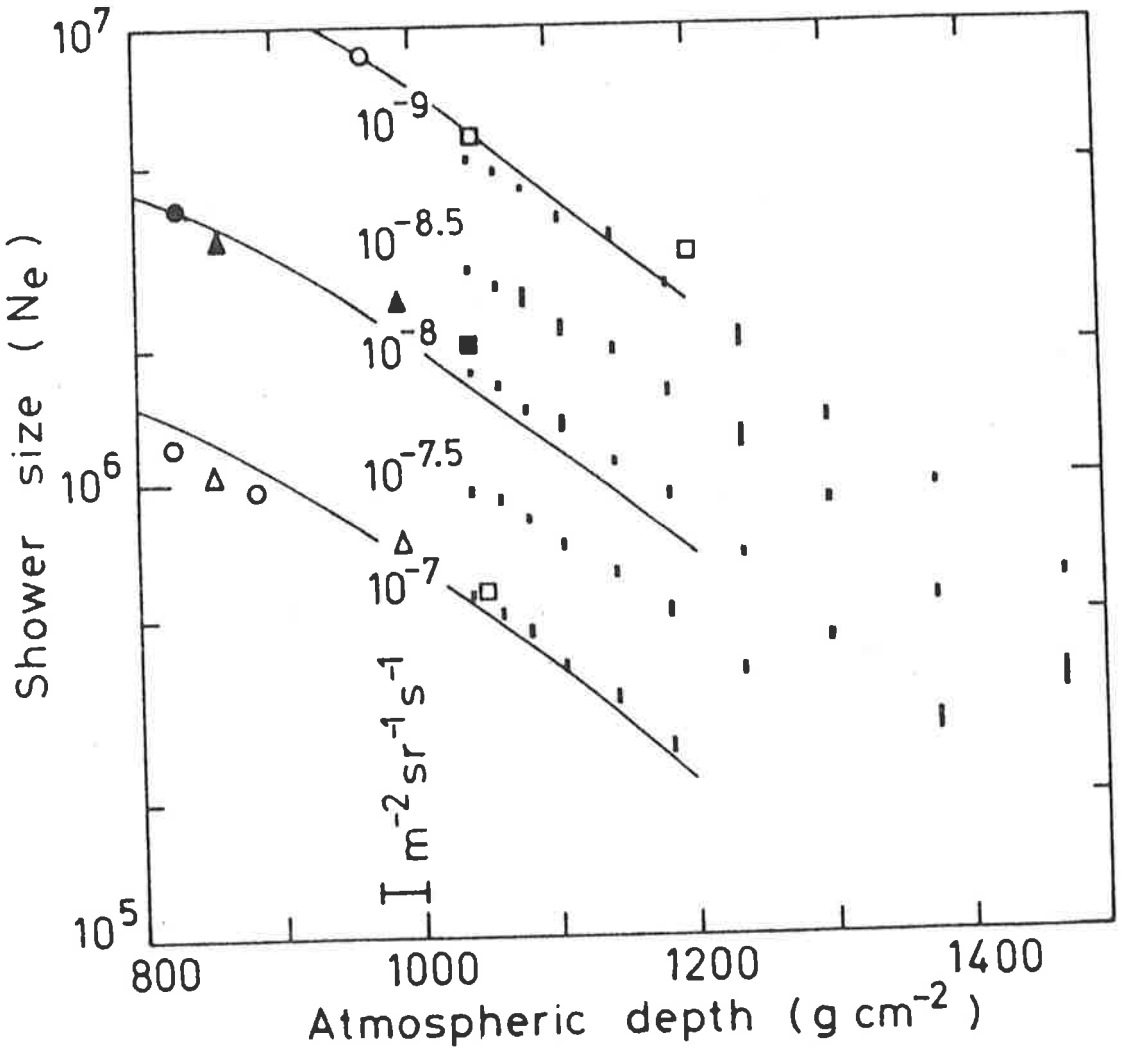

Figure 4.2 Longitudinal shower development data: the bars indicate the Buckland Park data derived from the size spectra in figure 4.1,the circles are the modified Mt Chacaltaya data (see text), the triangles are results from Tien Shan, squares are sea level data combined by Hillas (1979), lines are theoretical curves using scaling with rising cross sections.

lines in this diagram are the shower longitudinal development profiles derived by Hillas (1979) for a particular model of nuclear interactions - Feynman scaling with rising proton-proton cross sections. It is clear that these provide reasonable fits to the Mt Chacaltaya data up to depths of at least 600 g cm^{-2} and that extensions of these curves would also agree with the Buckland Park results.

Results from the high altitude array at Tien Shan (Danilova et al 1977, atmospheric depth of about 700 g cm^{-2}) also show good agreement with the modified Mt Chacaltaya data at common atmospheric depths. Boehm and Steinmann (1979) have presented data from the Pic du Midi array (730 g cm^{-2}) in which they noted a systemic deviation from the Mt Chacaltaya data and then modified the Pic du Midi shower sizes to fit the Mt Chacaltaya results. After this change, these sets of data gave smooth shower development curves. It was noted however, that there was no conflict between the unmodified Pic du Midi data and the sea level data from Kiel (Boehm 1977). Both these experiments used the same analysis programs. Agreement between the sea level size spectra from Kiel, Buckland Park, and others (see Catz et al 1975) imply that the renormalization factor suggested for the Mt Chacaltaya data is required. This brings shower profile data measured at various atmospheric depths into concord.

When combined with the Buckland Park data, the average shower longitudinal development from primary particles with energies near 10^{15} eV is well defined for atmospheric depths

between 600 g cm^{-2} and 1400 g cm^{-2}.

4.2 Shower Development Parameters (Past Maximum)

4.2.1 The Shower Size Attenuation Length

In early theories, the cosmic ray primaries were often considered to consist of either high energy electrons or photons, and thus the cascades produced by them (EAS) were thought to be pure electromagnetic cascades. Tests of these theories were provided by measurements of the way in which the showers varied in size as a function of the amount of atmospheric absorber through which they passed. These results could then be compared with the calculations on electromagnetic cascades which were available. It was largely on the basis of these measurements that the nuclear component of EAS was postulated to explain the slow shower size attenuation observed compared with the much more rapid attenuation expected from electromagnetic cascade theory (although other arguments such as the existence of penetrating particles and the form of the EAS lateral distribution were also available (see Dobrotin et al 1956)).

The shower size attenuation length parameter, λ, is derived from the assumption that, past shower maximum, the shower decay follows an exponential curve. Therefore it is defined by:

$$1/\lambda = -d(\ln N)/dt \qquad (4.1)$$

where N is the shower size as a function of atmospheric depth, t. Three obvious ways present themselves for the measurement of this parameter, each involving observations of the mean shower size at constant shower intensity with varying amounts of atmospheric absorber - altitude variations, ground level barometric pressure variations or zenith angle variations.

The last method was used with the Buckland Park data to derive the shower size attenuation length from the shower development profiles given in figure 4.2. For clarity, one of these (at integral intensity 10^{-8} $m^{-2}s^{-1}sr^{-1}$) is shown in figure 4.3. It was found from exponential best fits to these data that the attenuation length in the size range detected is nearly constant at 185+-5 g cm^{-2}. This agrees well with previous results utilizing the other techniques. For example, Krasilnikov et al (1962) find a value of 180 g cm^{-2} at shower size about 10^5 particles and the compilation of Cranshaw et al (1958) measure the value at 190 g cm^{-2} between shower sizes of 10^3 particles and 10^7 particles. More recently, Ashton et al (1975), using both zenith angle and barometric methods found the attenuation length to be 171 g cm^{-2}, however the errors on their individual measurements for the zenith angle technique are between 10% and 20%. With this parameter accurately known, it is possible to correct the shower sizes for EAS from all

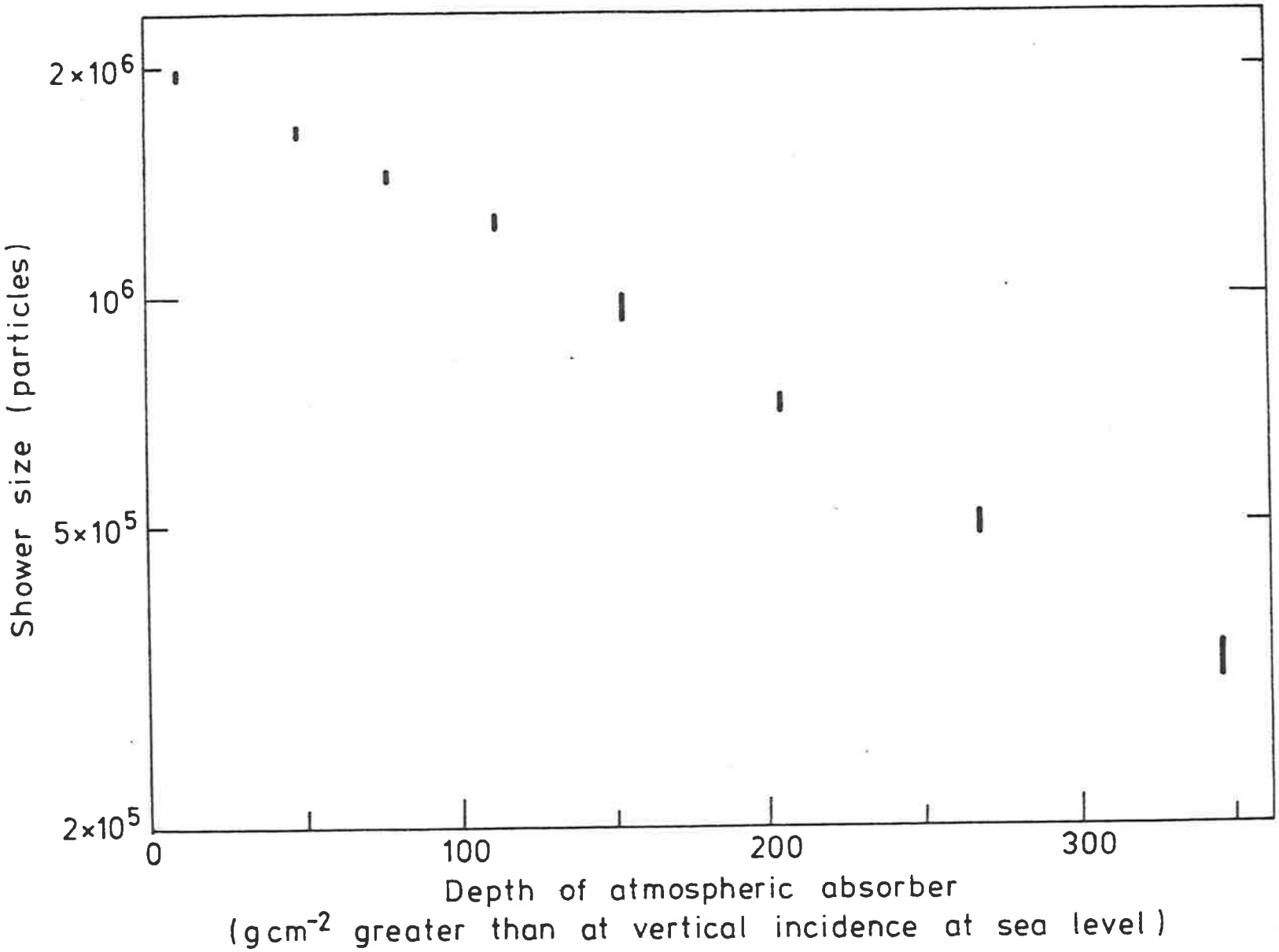

Figure 4.3 Longitudinal development data for integral intensity 10^{-8} m^{-2} s^{-1} sr^{-1}.

zenith angles to produce an accurate shower size for an isotropic (vertical) flux.

4.2.2 The Shower Frequency Absorption Length

In a similar way to the shower size attenuation length, a characteristic length - the shower frequency absorption length, can be introduced to describe the rate of change of the integral shower intensity with atmospheric absorber thickness. It is generally assumed, at least over small energy ranges, that the integral primary cosmic ray energy spectrum can be described by a power law, viz:

$$I(>E)=CE^{-\gamma'} \qquad (4.2)$$

Following the results of the previous section, the shower size produced by a primary particle of energy E, at atmospheric depth t, can be described by:

$$N(E,t)=K.E^{-\alpha}.\exp(-t/\lambda) \qquad (4.3)$$

It is generally assumed that α has a value near 1. The integral shower flux is then:

$$I(>N,t)=C.K^{\gamma}.N^{-\gamma}.\exp(-t/\Lambda) \qquad (4.4)$$

$$\text{where } \gamma = \gamma'/\alpha \text{ and } \Lambda = \lambda/\gamma \qquad (4.5)$$

Equation 4.4 then defines the shower frequency absorption

length, Λ, by:

$$1/\Lambda = -d(\ln I)/dt \qquad (4.6)$$

In this derivation of the absorption length definition, the assumptions of the power law shape of the energy spectrum and the simple relationship between shower size and primary energy (equation 4.3) are most important. As a result, variations from the simple relation between the attenuation and absorption lengths (equation 4.5) in detail can be used to probe the size spectrum. It has been shown (Bourdeau et al 1979, 1980) that accurate experimental determinations of the frequency absorption length can place strong constraints on the high energy interaction models used in shower development calculations. This is of particular interest in the region of the size spectrum knee.

Determinations of the absorption length can be made using the same three variable absorber techniques described in the previous section, the only difference being that, for absorption length measurements, the intensity is measured at constant shower size as a function of absorber thickness instead of vice versa.

Buckland Park data were used to derive values of the absorption length by employing again the variable zenith angle technique (Clay and Gerhardy 1981b). From the normalized integral shower size spectra at different zenith angles (atmospheric depth) shown in figure 4.1, cuts made at constant

shower size defined absorption curves. Examples of these data for three shower sizes ($3*10^5$, 10^6, and $3*10^6$ particles) are shown in figure 4.4. Absorption lengths for various shower sizes were then determined by fitting exponentials to these data. The results of these fits are shown in table 4.1 below:

Table 4.1: Frequency attenuation lengths at various shower sizes.

Shower Size (particles)	Absorption Length (g cm^{-2})
$2.3*10^5$	104+-2
$3.0*10^5$	102+-3
$4.0*10^5$	100+-6
$1.0*10^6$	99+-3
$2.5*10^6$	98+-3
$3.0*10^6$	95+-4

These results fill in the gap in measurements near shower size of 10^6 particles in the compilation by Bourdeau et al (1980). They are quite compatible with the other data although the Buckland Park data have much smaller error limits.

Assuming a power law primary energy spectrum with a 'knee' at $2.5*10^{15}$ eV, Bourdeau et al (1980) calculated the absorption length resulting from various shower development models and primary compositions. Their calculations clearly

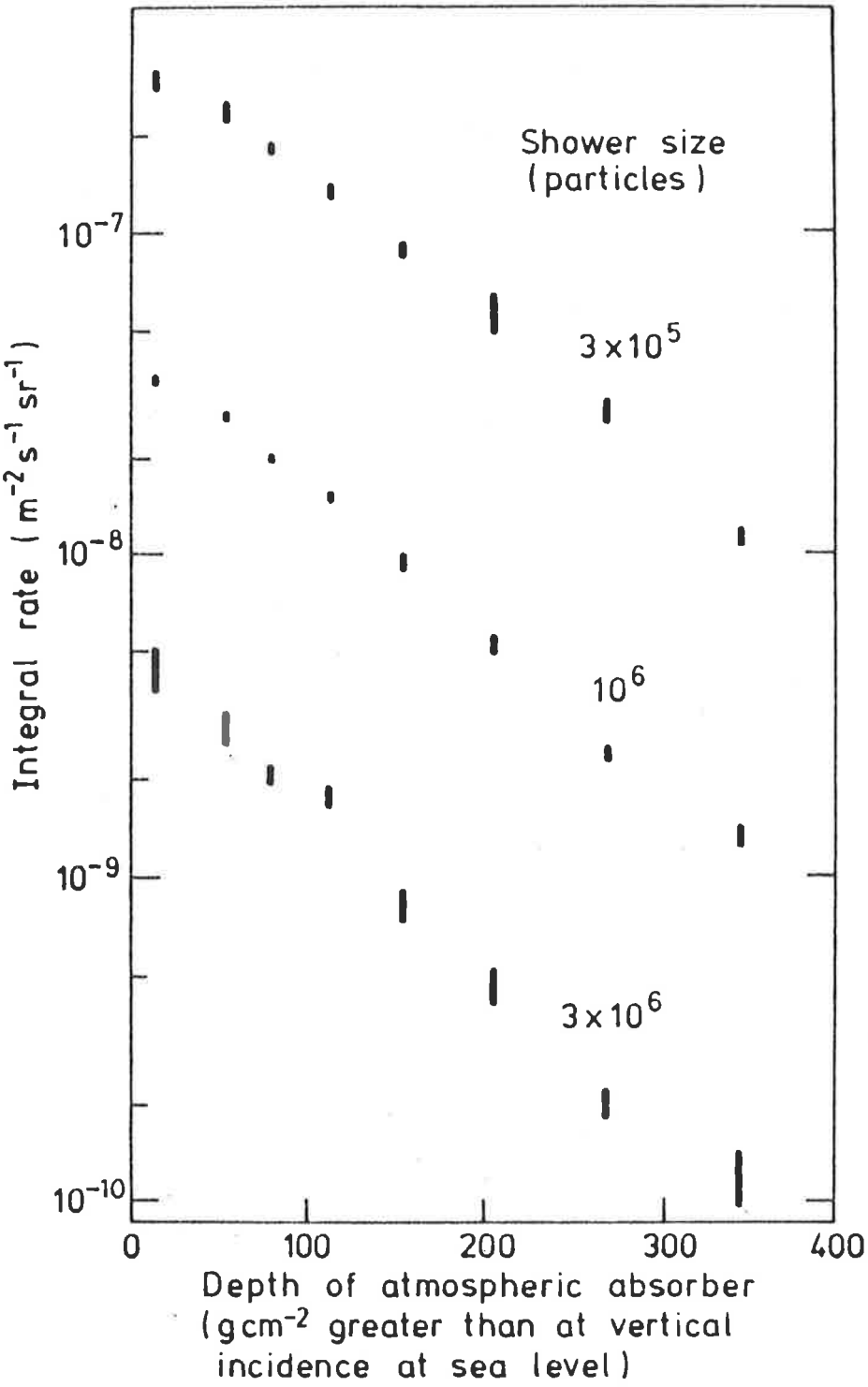

Figure 4.4 Shower frequency absorption curves from the data in figure 4.1.

show that a spectral knee is required to fit the observational data and although none of the models used are completely in agreement, some limits are placed on interaction models and composition. These will be discussed later in relation to the other observational data.

4.2.3 The Shower Lateral Age Parameter

For EAS analysed using the NKG function (equation 1.5) as an approximation to the real shower lateral distribution, a shower age parameter (s) can be defined. The NKG function was originally developed (Nishimura and Kamata 1950, 1951a,b) as an analytic description of the lateral distribution of particles in a pure electromagnetic cascade initiated by a single high energy photon. It is clear that the actual shape of this function must depend on the stage of development (age) of the cascade (see figure 3.2) and this shape change is described by the age parameter which increases monotonically between 0 and 2 as the cascade develops. The variation in the age parameter as a function of absorber depth (in this case atmosphere) and cascade size for various energies of the initiating photon is shown in figure 4.5 (taken from Cocconi 1961). Although the NKG function was developed for electromagnetic cascades, it has been found to be a useful approximation to EAS and is used (sometimes with slight variations) by a number of observatories in the analysis of their raw air shower data (e.g. Danilova et al 1977 - Tien Shan, Miyake et al 1979 - Mt Norikura, Hara et al 1979a -

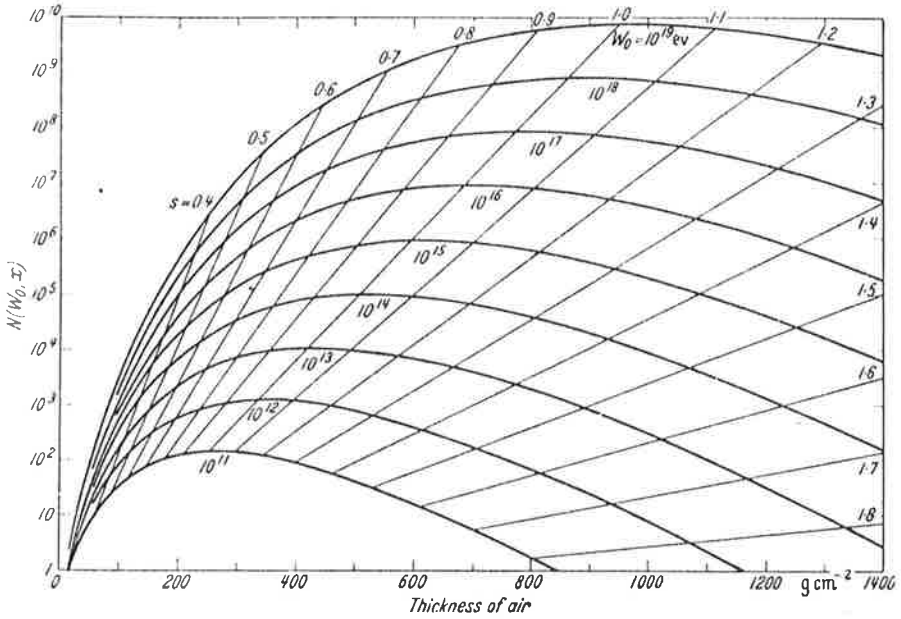

Figure 4.5 Electromagnetic cascade development curves showing the variation of the age parameter. (from Cocconi 1961)

Akeno).

Since EAS in reality consist of large numbers of superimposed electromagnetic cascades generated by a nuclear-active core, the age parameter defining the longitudinal development of the shower (s_{long}) is not equal to the age parameter determined from the shower lateral distribution (s_{lat}). It has been shown however (Dedenko et al 1979), that these age parameters for EAS at atmospheric depths greater than 200 g cm^{-2} may be related by:

$$s_{long}=s_{lat}+\Delta s \qquad (4.7)$$

where Δs is greater than about 0.15 (instead of $\Delta s=0$ which is the case for pure electromagnetic cascades). This relationship indicates that although the age parameters differ, their rate of change with atmospheric depth should be similar. Future references in this section to the age parameter imply only the lateral age parameter. For electromagnetic cascades, generated by cosmic ray photons in the atmosphere, the rate of change of the value of the age parameter is found to be about 0.06 per 100 g cm^{-2} of atmospheric absorber for shower sizes near 10^6 at sea level (Clay et al 1981b).

To investigate variations in the fitted lateral age parameter, data from the Buckland Park array (analysed with the NKG function) have been scrutinized. As usual, only well analysed showers (with reduced chi-squared less than 5) which

were detected with core locations and shower sizes in regions with near 100% triggering probability were used. The total number of showers accepted was about $3.3*10^4$. In order to see the variations as a function of atmospheric depth as well as size, the showers were sorted into three zenith angle ranges (0^o - 20^o, 20^o - 30^o, 30^o - 45^o) and shower size ranges a factor of $\sqrt{2}$ wide above the threshold of $2.3*10^5$ particles. The mean values of the age parameter in the size and angle bands are plotted in figure 4.6. To enable a clear comparison, the shower sizes have been normalized to equivalent vertical showers at an atmospheric depth of 1060 g cm^{-2} using the measured attenuation length of 185 g cm^{-2}. The data from each zenith angle range are displaced with respect to each other because of their different mean zenith angles.

At shower sizes below about $5*10^5$ particles, anomalous increases in age with size (and presumably primary energy) can be seen in each of the zenith angle ranges. That these increases are artifacts of the triggering requirements used to detect EAS by the Buckland Park array can be demonstrated by Monte Carlo simulations on the array. These were carried out for a number of fixed shower sizes with variable ages to determine the triggering probability as a function of shower age. The results of these simulations are shown in figure 4.7. It can be seen that above shower size of about $5*10^5$ particles, the shapes of the curves show little variation, indicating that the showers detected come from the same subset of the shower spectrum. Below this size however,

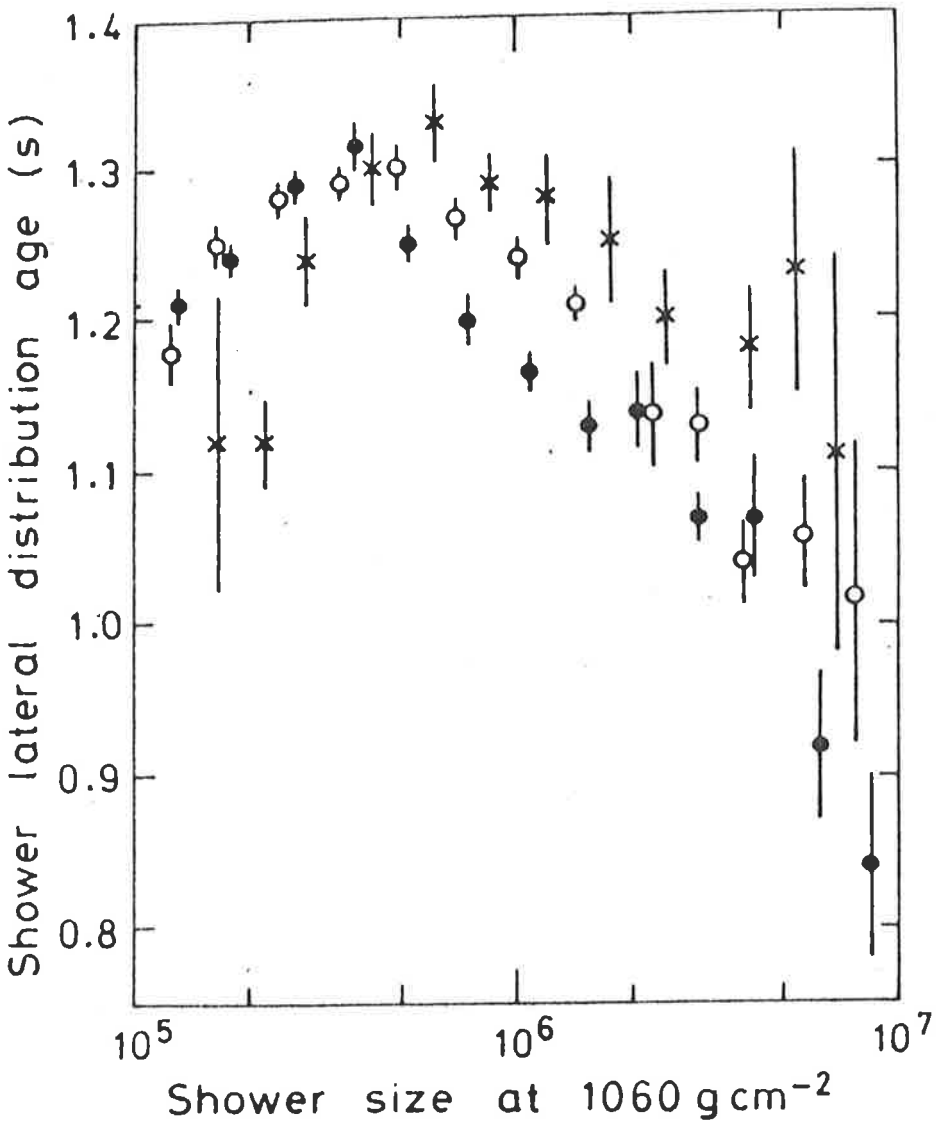

Figure 4.6 The shower lateral age parameter from Buckland Park data as a function of shower size and zenith angle (filled circles - less than 20°, open circles - 20° to 30°, crosses - 30° to 45°)

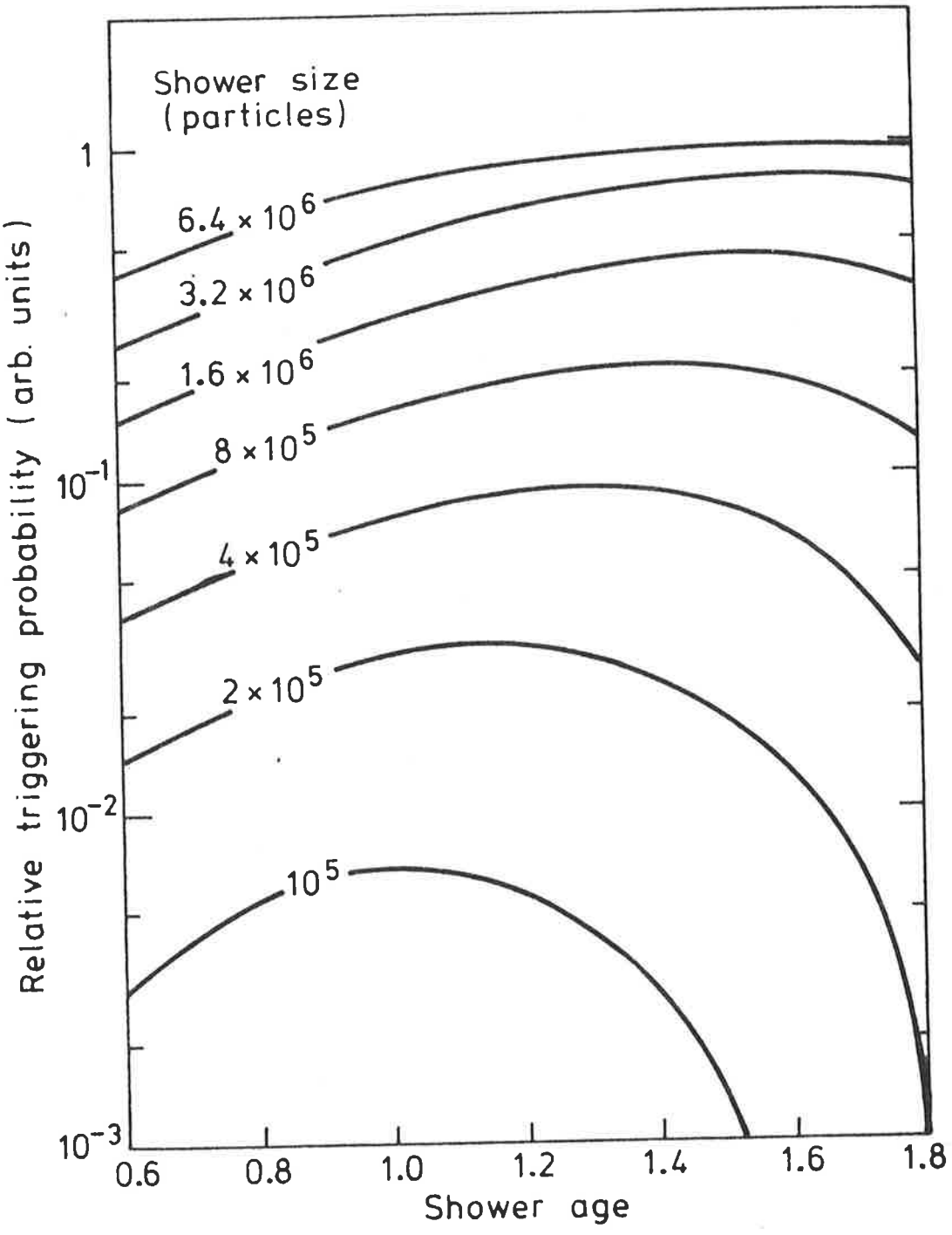

Figure 4.7 Triggering probability as a function of shower age and size.

an increasing bias toward the selection of showers with a lower age value is clear. These results are reflected in the actual measurements in figure 4.6. A similar effect has been noted in the results of Asakimori et al (1979) due to decreasing detection efficiency with reducing shower size.

Above shower size of $5*10^5$ particles, the data show a rapid decrease in the shower age in each of the zenith angle ranges. As expected, the rate of change for each of the zenith angle ranges is approximately the same. The rate of change is about 0.22 per decade of shower size. The change in mean zenith angle in each range corresponds to a change in mean atmospheric depth from about 1060 g cm^{-2} (zenith angles less than 20^o) to 1240 g cm^{-2} (zenith angles between 30^o and 45^o). From figure 4.6 this corresponds to a change in mean shower age of about 0.13. These data may be used to calculate an equivalent change in the depth of atmospheric absorber with changing shower size. If the change in depth of 180 g cm^{-2} corresponds to a change in the mean age of 0.13, then the change of 0.22 in shower age per decade of shower size corresponds to a change in the thickness of the atmosphere of about 300 g cm^{-2} per decade of shower size in the size range indicated ($6*10^5$ particles to $6*10^6$ particles). This means that the showers appear to be developing lower in the atmosphere very rapidly as the size increases. Although models of nuclear interactions with conventional primary compositions fail to predict this very rapid change, similar results, although with slightly smaller changes per decade have been observed by Thornton and Clay

(1979) and Andam et al (1982) who measured the change in depth of shower size maximum using Cerenkov techniques.

Rapid changes in the shower age parameter have also been reported by Hara et al (1979a) at the Akeno observatory (at atmospheric depth of 920 g cm^{-2}). They measure a change of over 0.32 between shower sizes 10^5 and 10^7 particles. At mountain altitudes Miyake et al (1979) at Mt Norikura (735 g cm^{-2}) find a decrease in the age parameter af nearly 0.2 for shower sizes increasing from 10^6 particles to 10^7 particles.

On the other hand, there is a good deal of disagreement between these results and other measurements. Khristiansen et al (1981) find that the variation in the age parameter is less than 0.05 between sizes $5*10^4$ particles and $2*10^6$ particles. In even worse agreement are the results of Abdullah et al (1981) who find an increase in the shower age between 10^6 particles and 10^7 particles. Both these results are from arrays located close to sea level.

Some explanations for the disagreements between all these results may be made from the calculations of Capdevielle and Gawin (1982). They show that, for EAS, a unique age parameter cannot be derived from the NKG function to give a good fit at all radial distances from the shower core. They have also derived a relationship between the theoretical or longitudinal age parameter, s_{long}, and the lateral age parameter, s_{lat} at shower core distance, r, of the form:

$$s_{lat}(r)=A.\log(r/r_0)+s_{long} \qquad (4.8)$$

for r between 15 metres and 150 metres and shower size between 10^5 particles and $4.5*10^6$ particles where r_0 is the Moliere radius. It can be seen from this that the values of the age parameter determined by any EAS array will depend on the distribution of detectors sampling the showers. To compare the actual results from different arrays, extensive Monte Carlo simulations are required, taking into account the array responses and triggering conditions.

In view of these data, the Buckland Park results must be carefully reinterpreted. The results of Capdevielle and Gawin (1982) indicate that at shower core distances between about 20 metres and 100 metres the change in age parameter as a function of core distance is not large since in this region the dependance goes through a minimum. This is just the distance at which most showers are sampled by the Buckland Park array as can be seen from the detector arrangement (figure 2.1). Therefore for the relatively unbiassed subset of showers detected with sizes above $5*10^5$ particles, the interpretation of a rapid change in the shower development at these shower sizes should still be at least qualitatively correct.

4.3 Atmospheric Rate Coefficients

Conditions in the atmosphere and especially the upper atmosphere can change the subset of primary energies investigated by varying the way that showers develop in the atmosphere. This occurs because, although it is obvious that the primary spectrum itself is not affected, the probability of detection of the resulting EAS produced by the primary particles is affected by atmospheric variations. The result of these variations is a modulation of the detection rate, since the shower size spectrum (and presumably the primary energy spectrum) is (at least roughly) a steep power law.

Variations in the barometric pressure imply variations in the mass of atmosphere vertically above the detector. The main effect of atmospheric pressure changes is to change the amount of atmospheric absorber above the detectors. For observatories where EAS are detected from a range of zenith angles, the simple absorption for vertical EAS is somewhat complicated by the factor of sec(θ) increase in the mass of absorber (where θ is the zenith angle) for inclined showers. This absorption effect means that shower sizes at sea level and hence the EAS detection probabilities are reduced when the barometric pressure increases. Another slightly less important although significant effect of barometric pressure variations is to change the atmospheric density which in turn changes the lateral spread of the showers due to scattering. The barometric coefficient of the shower rate is defined by:

$$dR/R = b.dp \qquad (4.9)$$

where R is the rate of shower detection and p is the barometric pressure.

Temperature variations in the lower atmosphere also change the air density and this effect is generally assumed (e.g. Bennett et al 1962) to be the cause of the temperature coefficient, a, of the air shower rate, defined by:

$$dR/R=a.dT \qquad (4.10)$$

where T is the atmospheric temperature. In a uniform atmosphere, the unit of lateral displacement of particles in electromagnetic cascades (the Moliere unit) is proportional to the radiation length (Cocconi 1961) which is inversely proportional (in metres) to the atmospheric density. Since it is the atmosphere above the detectors which determines the observed shower structure, it is expected that the temperature which is important is that some distance above the detectors. This distance has been shown to be one or two radiation lengths (Janossy 1948, Greisen 1956). Hodson (1951) found a correlation between the shower rate measured using a counter array and the atmospheric temperature about one radiation length above his apparatus. However, he also found that this correlation was relatively insensitive to the atmospheric thickness used and varied by less than 10% up to the 500 mbar level.

The atmospheric conditions at the top of the atmosphere are significant to shower development lower down

since this is the region where the primary cosmic ray particle undergoes its first few interactions. This is particularly important to the production of the muon component and measurements of the pressure and temperature effects have been conducted for many years (e.g. Duperier 1949, 1951, Trefall 1953, 1955a,b,c, Dutt and Thambyapillai 1965, Lyons 1981). These effects will not be discussed due to the lack of a complete set of upper atmosphere data for the Buckland Park array.

Since both the barometric pressure and lower atmospheric temperature have similar effects on the detected shower rate it is appropriate to use a multiple linear regression technique combining equations 4.9 and 4.10 to evaluate the respective coefficients, viz:

$$dR/R=c+b.dp+a.dT \qquad (4.11)$$

Barometric pressures and ground level atmospheric temperatures are recorded at Buckland Park along with the raw particle data at the time of each event. Mean coefficients have been calculated from these data using equation 4.11 and are:

$$b=-0.72\pm0.08\ \%\ mbar^{-1}\quad (-9.7\pm1\ \%\ cmHg^{-1})$$

$$a=0.12\pm0.08\ \%\ {}^{o}C^{-1}$$

Monthly values of the temperature coefficient indicate that it is consistent with zero and therefore it is probably not

significant. At different zenith angles, the mean equivalent vertical shower size varies due to the sec(θ) variation of the thickness of the atmospheric absorber. Unfortunately, measurements of the variation of barometric coefficient with size using data from different zenith angles are hampered by the relatively sharp zenith angle distribution of detected showers and also complicated by the competing effects of atmospheric attenuation of shower size, reduced detection efficiency at large zenith angles, and solid angle exposed. Measurement statistics were not sufficiently good to conclusively determine variations in the barometric coefficient with shower size.

The Buckland Park meteorological coefficients are in excellent agreement with those measured by other arrays (e.g. see the compilation of Cranshaw et al 1958).

Bennett et al (1962) have shown that the barometric and temperature coefficients are related to the shower frequency absorption length by:

$$1/\Lambda = -(b + a.T/p)/\langle \sec(\theta) \rangle \qquad (4.12)$$

where T is the absolute temperature and p is the pressure in appropriate units. In this case, the coefficients are those given by the simple linear regression equations, 4.9 and 4.10 (since the absorption length is determined by the total mass absorption). If it can be assumed that the temperature coefficient is entirely due to the density effect, the density

dependence may be removed from the barometric coefficient to give a coefficient entirely due to the mass absorption of the showers. To obtain the frequency absorption length, this coefficient must be modified to allow for the range of accepted zenith angles.

Using equation 4.12 and the Buckland Park data, the value obtained for the frequency absorption length is rather high, about 160 g cm^{-2}, compared with the direct determinations using the zenith angle technique of about 100 g cm^{-2}. The discrepancy may be explained by noting that the rate coefficients were obtained using the detected shower rate, taking no account of the variation in collection efficiency of the array over the area where showers are detected. Approximately 75% of detected EAS are collected in regions where the detection efficiency is less than 100%. This effect will tend to decrease the degree of modulation of the rate with pressure changes and hence reduce the barometric coefficient. The qualitative agreement between the results may then be considered to be satisfactory.

CHAPTER FIVE

THE COSMIC RAY ISOTROPY

5.1 Introduction

Attempts to measure preferred arrival directions of the primary cosmic ray flux have been made since the late 1940's with the aim of gathering information about the particle sources. Disentangling the real results from the spurious results produced by solar and atmospheric effects has proved difficult, however a pattern is beginning to emerge (Watson 1981) indicating that the flux is isotropic to within about 1% from the lowest energies (about 10^{12} eV) where solar modulation ceases to be important up to primary particle energies of about 10^{16} eV. At higher energies, the anisotropy appears to increase and for the highest energy cosmic rays above 10^{19} eV, although statistics are poor, very large deviations from isotropy (>10%) in the cosmic ray flux are indicated.

The high degree of isotropy observed in the lower energy range is the result of the propagation of particles through the magnetic fields which permeate the Galaxy, and probably extend large distances outside the Galaxy forming a halo. These fields may also possibly extend throughout the

local supercluster of galaxies. Measurements of the strength and direction of these fields using optical polarization of starlight (e.g. Mathewson 1968), Faraday rotation of radio waves from local pulsars and extragalactic sources (e.g. Morris and Berge 1964), Zeeman splitting of the 21cm hydrogen line (e.g. Davies 1964) and other techniques are difficult to interpret since they often involve only specific components of the Galaxy, for example, dust clouds or neutral hydrogen clouds. Despite these difficulties, it is generally accepted that the magnetic field in the Galaxy has a large scale (at least the order of 1 kpc) regular component along the spiral arms with a strength of a few microGauss, together with a disordered component (with a scale of about 100 pc) with comparable strength as well as perhaps smaller scale irregularities (Manchester 1974). The rather irregular structure of the field is probably the consequence of the motion of clouds of charged material carrying with them the frozen-in magnetic field. This occurs because the energy density of the magnetic field, at least in the large scale, is not great enough to affect these motions. Outside the galactic disc, data is more difficult to obtain. However, radio synchrotron measurements (e.g. Phillipps et al 1981) indicate a field in the halo (out to at least 10 kpc) not much weaker than that inside the disc, once reduced electron fluxes are allowed for (Hillas 1982). Although these fields are very weak (compared to say, the field near a pulsar), they extend over at least galactic distances and result in the deflection of the charged cosmic rays away from the original direction of their motion. The radius of gyration of the charged particles

may be roughly estimated by:

$$r=E/(Z.B) \qquad (5.1)$$

where r is measured in parsecs, E in units of 10^{15} eV, B in microGauss, and Z is the charge. This is illustrated in figure 5.1 where radii of gyration for protons and iron nuclei are plotted as a function of energy for a 3 μG magnetic field. It is clear that, only for protons of the highest energies (above about 10^{18} eV where the gyroradius becomes comparable with galactic dimensions) can the arrival directions measured at Earth be at all directly related to the direction of their source. Arrival directions will however, be related to the structure of the local magnetic environment, particularly for energies below 10^{15} eV. A useful summary of recent interstellar magnetic field measurements has been given by Heiles (1976).

For all but the highest energies then, the cosmic ray arrival directions are determined by the local magnetic field as well as the distribution and properties of the sources. On the other hand, since most models of cosmic ray sources and propagation may be used to predict anisotropies in the flux, the study of the way the flux anisotropy changes with energy may lead to important information about the sources.

Davis (1954) proposed one of the first detailed models of cosmic ray propagation which included the configuration of the galactic magnetic field. On the basis of a field similar

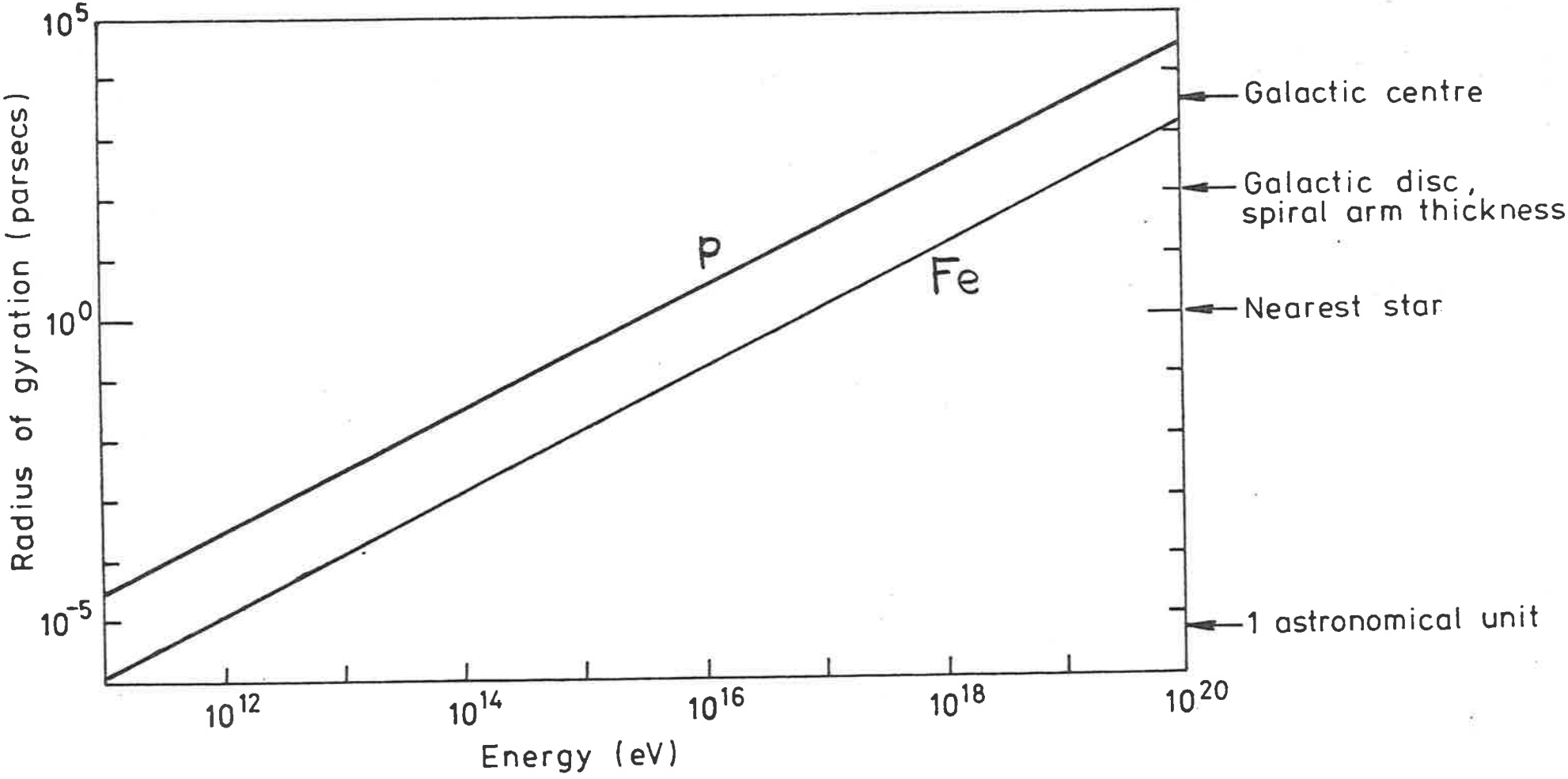

Figure 5.1 Radii of gyration of protons and iron nuclei in a 3μG magnetic field.

in structure but rather stronger than that presently postulated, he found tentative agreement with some early anisotropy measurements. By assuming a source spectrum, Hillas and Ouldridge (1975a,b) (and using a 'leaky box' model of confinement) were able to produce a model which matched the variation of anisotropy with energy. It had several problems however, not the least of which was the assumption of a source with a single power law production spectrum from 10^{11} eV to 10^{19} eV. The more elaborate model of Bell et al (1974) of galactic diffusion governed by magnetized gas clouds and the large scale magnetic field was useful although somewhat specific assumptions about the configuration of the scattering fields were required. Lloyd-Evans et al (1979) have considered a number of models of origin and propagation for particles of energy above 10^{15} eV. They find that all the models disagree with observations in some part of the energy spectrum although not all the models make use of the local interstellar magnetic field. An interesting point noted by Lloyd-Evans et al (1979) however, is that the two most obvious features of the energy (size) spectrum, the 'knee' near 10^{15} eV and the 'ankle' near 10^{19} eV appear to be associated with changes in the anisotropy. At 10^{15} eV, there seems to be a more rapid increase in the amplitude of the anisotropy than at lower energies. The onset of very large anisotropies occurs at 10^{19} eV where the spectrum flattens.

Of particular interest is the question of galactic or extragalactic origin of the cosmic rays. Although both points of view have strong proponents (e.g. Ginzburg and Syrovatskii

1964, Syrovatskii 1971, Burbidge and Brecher 1971, Brecher and Burbidge 1972), components of the spectrum from both sources seems a likely solution (Strong et al 1974a,b). Unless the cosmic rays of the highest energies are heavy nuclei, which seems unlikely (Coy et al 1981a) they cannot be trapped by the galactic magnetic field, and their arrival directions measured at Earth suggest an extragalactic origin (Wdowczyk and Wolfendale 1979) with its implications about the sources and mechanisms required for acceleration (Hillas 1982). Conversely, at lower energies the particles may be trapped and would then be expected to diffuse along the field lines (Karakula et al 1971). Anisotropies measured in the flux would then be the result of a cosmic ray gradient produced by the source direction and the field. The size and type of the anisotropy leads to source information although the interpretation of these data may not be simple (Hillas 1982).

5.2 Anisotropy Measurements

Measurements of anisotropies in the cosmic ray flux between energies of 10^{11} eV and 10^{20} eV have been summarized by Kiraly et al (1979), Linsley (1980) and Watson (1981) and the results are shown in figure 5.2 (after Linsley 1980 and references therein). The experiments producing these results will be examined in more detail below. However, it is appropriate to first discuss some of the mechanisms which may produce spurious measured anisotropies.

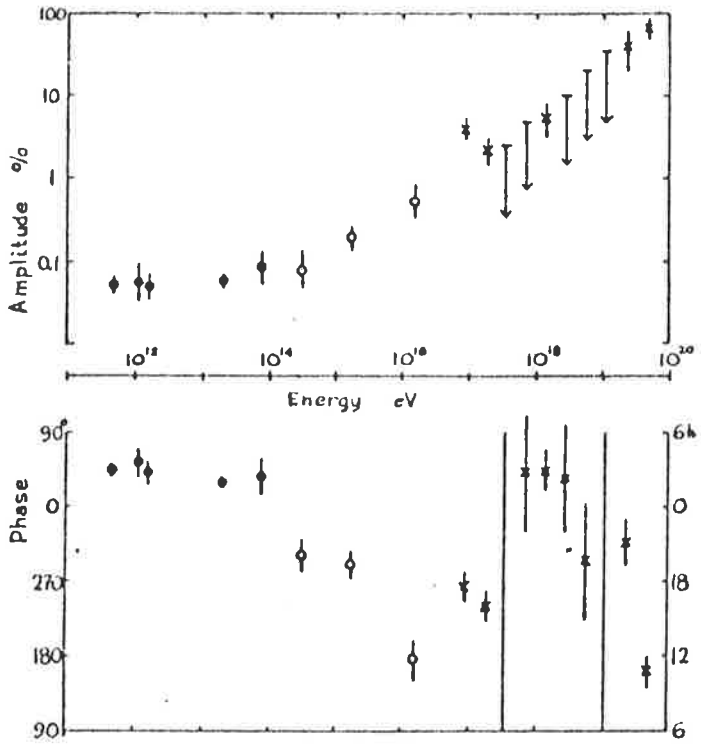

Figure 5.2 The dependence of the sidereal first harmonic anisotropy on energy (the compilation of Linsley 1980)

5.2.1 Spurious Effects

There are known to be a number of effects which change the measured anisotropy from its galactic value or produce spurious effects which add to the genuine anisotropy and distort the observations. These effects are especially important at low energies where the real flux anisotropy is expected to be small. The effects may be divided into two areas: those produced outside the terrestrial atmosphere, and those produced inside the atmosphere. In general, the spurious sidereal anisotropies arise from the modulation of regular variations occurring in solar time which produces apparent variations in sidereal time. This problem will be further discussed later.

At energies below about 10^{12} eV, the interplanetary magnetic field has a significant effect on the cosmic ray flux because of the small radius of gyration of the particles in the field. This effectively distorts the 'optics' for resolving genuine galactic anisotropies and attempts to correct for this effect require detailed knowledge of the configuration of the field (Marsden et al 1976, Davies et al 1979a) even though above 10^{11} eV, the motion of the particles is governed by only the large scale properties of the field. On the other hand, a knowledge of the field may make it possible to deduce the otherwise unobservable anisotropies from the polar directions (Davies et al 1979). The solar wind is also important because of the electric

potential produced by it which causes energy changes and resultant intensity changes in the flux (Kota 1976a,b).

Outside the atmosphere, two effects give rise to regular variations of the particle flux in solar time. Both are produced by the Compton-Getting effect (Compton and Getting 1935) where the motion of an observer through the cosmic ray gas (considered to be in equilibrium) produces a maximum in intensity in the direction of motion. The amplitude of this effect is clearly dependent on the velocity, v, of the observer and may be calculated from (Thambyapillai 1974):

$$\delta = (2+\gamma).v/c \qquad (5.2)$$

where $$\delta = (I_{max}-I_{min})/(I_{max}+I_{min})$$

and γ is the exponent of the differential rigidity spectrum, I is the cosmic ray intensity.

The first of these effects, the corotation anisotropy, is due to the motion of the solar magnetic field with respect to the Earth. If the cosmic ray gas is in equilibrium within the solar system, at low enough rigidities, (less than 100 GV (Thambyapillai 1974)), the gas may be considered to be frozen to the solar magnetic field as it sweeps past the Earth overtaking its orbital motion. This is obviously a rigidity dependent effect and should not be significant at the energies discussed in this thesis. The second effect is produced by the Earth's orbital motion about the sun. As opposed to the

corotation anisotropy, this effect should be energy independent with an amplitude of about 0.05% (for γ=2.6) with maximum at 06.00 hr local solar time outside the Earth's magnetosphere. A stylized illustration of these effects is shown in figure 5.3. Thambyapillai (1974) reports that there is no evidence of annual modulations of either of these effects to produce spurious sidereal anisotropies.

Another Compton-Getting effect is produced by the motion of the solar system with respect to the local interstellar medium, stationary in the frame of galactic rotation. At low energies, the amplitude of the anisotropy produced by this motion is about 0.03% in the direction of 18.6 hr sidereal time (Hillas 1982). This effect applies at all energies where the cosmic ray gas can be considered to be in equilibrium, and constitutes a genuine sidereal anisotropy.

Inside the atmosphere, periodic variations in the cosmic ray flux measured in solar time come from changes in the atmospheric conditions which change the density profile and mass absorption properties of the atmosphere (see Section 4.3). Of these the ground level temperature is the most obviously periodic in solar time but others such as the barometric pressure and the height and temperature at various pressure levels may also have significant solar diurnal components. If these components have annual amplitude modulation, spurious sidereal components will result.

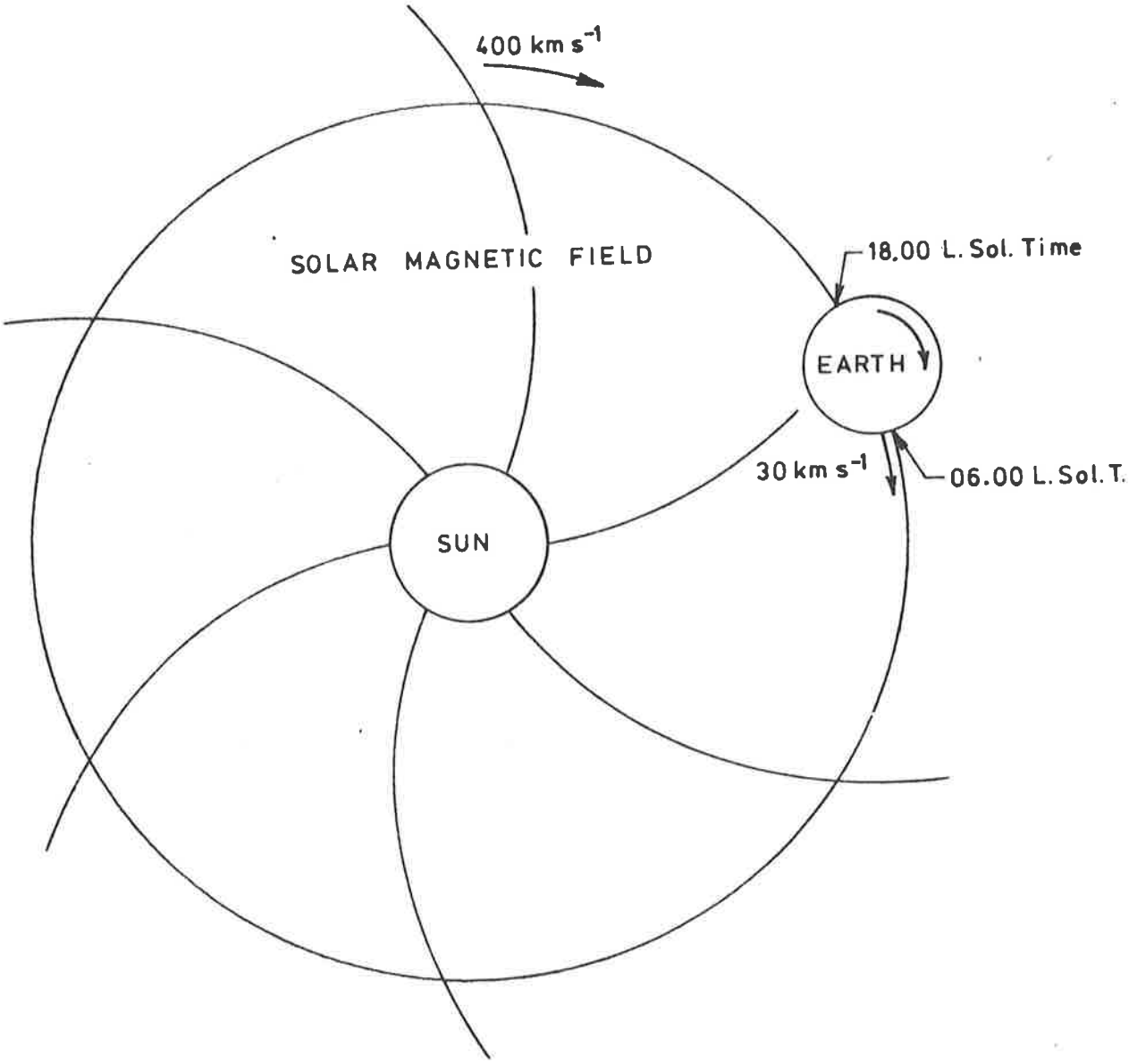

Figure 5.3 The mechanism of co-rotation and orbital anisotropy production.

As viewed from the southern hemisphere.

5.2.2 Low Energy Measurements

At primary energies below about 10^{14} eV, the cosmic ray flux may be monitored by means of the penetrating secondary muon component of air showers at sea level or in underground or shielded detectors or by the small air showers produced by these primaries at high altitudes. These monitoring experiments usually determine the flux by counting the rate of events as a function of sidereal and solar time, relying on atmospheric collimation for directional information. For an air shower experiment, the angular uncertainties produced by this technique are typically about 0.5 steradians. A useful method of eliminating atmospheric variations is achieved by the use of detectors only sensitive to events arriving from a small range of directions. If two cosmic ray telescopes are arranged pointing in different directions but similar altitudes, they are equally affected by atmospheric conditions and the flux anisotropy may be obtained from the vector difference between the results from each detector.

Below 10^{12} eV, anisotropy measurements have been made by the London (Davies et al 1979b) and Hobart (Fenton 1976, Humble and Fenton 1977) groups using underground muon telescopes. Both groups detected significant first harmonic anisotropies in sidereal time with amplitudes and phases of 0.048% at 0.27 hr and 0.031% at 05.7 hr respectively. However, both observatories noted large variations in the

measured anisotropies which were correlated with changes in the interplanetary magnetic field. This indicates the difficulty in deducing the anisotropy outside the heliosphere. In the same energy range, Sekido et al (1976) measured the anisotropy using an air Cerenkov telescope. Again a significant first harmonic in sidereal time was measured with amplitude 0.034% and phase 05.2 hr. This is in excellent agreement with the previously measured results although again solar effects were seen to be important. It should be noted that, because of the disturbing influence of the interplanetary magnetic field at these energies, the actual anisotropy outside the heliosphere may be very different to that measured (Wolfendale 1977).

It is expected that, for primary particle energies above 10^{12} eV, the effects of the interplanetary magnetic field should no longer be important for anisotropy measurements (Kota 1976a,b). Observations from the Poatina muon telescopes (Fenton and Fenton 1976, Fenton et al 1977) have however given some indication that solar effects may still be operating at the median energy of $1.5*10^{12}$ eV. Although a significant sidereal first harmonic was observed (0.046%, 02.3 hr) for all collected data, there appeared to be some correlation of the anisotropy with the direction of the interplanetary magnetic field in a similar way to that measured at Hobart (Humble and Fenton 1977) for primaries near 10^{11} eV. At a similar median primary energy, Bergeson et al (1979a) have reported anisotropy measurements from the Utah underground muon monitor using a discrete Fourier transform

analysis technique (Bergeson et al 1979b) rather than the usual harmonic analysis approach (see Section 5.3, Appendix 3). This technique clearly shows the sidereal variations and noise fluctuations from other sources. The measured sidereal anisotropy had an amplitude of 0.038% and phase of 01.5 hr.

Anisotropy measurements between 10^{13} eV and 10^{14} eV are dominated by the air shower measurements from Baksan (Alexeenko et al 1981), Mt Norikura (Nagashima et al 1977, Sakakibara et al 1979) and Musala Peak (Gombosi et al 1975, 1977). The experiment conducted at Baksan (mean primary energy 10^{13} eV) was an air shower rate counting experiment with corrections for barometric pressure variations and using atmospheric collimation for directional information. A total of 10^{9} events at a mean rate of 55 s^{-1} were detected in 1980-1981 with resultant sidereal anisotropy of 0.057% at 01.4 hr. Observations of the sidereal anisotropy were made at Mt Norikura (mean primary energy $3*10^{13}$ eV) between 1970 and 1979. The yearly results from this array show remarkable consistency and the mean sidereal first harmonic amplitude was 0.053% with maximum at 00.9 hr. To test for atmospheric effects, directional detectors sensitive to only air showers from the east and west were also used, however the vector difference obtained from this experiment was almost identical to the result from the omnidirectional detector, indicating that atmospheric effects were unimportant for this experiment. At a mean energy of about $6*10^{13}$ eV the arrival times of about 10^{8} air showers collected by the Musala Peak array were analysed for sidereal variations (Gombosi et al 1975).

Spurious effects produced by atmospheric fluctuations etc. were accounted for in the analysis by determining the coefficients of the atmospheric parameters as well as the solar and sidereal waves simultaneously. As a further test of the significance of the measured sidereal variation (0.073%, 01.7 hr), the amplitude of variations with frequencies near the sidereal frequency were also determined (Gombosi et al 1977). These indicated clearly the significance of the sidereal anisotropy.

In figure 5.4, a summary is presented of anisotropy measurements below 10^{14} eV. The data are uncorrected for the Compton-Getting effect of solar motion through the interstellar medium. Second harmonics of the sidereal variations are also measured to provide further information on the actual configuration of the galactic flux anisotropy, however most of the measurements are nearly consistent with isotropy. Although these results give no direct indication about the origin of the primary particles, the remarkable consistency of the sidereal first harmonics in both amplitude and phase indicates that the mode of propagation of cosmic rays in the galaxy probably changes little in the energy range from 10^{11} eV to 10^{14} eV. Since the radii of gyration of these particles change by three orders of magnitude over this energy range, these data suggest that the interstellar magnetic field is smooth on these scales from about 10^{-5} to 10^{-2} parsecs.

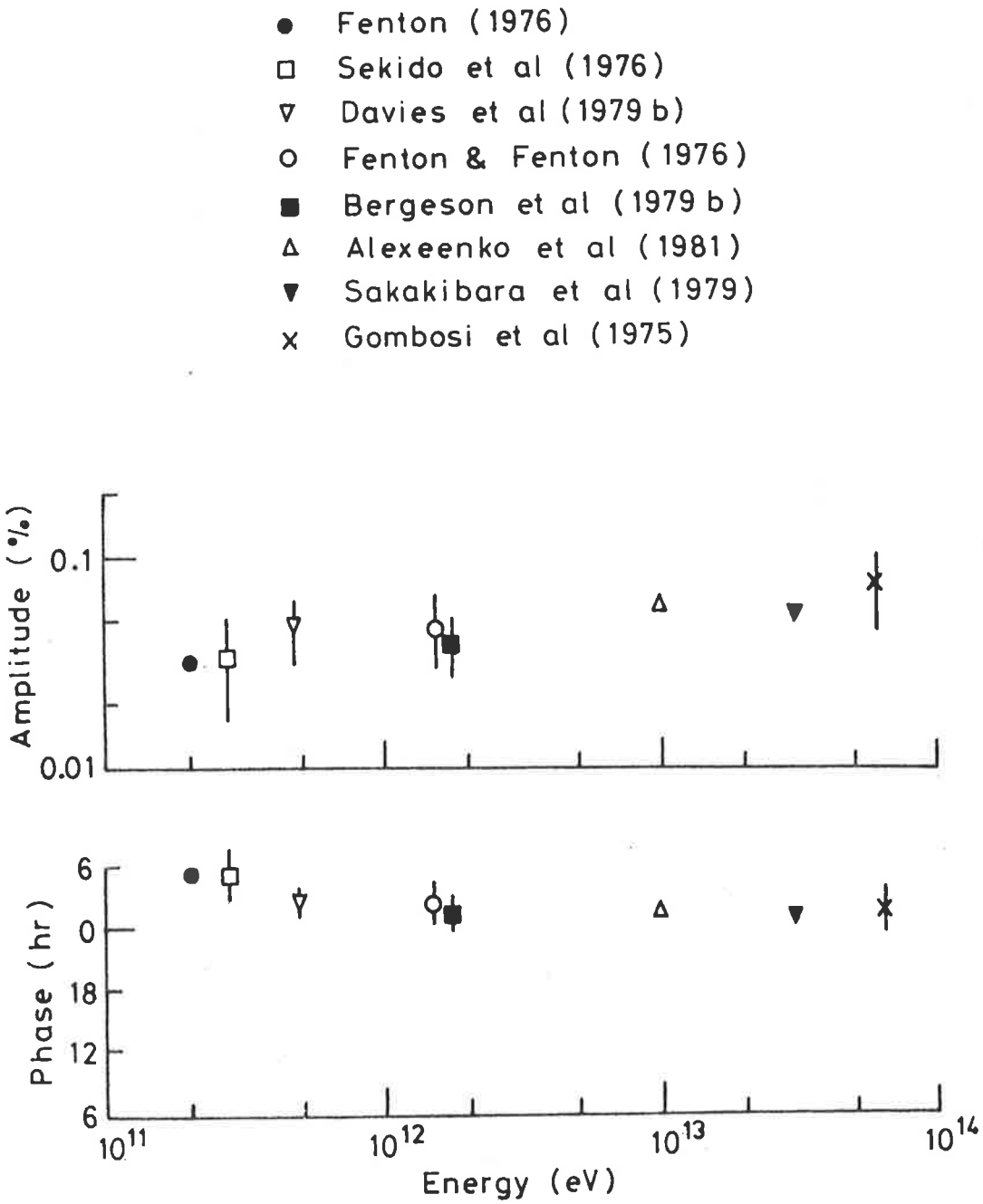

Figure 5.4 Compilation of low energy anisotropy measurements.

5.2.3 Medium Energy Measurements

the greatest difficulty in anisotropy measurements of the cosmic ray flux above the low energy region is the gathering of sufficient data for a statistically significant result. Solar and interplanetary magnetic field effects are negligible above 10^{14} eV, however with the integral spectrum falling as an inverse power law with exponent near 2, detectors with large sensitive areas exposed for long continuous periods are required to register sufficient events to give a result significantly above that which would be due simply to cosmic rays arriving from completely random directions. This means that the exposure to the flux must be increased by a factor of near 100 for each decade higher in energy to maintain the same statistics.

A comprehensive survey of anisotropy determinations conducted between 1951 and 1965 in the medium energy region has been made by Linsley and Watson (1977) (following the work of Sakakibara (1965)). This survey included 42 measurements from 20 independent experiments. With a few exceptions, these experiments were air shower rate counting experiments, relying on atmospheric collimation for directional information and having only rather crude energy resolution based on estimations of the mean number of shower particles. Atmospheric attenuation of the EAS was minimised expecially for the lower energy experiments by conducting them at high altitudes. Despite these limitations, some interesting

features were evident in the data, the most interesting of which was the apparent clustering of the directions of maximum of the sidereal first harmonics about 17.5 hr when the experimental results were given equal weight. On the other hand, the second harmonics in sidereal time showed no significant agreement. The energy dependence of the measurements was investigated by grouping the data by energy into the three energy decades below 10^{17} eV. The resultant for each energy (shown in table 5.1 below) was obtained by the vectorial addition of the various results.

In group A, a total of over $5.8*10^{7}$ events were collected. Of these over 70% come from the air shower rate counting experiment of Daudin et al (1956), conducted at Pic du Midi (altitude 2860 m, latitude 43^{o} N) using five trays of Geiger-Muller counters separated by up to about 80 m. Different coincidence requirements between these counters enabled different mean primary energies for the air showers to be selected up to about $4*10^{15}$ eV (used in group B). To improve the reliability of the results, corrections were made for chance coincidences between the detectors and variations in the high tension supply to the detectors as well as atmospheric variations. The validity of the sidereal anisotropy was demonstrated when the data were divided into half yearly bins; the event rate in sidereal time showed constant phase whereas the variations of solar origin changed phase between the bins as expected. Other experiments in group A contributed little to the apparent amplitude of the anisotropy although some phase agreement could be seen.

Table 5.1 (after Linsley and Watson (1977))

Energy Group	Average Energy (eV)	Apparent Amplitude (%)	Phase (hours sidereal time)
A	3.0×10^{14}	0.075 ± 0.020	20.1 ± 1.3
B	1.7×10^{15}	0.190 ± 0.045	19.4 ± 1.1
C	1.6×10^{16}	0.53 ± 0.25	11.7 ± 1.8

Nearly $1.3*10^7$ events from 15 independent experiments were collected in the energy decade above 10^{15} eV (group B). The largest contribution again came from the experiment of Daudin et al (1956) however significant contributions were also made by Citron and Stiller (1958) and Farley and Storey (1954,1957). Citron and Stiller, using Geiger-Muller counters in two sets of identical apparatus at Schauinsland (latitude 48^o N, altitude 1230 m) (duplicated so that the behaviour of each set could be monitored) found significant variations in solar time, however the sidereal variations were small, changed from year to year, and could to some extent be accounted for by atmospheric influences. Alternatively, the atmospheric effects were large enough to disguise genuine sidereal variations. This apparent and unexpected variation in the sidereal anisotropy, since then attributed to the counting statistics (Linsley and Watson 1977), was also observed in the independent experiments of Farley and Storey (1954,1957) at Auckland (latitude 37^o S, altitude 40 m). The large sidereal anisotropy measured in the first experiment was much less significant in the second experiment which had better statistics. Although the experiments of Clark (1957) and Chitnis et al (1960) made only small contributions to the statistics of the measurements in this energy group, they are important since rather than atmospheric collimation, fast timing of the EAS front was used to obtain directional data. This technique which has since become almost universal at these and higher energies, enables variations in the declination as well as the right ascension

of the cosmic ray flux to be observed.

The statistics in energy group C, 10^{16} eV to 10^{17} eV, are much poorer, deriving from seven experiments with only about $3.7*10^5$ events. Of these, the most important contributor is the Ithaca experiment of Delvaille et al (1962) using atmospheric collimation at low energies below 10^{15} eV, but individual analysis of fast timing data for each event at higher energies. Fifteen scintillator detectors in an array of diameter nearly 1 km were used in this experiment enabling showers with sizes up to 10^8 particles to be analysed. Corrections (not used in the Linsley and Watson survey) for spurious sidereal variations were made using the antisidereal analysis of Farley and Storey (1954) (see Section 5.3). Although the evidence for genuine anisotropies in these results was not conclusive, Delvaille et al (1962) noted the consistency in phase measurements.

Apart from the Linsley and Watson summary, the most important anisotropy measurements in the medium energy region have come from the Haverah Park array (Edge et al 1977). This array, using large deep water Cerenkov detectors in a number of sub-arrays with characteristic spacings of between 50 m and 2 km, is able to detect and analyse EAS with energies from about 10^{15} eV up to the most energetic events detected (above 10^{21} eV). Below $6*10^{16}$ eV, data was collected from the 50 m array ($2.4*10^5$ events) and the 150 m arrays ($1.5*10^5$ events) (Lloyd-Evans 1982). These experiments were very carefully investigated for spurious effects, and the

results, although their significance is relatively low, are in agreement with the Linsley and Watson survey. Above $6*10^{16}$ eV, a large and highly significant anisotropy was reported from measurements with the 500 m array (Edge et al 1978, Pollock 1978, Lapikens et al 1979), however this result was inconsistent with that from the 150 m arrays (Coy et al 1981b). It was concluded that this discrepancy could be removed by correcting the 500 m data for triggering variations in solar time and also variations in the lateral distribution as a function of temperature. The resultant however, still indicates a measured anisotropic flux near 10^{17} eV.

A summary of the results of anisotropy measurements between 10^{14} eV and 10^{17} eV is given in figure 5.5. The apparent change in both the amplitude and phase of the anisotropy is of great interest because of its coincidence with the change in the energy spectrum. This may suggest galactic origin (Kiraly et al 1979) for these primary cosmic rays although the inferred mass composition of the particles presents some difficulties.

5.2.4 High Energy Measurements

Early measurements of the anisotropy at the highest energies were made using counter experiments like those used at lower energies although on a larger scale. The bulk of data, however, has come from the giant air shower arrays which use fast timing directional analysis. Of these, by far the

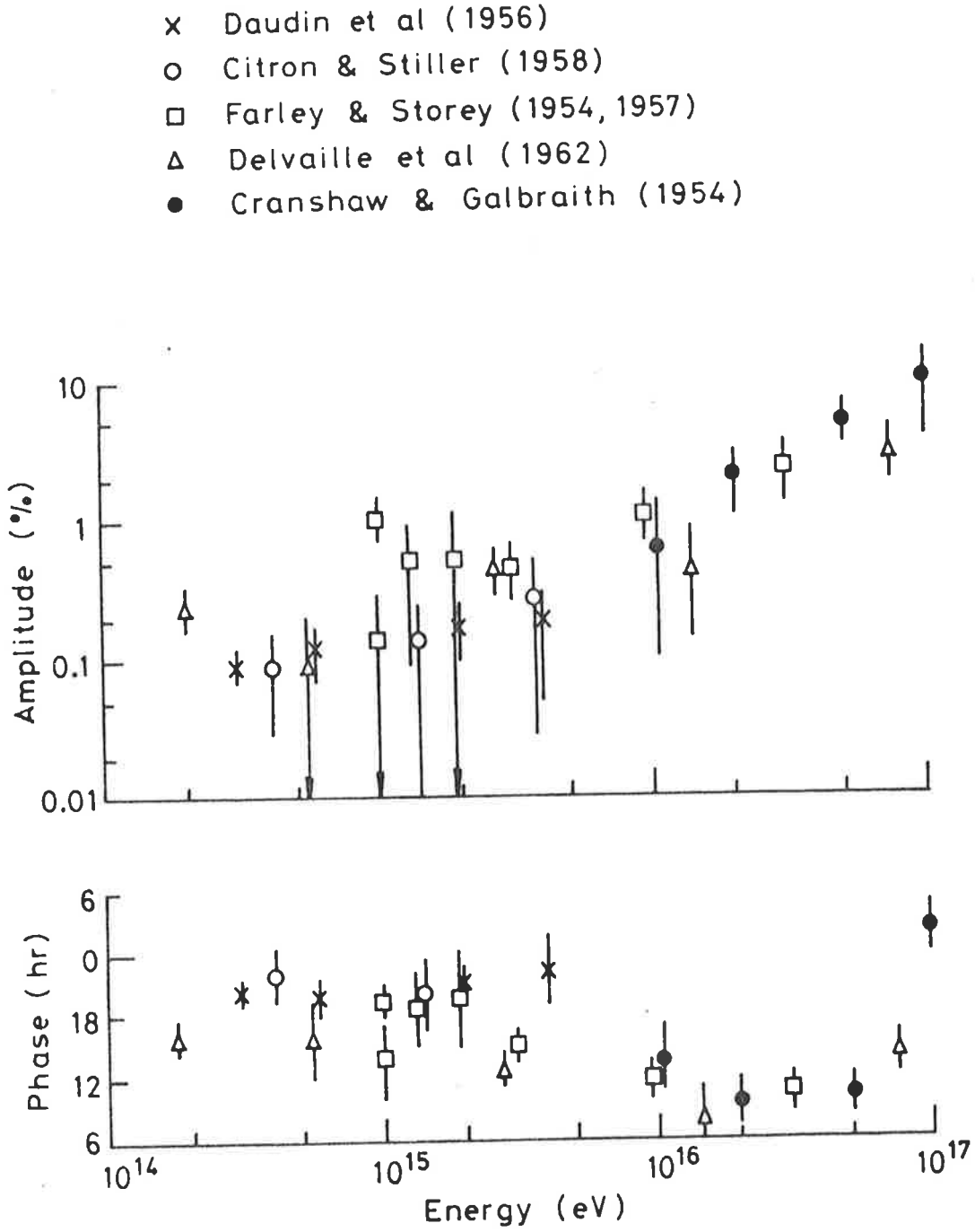

Figure 5.5 Compilation of medium energy anisotropy measurements.

most important is the Haverah Park array (Lloyd-Evans 1982), although useful contributions have been made by other arrays - Volcano Ranch (Linsley 1975c), Ithaca (Delvaille et al 1962), Mt Chacaltaya (Aguirre 1974), Yakutsk (Krasilnikov et al 1977) and Agassiz (Clark et al 1961). Results from the early fast timing experiments (Clark et al 1961, Delvaille et al 1962) were obtained near the upper energy limits accessible to the arrays concerned. Consequently, the statistics of these experiments were rather poor. The Sydney group (Bray et al 1975) have also produced data using the giant array at Narrabri. However this data is not discussed here due to energy calibration difficulties. A useful summary of these measurements may be found in Edge et al (1978) and they are illustrated in figure 5.6.

The first measurements of the high energy anisotropy were made by Cranshaw and Galbraith (1954, 1957) using a large array of Geiger-Muller counters. These experiments at primary energies just above 10^{17} eV counted the rates of various counter coincidences as a function of both sidereal and solar time and no corrections were made for atmospheric effects. Although significant variations were noted in solar time, the sidereal rates showed no significant variations. A similar experiment was carried out by Crawshaw and Elliot (1956). Again the sidereal variation measured was not statistically significant although a large and unexplained solar variation was seen. The total number of events detected in these experiments was nearly 10^4.

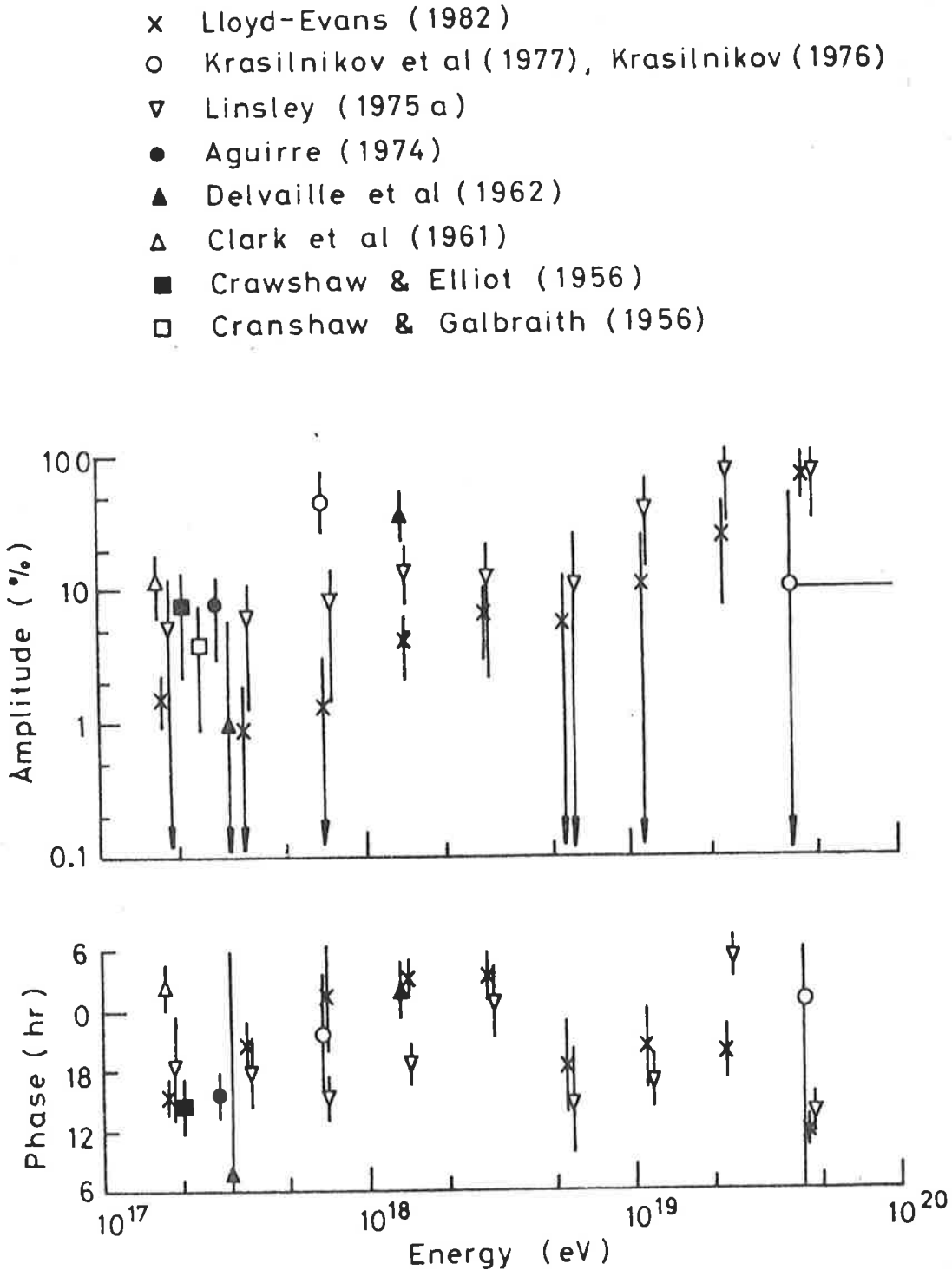

Figure 5.6 Compilation of high energy anisotropy measurements.

At Agassiz, Clark et al (1961) detected 652 events with mean energy $2*10^{17}$ eV using a fast timing array. With the arrival directions plotted in celestial coordinates, chi-squared tests were performed on declination bands with the results being consistent with isotropy. Special regions, the galactic plane, a perpendicular to the galactic plane, and the region of the spiral arm were also tested with the same result. The 853 largest EAS detected by Delvaille et al (1962) with mean primary energy of $3*10^{17}$ eV showed no significant sidereal or solar variations.

Apart from the Narrabri experiment, the only other high energy experiment performed in the Southern hemisphere was conducted at Mt Chacaltaya (altitude 5200 m). Aguirre (1974) attempted to correlate the arrival directions of about $2.6*10^{3}$ events at energies between 10^{17} eV and 10^{18} eV with known pulsar positions and found a positive result. Since this assumes neutral primary particles (neutrinos, gamma rays or neutrons - at energies over 10^{17} eV neutron decay is no longer important for sources within 1 kpc due to the Lorentz factor (Kiraly et al 1975)) the flux of which at these energies is unknown, the result of this correlation is somewhat problematical. However, the data (for declinations greater than 0) were reanalysed by Edge et al (1978) with an insignificant sidereal result.

In contrast with the previous insignificant anisotropy measurements, the results (using about $3*10^{3}$ events) from Volcano Ranch (Linsley 1975c) indicate a strongly energy

dependent anisotropy above 10^{17} eV. To explain the discrepancy with previous results, this author invoked the radical proposal of time dependence in the sidereal anisotropy. If this modulated sidereal effect could produce a spurious solar result, the results of Cranshaw and Galbraith (1957) and Crawshaw and Elliot (1956) might be explained.

Krasilnikov et al (1977) have presented data from the Yakutsk array for particles with primary energies above about 10^{18} eV. This array detects EAS by means of the visible Cerenkov radiation emitted by the ultrarelativistic particles in the shower. Unfortunately, this restricts the observing periods available and the collection statistics are therefore low, however especially above 10^{19} eV the flux appears to be very anisotropic.

By far the most important results in this energy range come from Haverah Park with over $9.1*10^{4}$ events with energies greater than $6.25*10^{16}$ eV detected by the 500 metre array (from the most recent analysis of Lloyd-Evans 1982). Apart from a dip in the amplitude of the anisotropy near $5*10^{17}$ eV, the amplitude increases from about 1.6% near 10^{17} eV up to about 70% above $3*10^{19}$ eV. Changes in the phase of the anisotropy are also apparent at $2*10^{17}$ eV and $4*10^{18}$ eV.

Above primary energies of about 10^{19} eV, the data from all arrays is often combined because of the very low flux (Krasilnikov et al 1974, Krasilnikov 1979). A striking result

of this combination is the large number of events arriving from high galactic latitudes. Unless the primary particles are heavy and an ordered magnetic field exists as a halo outside the galactic disc, this result argues against a galactic origin for these particles. Acceleration by magnetic fields and turbulent gas motions in the local supercluster of galaxies as argued by Hillas (1982) must then be considered.

Although the variation in the anisotropy below 10^{19} eV indicates changing propagation and/or source distribution, it is not yet possible to determine the relative importance of these effects without definite composition data. More complete measurements of the anisotropy in the Southern Hemisphere would be very important to this determination since they would allow complete maps of the flux anisotropy over the sky to be drawn.

5.3 Harmonic Analysis

The technique chosen for the analysis of the Buckland Park data was harmonic analysis. Although the use of this technique on anisotropy measurements has been critisized (Kiraly and White 1975, Kiraly et al 1975) in comparison to chi-squared tests, its use may be justified on a number of grounds, the most important of which is that the sinusoidal analysis is of the same form as the variations in solar and sidereal time being investigated. The use of this technique also allows a good test for spurious variations in sidereal

time produced by fluctuations in solar time. Also, this analysis method has been used by most experimentalists in this field and hence the results from the Buckland Park experiment using harmonic analysis may be conveniently compared with the other results.

Given that data are collected over a number of complete cycles in sidereal or solar time, the statistics of the analysis of these data are analogous to the solution of the two-dimensional random walk with equal step lengths and random angles. This problem, first analysed by Lord Rayleigh (1880) in the asymptotic ($n \to \infty$) case, has been solved in detail by Chapman and Bartels (1940) for applications in geomagnetism. In the analysis used here, the terminology of Linsley (1975a,b) is followed. Details of the harmonic analysis technique in its adaptation to anisotropy measurements are given in Appendix 3, however the following terms are introduced here:

r, the harmonic amplitude,

θ, the phase of maximum,

$k_0 = n.r^2/4$,

where n is the total number of events. The statistic k_0 provides a useful measure of the probability of measuring an amplitude greater than r from n unit steps with randomly distributed angles. This probability is given by the Rayleigh formula:

$$W(>r) = \exp(-k_0) \qquad (5.3)$$

Hence the measured anisotropy amplitude in sidereal time or Right Ascension may conveniently be compared to that expected from an isotropic cosmic ray flux. k_0 may also be defined in terms of r_{RMS}, the root mean squared amplitude expected from n random steps by:

$$k_0=(r/r_{RMS})^2, \quad r_{RMS}=2.n^{-0.5} \qquad (5.4)$$

r_{RMS} then defines the approximate noise level of a random distribution. For significant results the measured amplitude should be greater than the noise, that is, k_0 should be greater than 1. If n is large enough ($k_0>>1$), it may be shown that the probability distributions of the amplitude and phase tend to Gaussian (Linsley 1975a,b) so that the formal statistical error limits in the measured parameters are given by:

$$\sigma_r=(2/n)^{0.5}, \qquad \sigma_\theta=\sigma_r/r \qquad (5.5)$$

These values must be treated with care however since as n decreases, the probability distributions of these parameters become definitely non-Gaussian.

Using this statistical background, the antisidereal analysis of Farley and Storey (1954) may be used to detect spurious sidereal variations as follows. It is assumed that there are only two natural frequencies in the variations detected in the cosmic ray flux, the sidereal variations caused by genuine flux anisotropies, and the solar variations

produced by, for example diurnal temperature fluctuations. Suppose the solar variation is described by:

$$S(t)=S_0+S.\cos(2\pi Nt-\alpha) \qquad (5.6)$$

where S_0 is the mean annual rate in solar time, N is the number of solar days in the year, t is in years, and S and α describe the relative solar amplitude and phase. If this amplitude is made to undergo annual modulation such that:

$$S=S(1+A.\cos(2\pi(t-\beta))) \qquad (5.7)$$

then:
$$S(t)=S_0+S.\cos(2\pi Nt-\alpha)+S.A.\cos(2\pi Nt-\alpha)\cos(2\pi(t-\beta))$$

or:
$$S(t)=S_0+S.A.\cos(2\pi(N+1)t-\alpha-2\pi\beta)/2$$
$$+S.\cos(2\pi Nt-\alpha)$$
$$+S.A.\cos(2\pi(N-1)t-\alpha+2\pi\beta)/2 \qquad (5.8)$$

Since there are exactly (N+1) sidereal days in a year, it can be seen that the annual amplitude modulation of variations in solar time produces a spurious variation in sidereal time. The (N-1) term is known as the antisidereal term corresponding to a year with (N-1) days. It should be noted that these spurious sidebands have identical fractional amplitudes and are distributed symmetrically about the solar vector. If the genuine sidereal variation can be described by:

$$R(t)=R_0+r.\cos(2\pi(N+1)t-\theta) \qquad (5.9)$$

then the total detected flux can be represented by:

$$J(t)=J_0+T_1+T_0+T_{-1} \qquad (5.10)$$

where T_i are the terms at the various frequencies and T_1 is the sum of the real sidereal variation (equation 5.9) and the spurious term from equation 5.8.

$$r'.\cos(2\pi(N+1)t+\theta')=r.\cos(2\pi(N+1)t-\theta) + S.A.\cos(2\pi(N+1)t-\alpha-2\pi\beta)/2 \qquad (5.11)$$

Time t is zero at 00.00 hours on the 22nd September when sidereal and solar times coincide. Data must be collected for complete years to avoid spurious variations at other frequencies. If data from a full year is analysed, the terms T_i are orthogonal so that they can be determined easily. Once the components have been determined, the real sidereal vector (r,θ) may be deduced by vector subtraction of the reflection of the antisidereal vector in the solar vector from the measured sidereal vector (r',θ') as illustrated in figure 5.7.

Unfortunately, this technique is not applicable if annual phase modulation of the solar vector is also important. In this case, the situation becomes more difficult. If the phase modulation goes as:

$$\alpha=\alpha_0(1+\delta.\cos(2\pi(t-\gamma))) \qquad (5.12)$$

then without loss of generality, α may be set to 2π. The

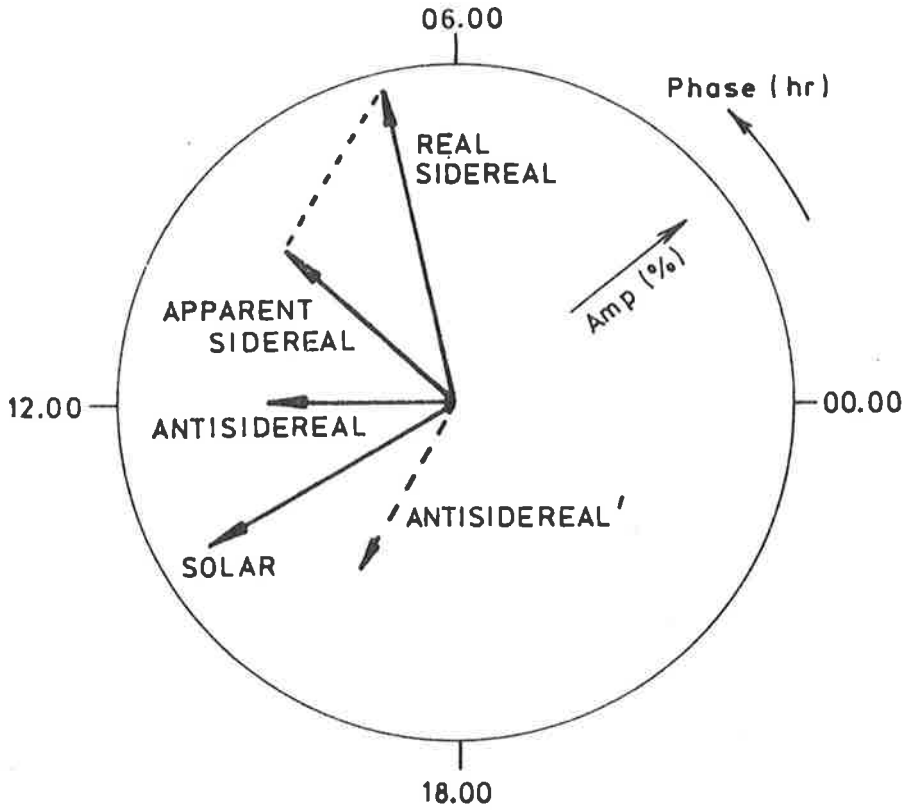

Figure 5.7 Farley and Storey antisidereal analysis technique.

total solar variation is given by:

$$S(t)=S_0+S.(1+A.\cos(2\pi t-\beta).\cos(2\pi(Nt-\delta.\cos(2\pi(t+\gamma))))) \quad (5.13)$$

This variation has harmonic components at all frequencies ω_i:

$$\omega_i=2\pi(N+i) \quad (5.14)$$

and may be expressed by:

$$J(t)=J_0+\sum_i T_i$$

where

$$T_i=U_i.\cos(2\pi(N+i)t-\phi_i) \quad (5.15)$$

Here U_i is the amplitude of the i^{th} component and ϕ_i is the corresponding phase. Pollock (1978) has provided a detailed solution for this problem with the following results for the solar, sidereal and antisidereal components:

$$T_0/S=B.\cos(2\pi Nt)+C.A.\cos(2\pi(\beta-\gamma)).\sin(2\pi Nt)/2$$

$$T_1/S=B.A.\cos(2\pi(N+1)t-\beta)/2+C.\sin(2\pi((N+1)t-\gamma))/2$$
$$+D.A.\cos(2\pi((N+1)t+\beta-2\gamma))/4$$

$$T_{-1}/S=B.A.\cos(2\pi(N-1)t+\beta)/2+C.\sin(2\pi((N-1)t+\gamma))/2$$
$$+D.A.\cos(2\pi((N-1)t-\beta+2\gamma))/4 \quad (5.16)$$

where B, C, and D are constants depending only on δ. The components at other frequencies have similar expressions (Pollock 1978). The T_2 and T_{-2} terms have been named ultra-sidereal and ultra-antisidereal terms respectively.

Clearly, for phase modulation the simple symmetry demonstrated in figure 5.7 no longer holds and determination of the spurious sidereal signal depends on the evaluation of a number of parameters. It can be seen however, that amplitude and phase modulation of the solar variation can easily be tested for by analysing the collected data for significant variations at frequencies other than the sidereal and solar frequencies. On this basis, the collected data may now be analysed for the presence of significant deviations from isotropy in the cosmic ray flux.

5.4 Buckland Park Anisotropy Results

The data analysed here came from three complete years, 1979, 1980 and 1981 during which time approximately $1.33*10^5$ events were detected by the Buckland Park array. In this period, the array was set to run (nominally) continuously (excluding routine maintenance and breakdowns) with constant triggering conditions as described in Chapter 2.

5.4.1 Spurious Effects

Before significant measurements of the sidereal anisotropy can be made, the data must be examined for effects which may introduce coincidental or spurious variations into the results. Although the zenith and azimuth angle

distributions are non-uniform so that only a small part of the celestial sphere is accessible to the array at any given time, the rotation of the earth means that in one complete sidereal day, the Right Ascension exposure of the array is uniform. Therefore, if the on-time of the array is uniform in sidereal time, the Right Ascension exposure will also be uniform and unbiassed measurements of the cosmic ray flux as a function of Right Ascension may be made simply by observing the number of showers from given celestial coordinates. To achieve this uniform data train however, requires the array to be sensitive at all times without interruption - an ideal impossible to attain in practice.

Variations in the total array exposure time are introduced especially by the routine tape changing and maintenance procedures which naturally occur at similar times during the solar day. This produces a considerable non-uniformity in the exposure of the array to the sky in solar time as shown in figure 5.8. The efficiency of the array during the period considered (1979 - 1981 inclusive) was 71%, most of the off-time being attributable to equipment breakdowns. Because of the approximately 0.3% difference between solar and sidereal time scales (one day difference per year), the variation in sidereal time is much less (figure 5.9). First and second harmonics of the array exposure in solar, sidereal, and antisidereal time scales are shown in table 5.2 below. The actual variation in the Right Ascension distribution of events is less than this, since the width of the zenith angle distribution makes the array sensitive to a

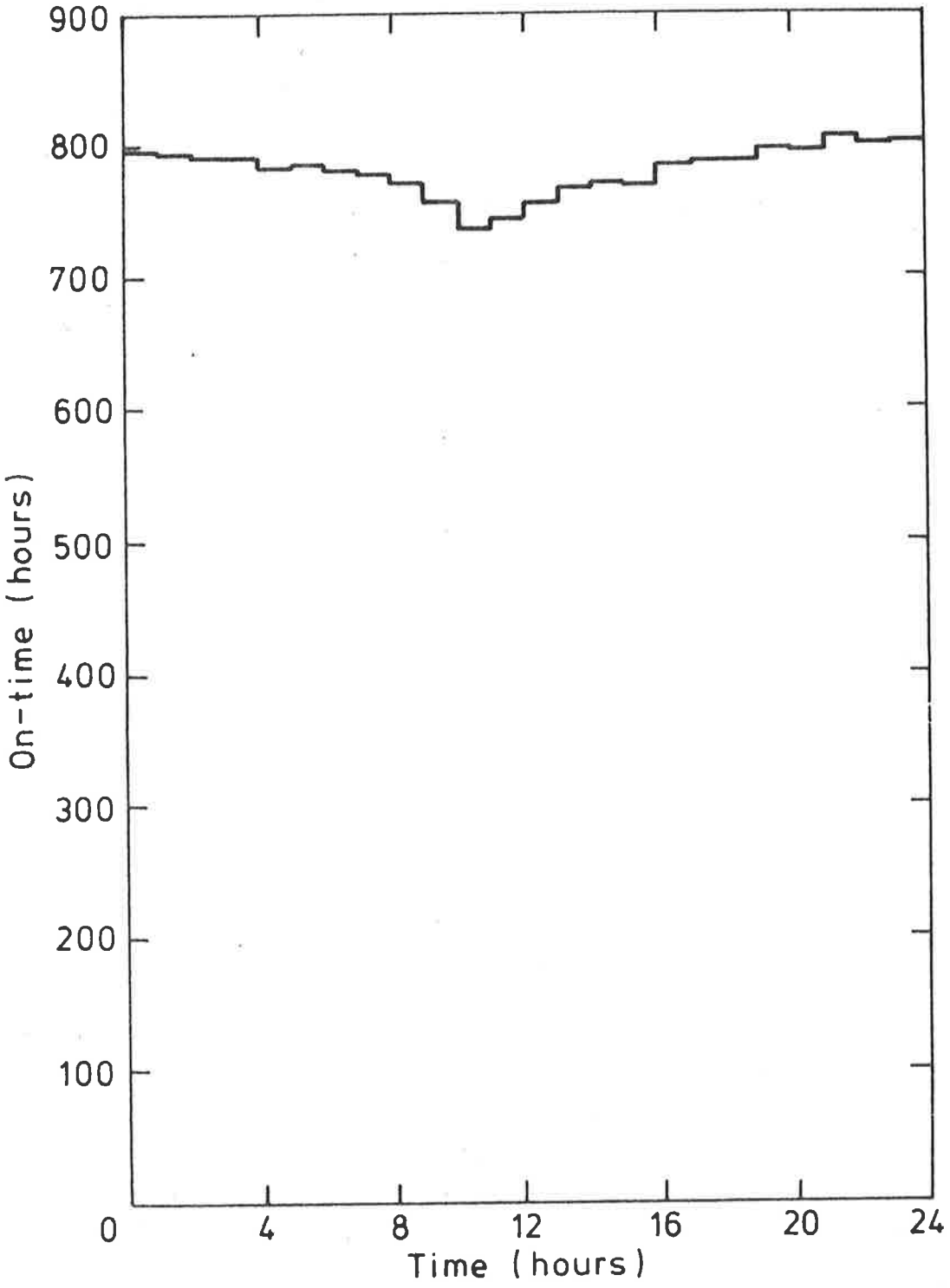

Figure 5.8 The array exposure in solar time.

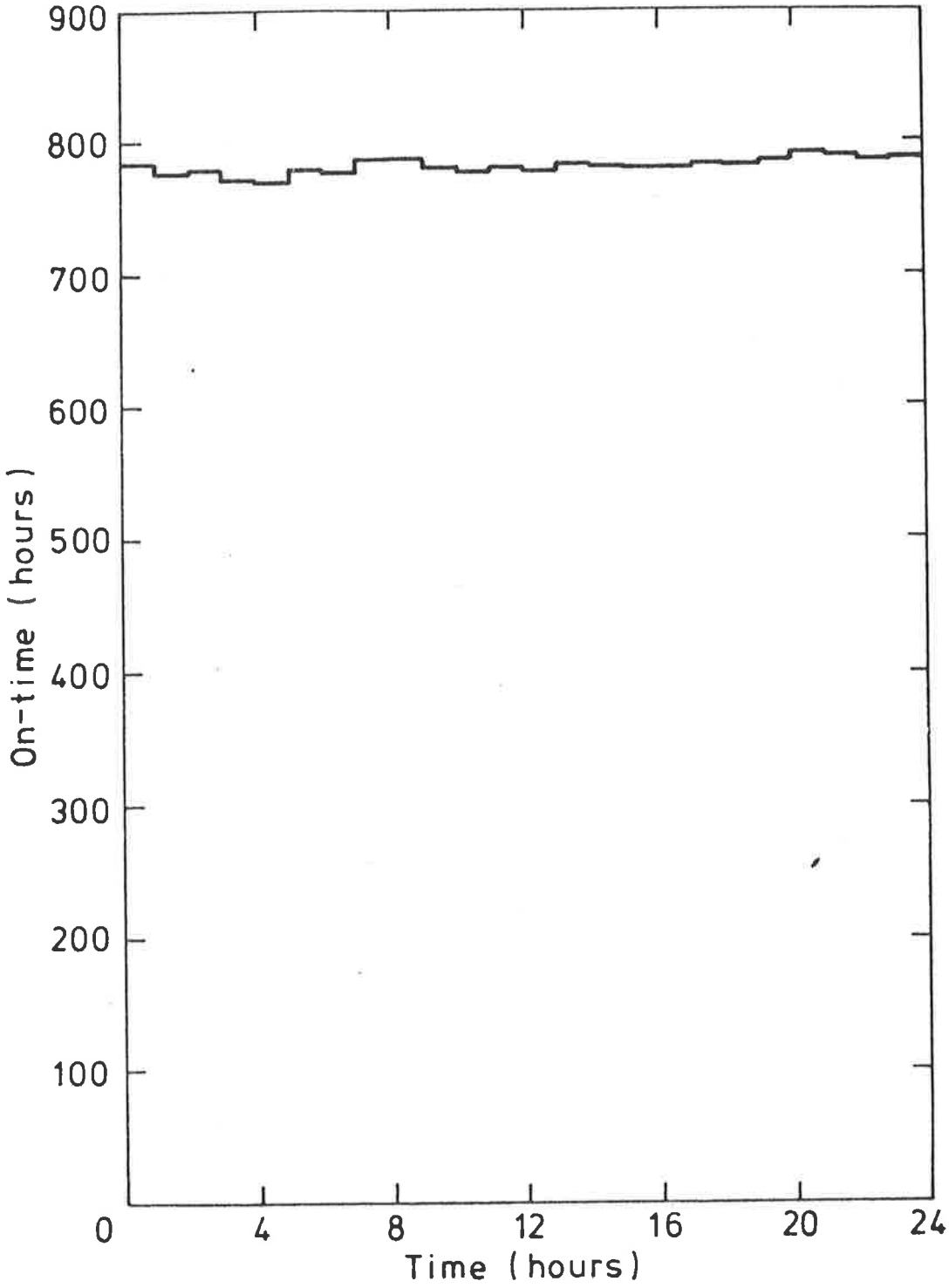

Figure 5.9 The array exposure in sidereal time.

Table 5.2 - HARMONICS OF THE ARRAY EXPOSURE TIMES

Timescale	1st Harmonic		2nd Harmonic	
	Amplitude (%)	Phase (hr)	Amplitude (%)	Phase (hr)
Sidereal	0.22	19.1	0.28	06.8
Solar	1.48	23.6	0.41	00.4
Antisidereal	0.31	19.3	0.13	11.9

range of Right Ascensions at any given sidereal time. Figure 5.10 shows the range of Right Ascensions of events detected in the sidereal time interval from 11.00 to 12.00 hours. The width of this distribution is about four hours (sidereal time). Variations in the sidereal exposure are therefore smeared out by this effect. Another factor reducing the spurious result due to sidereal on-time fluctuations is the determination of the Fourier components of the sidereal anisotropy in terms of the rate of events as a function of Right Ascension weighted by the sidereal on-times. Because of these effects, the spurious sidereal variation produced by on-time fluctuations is reduced well below the RMS noise level expected from $1.3*10^5$ events (about 0.55%). For this reason, no attempt has been made in the anisotropy determinations presented here to produce uniformity in the sidereal exposure time.

Coincidental sidereal variations may also be introduced by the atmospheric effects noted in the previous chapter as well as fluctuations in the detection equipment gains produced by temperature changes. Figure 5.11 is an extract from the pressure and temperature records produced at the Buckland Park array. The thermal lagging around the detectors clearly reduces the amplitude of temperature fluctuations of the detectors by a considerable amount as well as changing their time profile, but does not damp them right out. If any of these variations have Fourier components in sidereal time, spurious sidereal variations in the detection rate will be produced. It can be seen that temperature

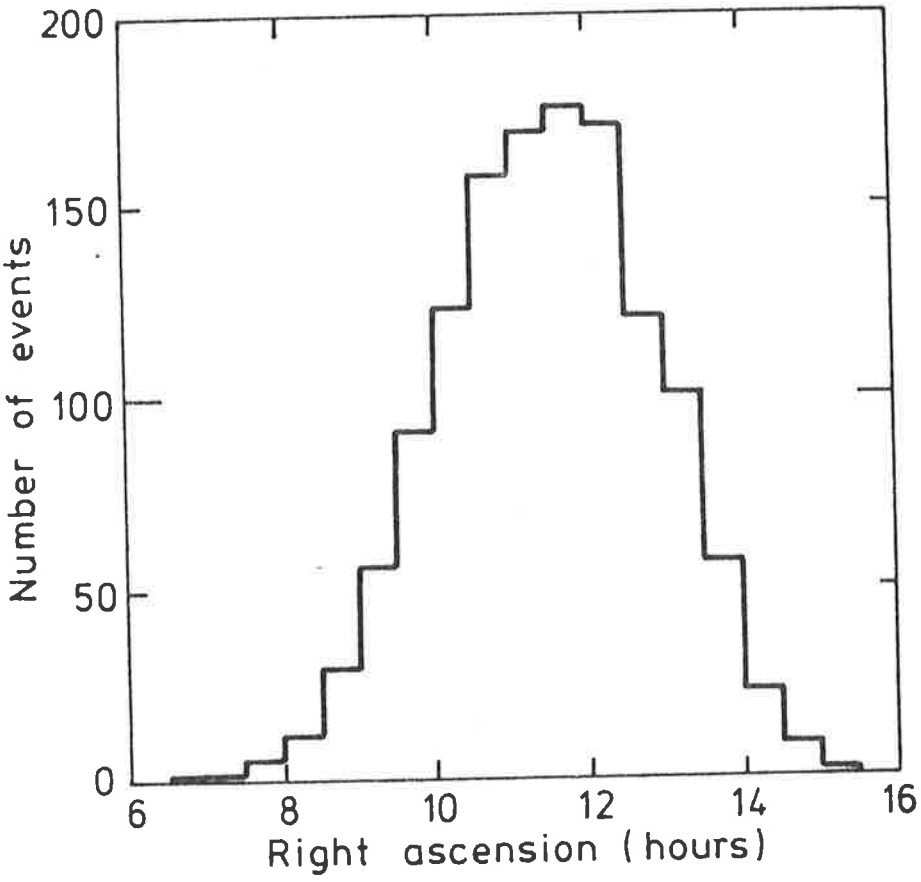

Figure 5.10 The range of Right Ascensions of detected showers during the local sidereal time interval from 11.00 to 12.00.

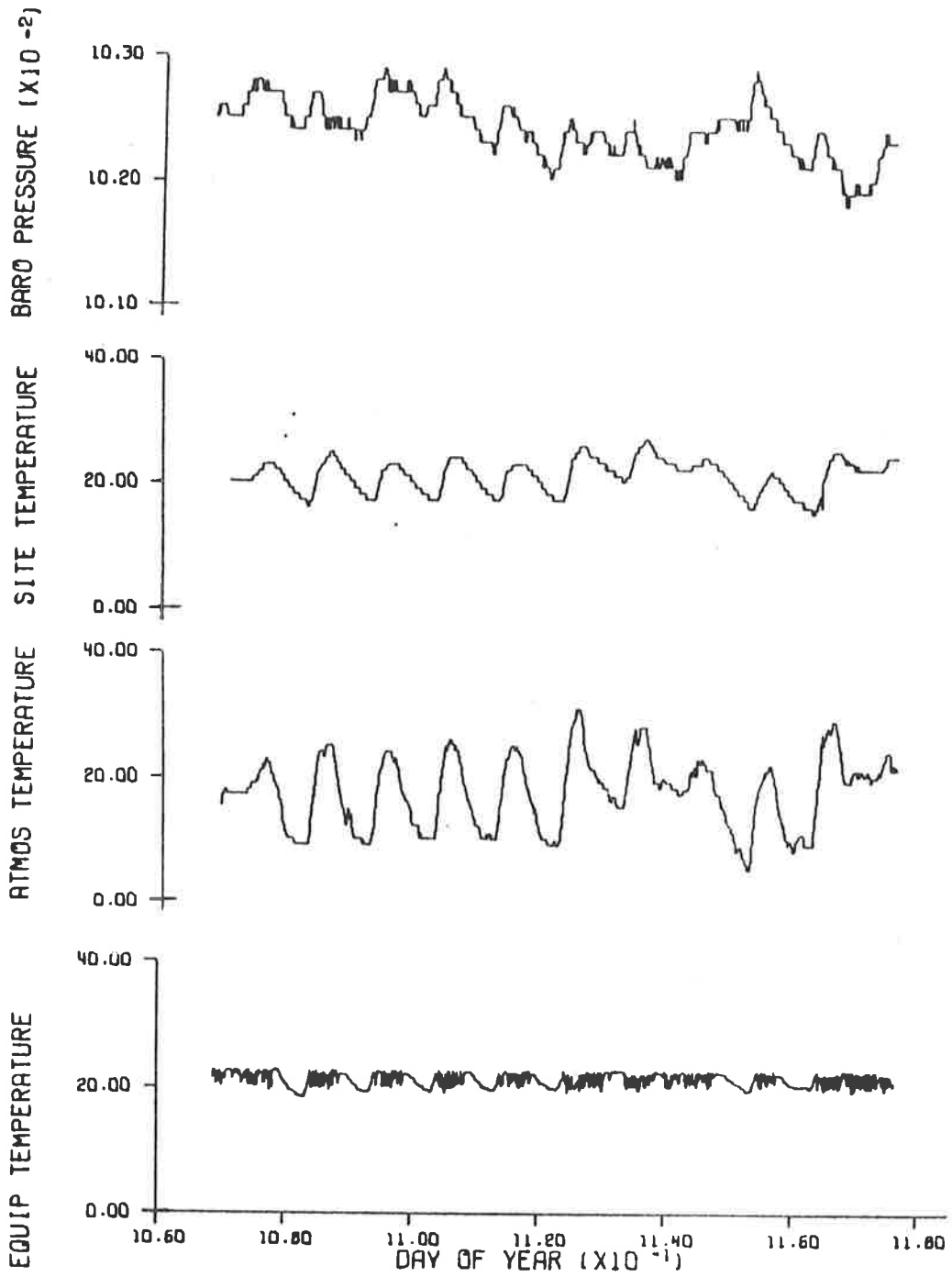

Figure 5.11 An extract from the Buckland Park Temperature and Pressure records. The site temperature referred to is C detector.

Table 5.3 Fourier Components of the Temperature and Pressure Variations

Frequency	Atmospheric Temperature		Detector Temperature		Barometric Pressure	
	(a)	(b)	(c)	(d)	(e)	(f)
(First Harmonics)						
Sidereal	2.3	21.2	1.1	00.4	0.53	19.6
Solar	13.4	14.1	5.7	16.4	2.55	12.6
(Second Harmonics)						
Sidereal	0.5	03.6	0.3	08.3	0.17	09.4
Solar	2.7	01.1	1.2	02.9	2.0	08.5

(a) = Amplitude (K)

(b) = Phase (hr)

(c) = Amplitude (K)

(d) = Phase (hr)

(e) = Amplitudes (mb)

(f) = Phase (hr)

variations of the analysing and recording electronics are minimized by the air-conditioning of the main recording hut, and they have been ignored in this analysis. The complete data train of the pressure and temperature data (weighted by on-times) have been analysed for their Fourier components at sidereal and solar frequencies with the results shown in table 5.3.

These data, in combination with the results of multiple linear regression analysis on the same parameters with respect to the rate of event detection, have been used to produce the resultant spurious harmonics of the event rate for each frequency component (table 5.4) . Finally the total spurious anisotropy amplitudes and phases were calculated from the vector additions (figure 5.12) of these results and these are displayed in table 5.5.

The spurious sidereal resultants are small indicating that atmospheric modulations of the detection rate do not have a serious effect on measurements of the cosmic ray flux anisotropy. Even if the maximum results from the on-time irregularities are added to these sidereal vectors, the spurious first and second harmonics have amplitudes of only about 0.28% (21.0 hr) and 0.33% (05.3 hr) respectively. This indicates that measurements of the deviation of the flux from isotropy in Right Ascension can be made with some confidence.

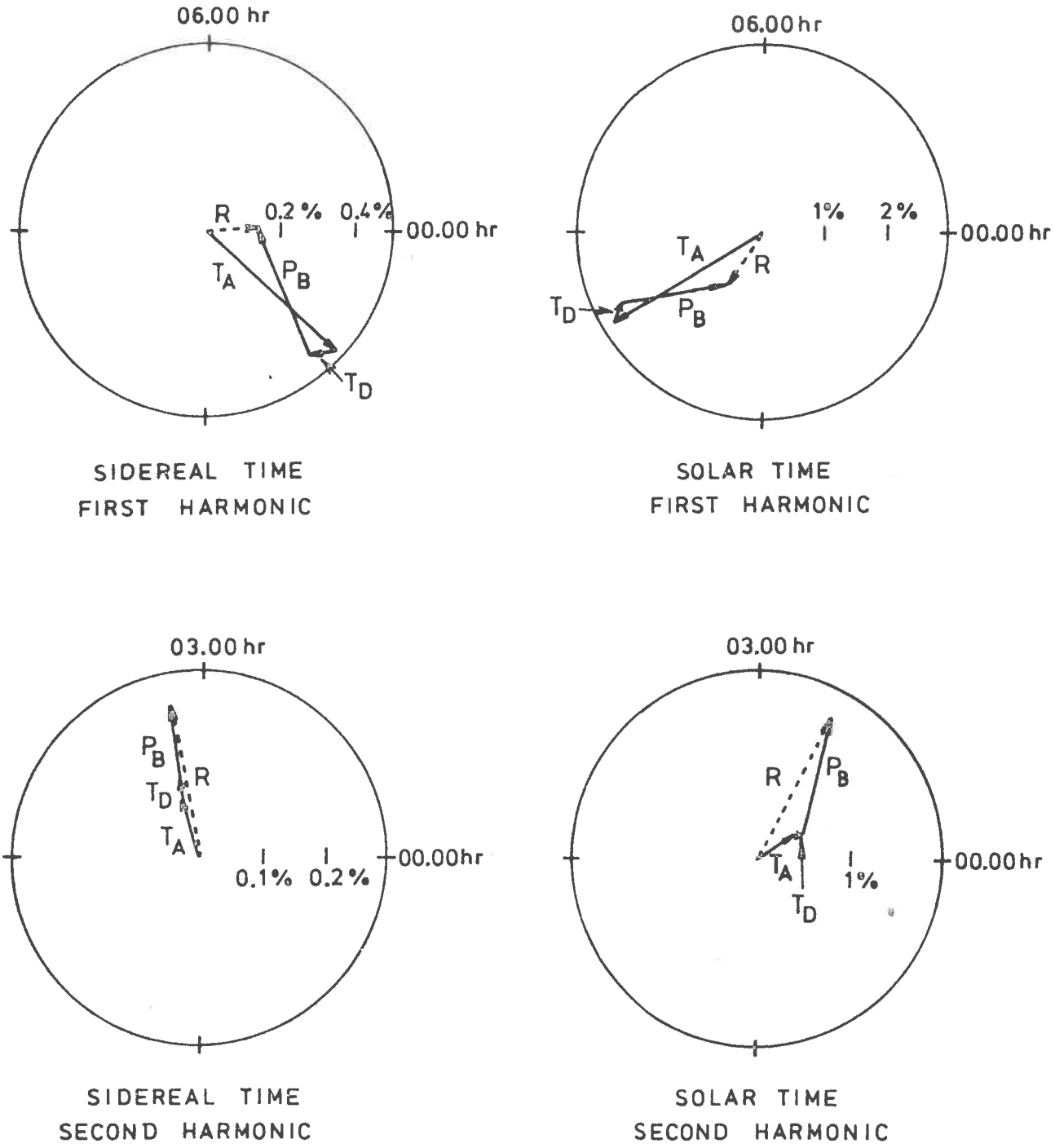

Figure 5.12 The spurious first and second harmonics from atmospheric effects.
R, resultant total
T_D, detector temperature
T_A, atmospheric temperature
P_B, barometric pressure

5.4.2 Analysis Produced Effects

Using the statistical basis established in the previous sections, determinations of the anisotropy may now be made. Although obvious sources of spurious results have been investigated, the array and the atmosphere form a complex and open detector system and only relatively few of the parameters of the system are easily monitored or controlled. For this reason, the data must still be checked for the presence of amplitude and phase modulations of the solar signal which are due to changes in the detection probability.

If it can be assumed that the harmonics at the frequencies being investigated are relatively independent of declination and shower size in the size interval detected, then the antisidereal technique of Farley and Storey (1954) may be applied to the whole set of recorded data (January 1979 - December 1981). In this way, maximum statistical weight can be obtained for the measurement of spurious results.

Events which were badly analysed (with reduced chi-squared greater than 5) or which had recording errors have been eliminated from the data set. This reduces the total number of available events to about $1.2*10^5$. Using the arrival times of the events, the geographical coordinates (zenith and azimuth angles) for arrival directions have been converted to celestial coordinates (Right Ascension and declination). Unless otherwise stated, the data have been

Table 5.4 Spurious Event Rate Harmonics From Atmospheric Coefficients

Frequency	Atmospheric Temperature		Detector Temperature		Barometric Pressure	
First Harmonics	(a)	(b)	(c)	(d)	(e)	(f)
Sidereal	0.48	21.2	0.07	12.4	0.37	07.6
Solar	2.82	14.1	0.37	04.4	1.78	00.6
Second Harmonics						
Sidereal	0.11	03.6	0.02	02.3	0.12	03.4
Solar	0.57	01.1	0.08	08.9	1.36	02.5

(a) = Amplitude (%)

(b) = Phase (hr)

(c) = Amplitude (%)

(d) = Phase (hr)

(e) = Amplitude (%)

(f) = Phase (hr)

Table 5.5 Spurious Anisotropy Vectors from Atmospheric Coefficients

	Amplitude (%)	Phase (hr)
First harmonics		
Sidereal	0.14	00.3
Solar	0.99	16.0
Second harmonics		
Sidereal	0.25	03.4
Solar	1.75	02.1

summed over all the observed declinations. When divided by the appropriate array exposure times, these data give the mean rate as a function of Right Ascension (or sidereal time).

These data have been Fourier analysed for first and second harmonics at ultra-sidereal, ultra-antisidereal, and antisidereal frequencies as well as solar and sidereal frequencies, that is, at frequencies one and two cycles per year different from solar time. The sidereal vector (r, θ) measured is the resultant of genuine and spurious sidereal signals. Information on any amplitude modulation of the solar vector can be derived from the antisidereal vector, while the ultra-sidereal and ultra-antisidereal vectors give complementary information on phase modulation. Phase relationships between the vectors are derived from 00.00 hours on the September equinox when all the time frames coincide.

The results of the analysis are shown in table 5.6. In the table, the probability referred to is that of a random distribution giving rise to a variation with less than or equal to the same amplitude. A number of interesting features emerge from this analysis. From the first harmonics, the sidereal variation has the greatest significance while the chance probability of the solar vector is fairly high. The amplitude of the solar vector is well below the statistical noise level expected from the sample. Evidence of phase modulation from the ultra-sidereal and ultra-antisidereal variations is somewhat contradictory, each showing one amplitude with low and one amplitude with very high

Table 5.6 Harmonic Analysis of All Data 1.20×10^5 events

Frequency	Amplitude (%)	Phase (hrs)	Probability (%)
first harmonics			
Ultrasidereal	0.15	18.1	93.8
Sidereal	0.84	08.0	12.3
Solar	0.38	15.3	64.7
Antisidereal	0.07	20.7	98.5
Ultra-antisidereal	0.82	15.4	13.5
2nd Harmonics			
Ultrasidereal	1.01	00.6	4.7
Sidereal	0.87	02.4	10.1
Solar	0.37	02.2	66.4
Antisidereal	0.43	03.4	56.7
Ultra-antisidereal	0.19	05.5	89.4

probability of being produced by a random distribution. Since these vectors are complementary, both being produced from the solar variation, the probability of them being significant is not high and no information about phase modulation of the solar variation can be extracted. It is therefore assumed, in agreement with Pollock (1978), that phase modulation has not been observed. Similarly, these results indicate that the antisidereal variation is consistent with being produced by a random distribution. It should be noted that from equations 5.7 and 5.12, the modulation amplitudes are by definition fractional compared with the solar variation amplitude so that for a solar vector with an insignificant amplitude, no significant conclusions about the phase and amplitude modulations of this variation can be expected. An interesting point however, is the agreement in phase of the solar vectors with the results produced for expected atmospheric variations in table 5.5. The sidereal vectors are much larger than the expected spurious results from table 5.5 and only show phase agreement in the second harmonics.

Since this data has the highest statistical significance and no conclusive evidence for either phase or amplitude modulation can be found, in further analyses of the data, no corrections (using the antisidereal analysis technique) will be applied to the sidereal signal by way of attempts to measure the genuine cosmic ray sidereal anisotropy.

As a check on these conclusions, the data set has been

subdivided into individual complete years and reanalysed in the same way with the results shown in table 5.7. The RMS noise levels associated with these results are all about 1%. Although a number of these vectors have large amplitudes, it is interesting to compare the phases for each year. These are plotted on harmonic dials in figure 5.13. It can be seen that only the sidereal first harmonic shows substantial consistency over the three years, although the low number of independent estimates makes this difficult to test statistically. This tentative result supports the earlier conclusion that only the sidereal signal shows a significant amplitude.

Reducing the data to shorter time periods introduces difficulties into the interpretation of the results since at all frequencies other than the solar frequency, the number of cycles is non-integral. If the sidereal and antisidereal signals are produced by modulation of the solar wave, over the period of a year, it would be expected that the solar vector should maintain a constant phase with the sidereal and antisidereal phases rotating in opposite directions and coinciding with the solar phase at the September equinox. The data were therefore divided into three month periods. Results of this analysis are given in table 5.8 and plotted in figure 5.14.

At the second harmonic frequencies, the result is as expected for modulation of the solar variation, with a fairly constant solar vector and the sidereal and antisidereal vectors rotating in opposite directions. However, the

Table 5.7 Analysis of the Data by years

Frequency	1979		1980		1981	
1st harmonics	Amp.(%)	Phase(hr)	Amp.(%)	Phase(hr)	Amp.(%)	Phase(hr)
Ultrasidereal	0.21	11.8	0.66	13.3	0.62	22.5
Sidereal	1.73	10.6	1.13	05.0	0.42	07.7
Solar	0.97	16.0	1.36	10.7	1.36	22.0
Antisidereal	0.76	18.5	0.89	03.7	0.43	05.8
Ultra-antisidereal	1.68	17.0	1.12	12.4	0.38	19.6
2nd harmonics						
Ultrasidereal	1.93	02.5	0.67	11.3	1.01	10.2
Sidereal	2.29	01.2	0.41	03.5	0.55	06.8
Solar	1.17	03.3	0.76	11.1	1.28	10.6
Antisidereal	1.33	11.6	0.90	11.9	1.34	04.0
Ultra-antisidereal	0.24	08.1	0.66	03.6	0.56	10.9
No. of Events	$3.6*10^4$		$4.6*10^4$		$3.8*10^4$	

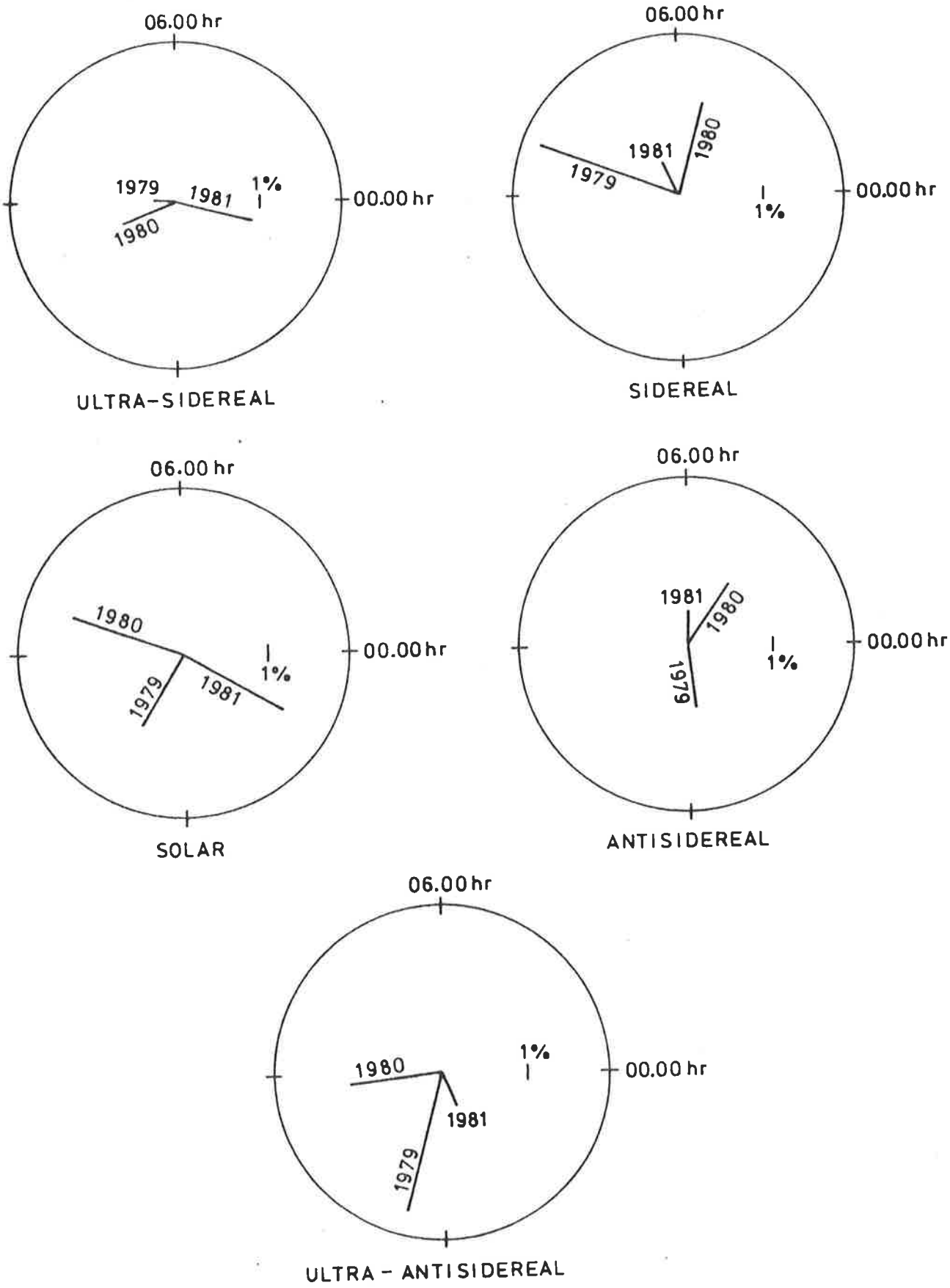

Figure 5.13a Yearly first harmonic vectors

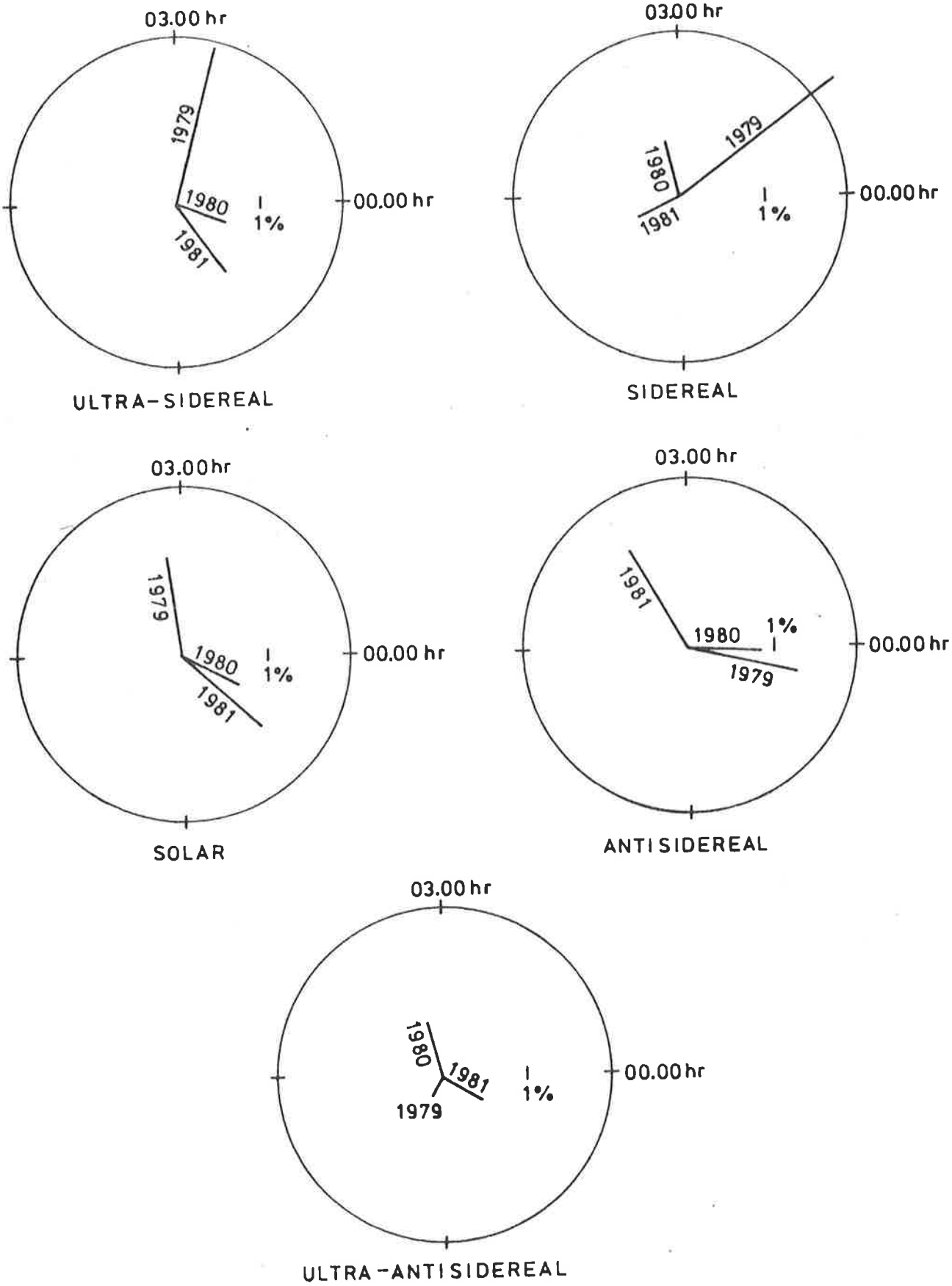

Figure 5.13b Yearly second harmonic vectors

Table 5.8 Quarterly Data Analysis

	Sidereal		Solar		Antisidereal	
	(a)	(b)	(c)	(d)	(e)	(f)
First Harmonics						
Quarter						
First	0.54	03.5	0.32	14.0	0.67	02.1
Second	1.67	09.0	1.43	18.1	1.09	03.8
Third	1.08	09.0	1.53	11.1	1.43	13.9
Fourth	0.37	08.3	0.51	00.5	0.82	18.9
Second Harmonics						
Quarter						
First	1.14	09.1	0.88	07.4	1.36	11.7
Second	1.19	05.4	0.96	04.6	1.47	01.3
Third	0.63	02.5	1.87	05.9	2.07	10.0
Fourth	1.86	03.5	0.90	07.9	0.11	9.9

(a) = Amplitude (%)

(b) = Phase (hr)

(c) = Amplitude (%)

(d) = Phase (hr)

(e) = Amplitude (%)

(f) = Phase (hr)

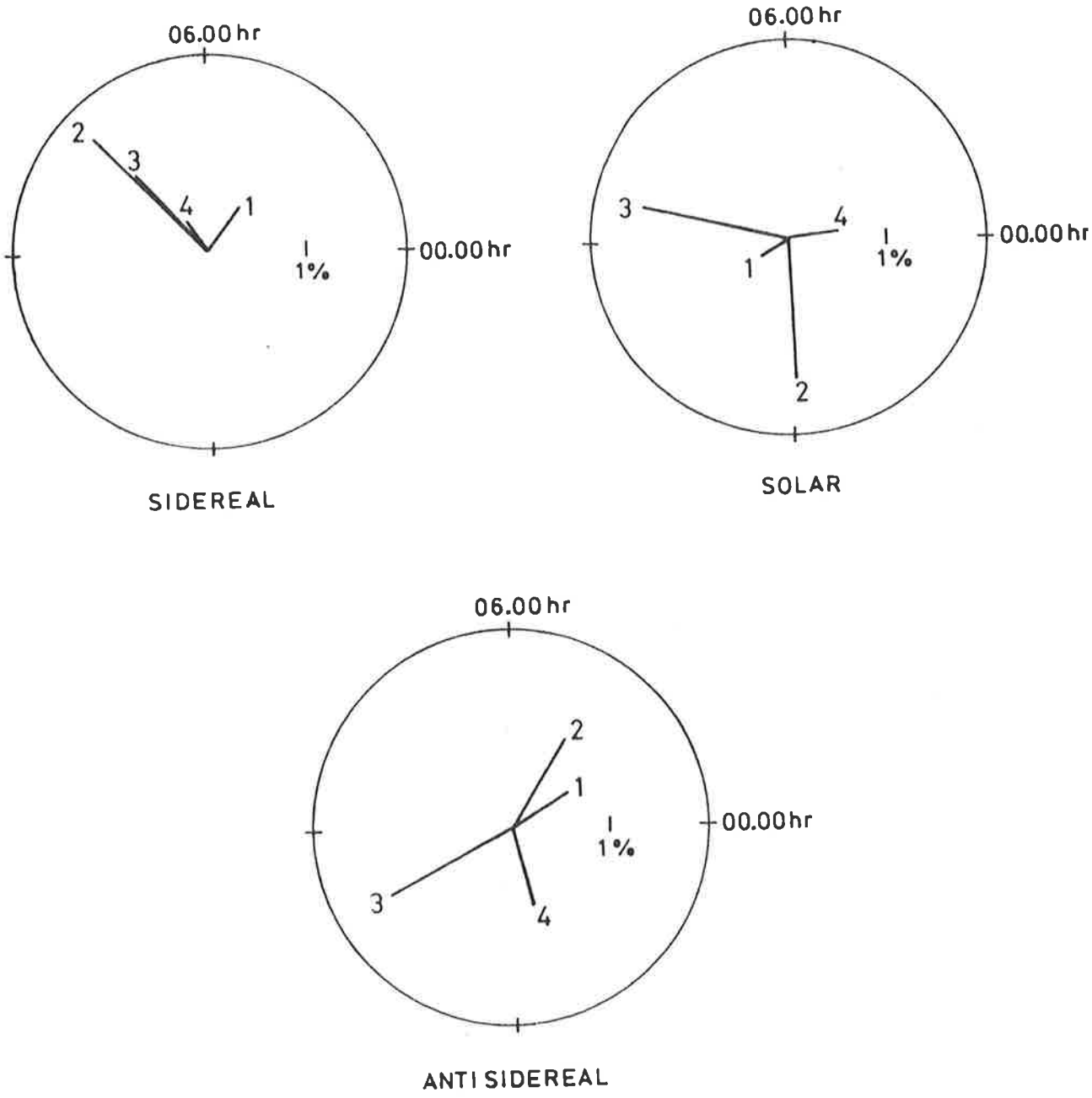

Figure 5.14a Quarterly first harmonic vectors

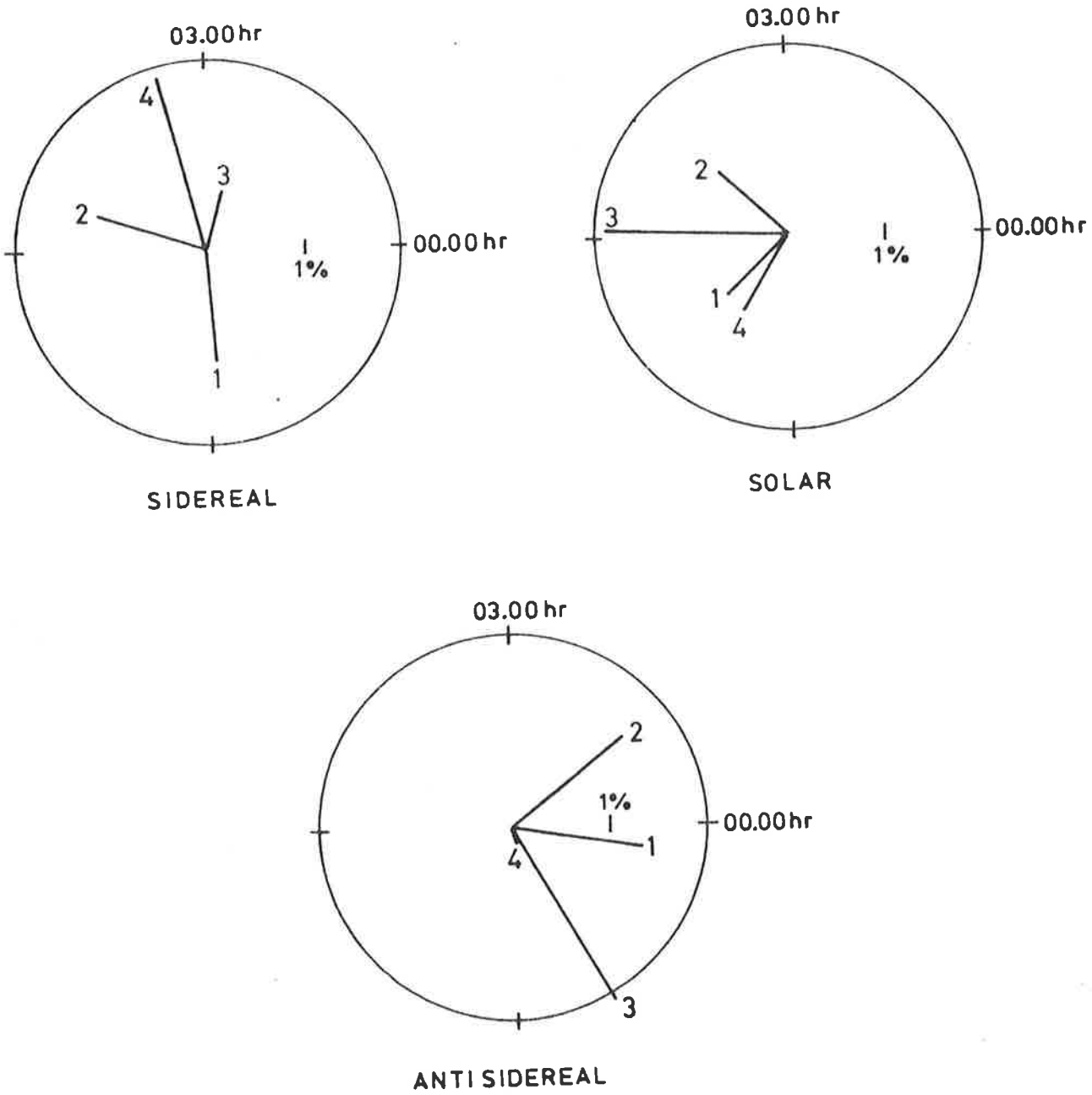

Figure 5.14b Quarterly second harmonic vectors

sidereal first harmonic shows remarkable consistency while the solar and antisidereal vectors are variable in phase.

Taken together with the previous results, there is strong evidence for a genuine sidereal first harmonic, while signals at other frequencies appear to be consistent with random distributions. On the other hand, the situation at second harmonic frequencies is more confused although the possibility of a genuine sidereal signal cannot be discounted. Due to the low significance of the sidereal, solar, and antisidereal first harmonics, no positive corrections can be made via the Farley and Storey antisidereal method without simply increasing the uncertainty of the sidereal vector.

5.4.3 Right Ascension Distributions

The assumption made in the previous section that the real anisotropy in the cosmic ray flux is independent of energy and declination in the detected sample, has no strong theoretical basis. To investigate any possible dependence, the data have been arbitrarily divided into three size bins - N_1 ($5*10^5$ - 10^6 particles), N_2 (10^6 - $2*10^6$ particles), and N_3 ($>2*10^6$ particles). Contamination of these size bins was minimized by converting the detected events to the equivalent vertical size before binning (including corrections for atmospheric variations) using the previously measured attenuation length of 185 g cm^{-2}. Using the calculations of Protheroe (1977), the size bins N_1, N_2

and N_3 correspond to mean primary energies of about $8*10^{15}$ eV, $1.3*10^{16}$ eV and $3*10^{16}$ eV. Only showers with near 100% detection probability were accepted. Unfortunately, due to the lack of adequate meteorological data in early 1979, it was necessary to reject a full year's data. These rejections reduced the number of events in each size bin to about $5*10^3$. Previous results, e.g. Linsley and Watson (1977) have indicated that the Right Ascension anisotropy in the vicinity of these energies is of the order of 1%. Clearly the statistics available in this experiment are insufficient to accurately determine such a small variation although upper limits will be given.

The results are given in table 5.9. Apart from the anomalously high Right Ascension first harmonic in the low energy bin, the sidereal signals are not well resolved from the statistical noise although a phase change between N_1 and N_2 is apparent. Solar and antisidereal vectors have been determined in case these signals give information not clear in the large data groupings. The first harmonics at these frequencies give somewhat contradictory information with large antisidereal signals appearing together with small solar signals and vice versa. Considering the earlier statistically more important results, these are probably the products of statistical fluctuations. Similarly, the second harmonics at these frequencies give little information - most of the variations remain below the RMS noise level. Second harmonic Right Ascension signals are generally slightly larger than their counterparts and some phase consistency is evident.

Table 5.9 Analysis for Size Dependence (2 years data)

Size	Right Ascension			Solar	Antisidereal	
First Harmonics	Amp%	Phase	Amp%	Phase	Amp%	Phase
N_1	6.64	19.5	3.79	18.6	1.09	03.2
N_2	1.90	09.0	1.24	19.7	4.01	04.9
N_3	2.84	05.8	4.11	10.7	2.70	19.8
		Prob.		Prob.		Prob.
N_1		0.3		15.4		85.8
N_2		62.0		81.6		12.0
		35.3		11.3		39.0
Second Harmonics	Amp%	Phase	Amp%	Phase	Amp%	Phase
N_1	2.06	06.9	3.93	00.3	2.14	03.3
N_2	2.21	04.9	1.28	06.7	0.91	04.7
N_3	3.25	06.0	1.95	00.3	1.57	02.9
		Prob.		Prob.		Prob.
N_1		57.5		13.3		55.0
N_2		53.2		80.6		89.6
N_3		25.6		61.3		72.7

To investigate the large Right Ascension first harmonic in N_1, the data from the third year were included in a second analysis. The showers were corrected to their equivalent vertical size, however the (relatively small) atmospheric corrections were not made for this extra year. The results, shown in table 5.10 are generally quite consistent with the two year data for the solar and antisidereal harmonics with some amplitude fluctuations occurring although these are most often downwards. Similarly, the Right Ascension amplitudes show fluctuations although the general reduction is not so obvious. The large first harmonic is considerably smaller although still highly significant. It is interesting to note that for both first and second harmonics in Right Ascension, there is a phase change between size bins N_1 and N_2 while the phase is approximately constant between bins N_2 and N_3. Because of this phase consistency, the two largest shower size bins may be combined (N_4) to improve the statistics for showers with size greater than 10^6 particles (table 5.11).

It can be seen from these results that the solar and antisidereal variations are consistent with random noise distributions. The Right Ascension harmonics are both significant and with the data from table 5.10, estimates may be made of the genuine flux anisotropy. Linsley (1975a,b) has shown that, if $\underline{s}$ is the genuine vector anisotropy, then:

$$\underline{s} = \underline{r} + \underline{x}$$

Table 5.10 Analysis for Size Dependence (3 years)

Size	Right Ascensions		Solar		Antisidereal	
First Harmonic	Amp%	Phase	Amp%	Phase	Amp%	Phase
N_1	3.66	19.2	3.05	20.3	2.46	03.6
N_2	2.30	10.0	1.09	17.3	2.33	03.8
N_3	2.07	10.6	2.81	09.0	3.23	19.8
		Prob.		Prob.		Prob.
N_1		7.3		16.2		30.6
N_2		35.3		79.1		34.3
N_3		45.0		22.9		14.3
Second Harmonics	Amp%	Phase	Amp%	Phase	Amp%	Phase
N_1	2.72	07.82	2.98	01.43	0.63	06.49
N_2	2.38	04.84	0.20	07.20	1.82	00.67
N_3	4.33	03.56	3.41	01.27	0.45	09.02
		Prob.		Prob.		Prob.
N_1		23.4		17.5		92.5
N_2		32.5		99.2		50.9
N_3		3.0		11.5		96.3

Table 5.11 Anisotropy for size > 10^6 Particles

	Right Ascension		Solar		Antisidereal	
	1st hr.	2nd hr.	1st hr.	2nd hr.	1st hr.	2nd hr.
Amp%	2.18	3.29	1.15	1.66	1.42	0.84
Phase(hr)	10.3	04.0	10.6	01.5	22.9	01.5
Prob.	16.2	1.6	60.2	34.7	46.1	76.1

where $\underline{r}$ is the measured vector and $\underline{x}$ is the contribution from the Rayleigh statistical fluctuations. The amplitude of $\underline{s}$ may then be estimated by:

$$\langle s \rangle = r.(1-1/(2k_0))^{0.5} \qquad (5.17)$$

Table 5.12 gives the estimates of the genuine anisotropy calculated from equation 5.17. These are also shown in figure 5.15. The limits are those given by statistics from equation 5.5. Although the amplitudes of these sidereal signals are larger than the estimates made by Linsley and Watson (1977), it is significant that the phases are in excellent agreement. These results support the comment of Linsley (Pollock 1978) that for a population amplitude equal to the RMS noise, in a series of experiments the observed amplitude will only be significant in one experiment out of ten, whereas the phase will be within 50^{o} of the true phase in two experiments out of three.

The assumption of declination independence of the data has also been investigated. Unlike the Right Ascension exposure which is uniform over one sidereal day, the declination exposure is very non-uniform (figure 5.16). The declination exposure is determined by the azimuth and zenith angle distributions and may in principle be determined theoretically. However, the azimuth and angle distributions are themselves functions of the rather complex interaction between the atmosphere and the array triggering conditions,

Table 5.12 Best Estimates of the Genuine Anisotropy in Right Ascension

Size Range	Mean Energy (eV)	No. of Events	R.A. (First harmonic)		R.A. (Second harmonic)		σ_r	σ_{θ_1}	σ_{θ_2}
			s	θ	s	θ			
$5\times10^5-10^6$	8×10^{15}	7831	3.29	19.2	2.20	07.8	1.60	1.9	2.8
$> 10^6$	1.7×10^{16}	15340	1.86	10.3	3.09	04.0	1.14	2.3	1.4

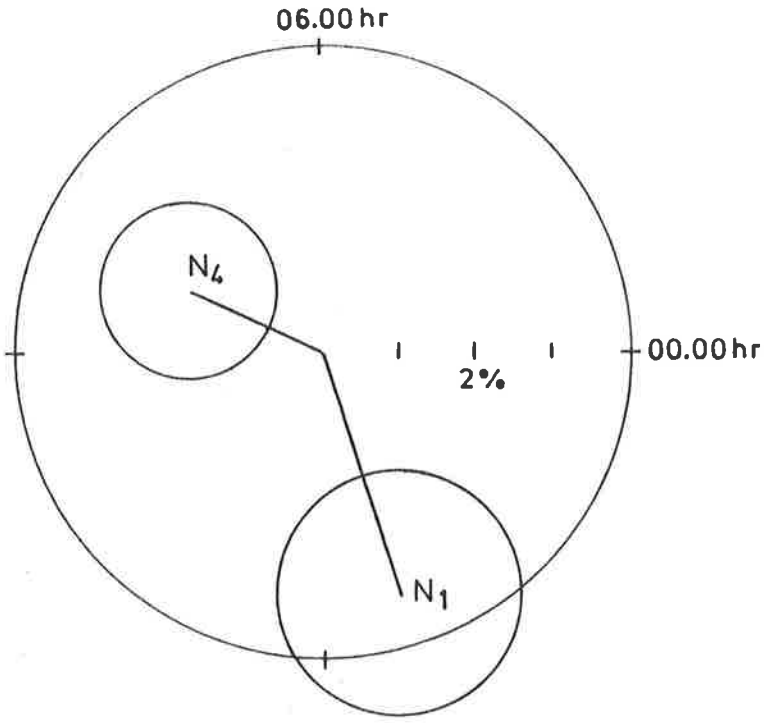

(a) RIGHT ASCENSION – FIRST HARMONIC

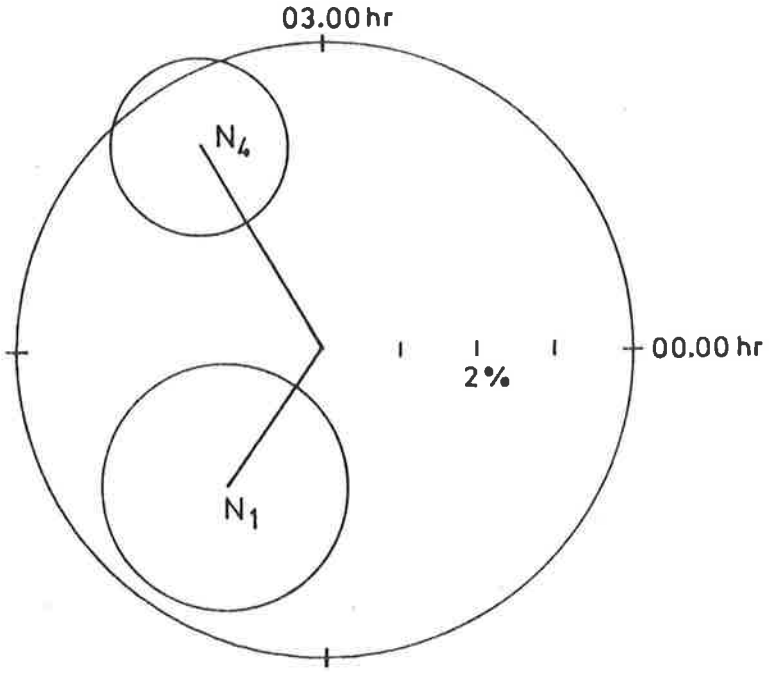

(b) RIGHT ASCENSION – SECOND HARMONIC

Figure 5.15 Shower size dependence of the measured Buckland Park anisotropy

N_1 less than 10^6 particles

N_2 greater than 10^6 particles

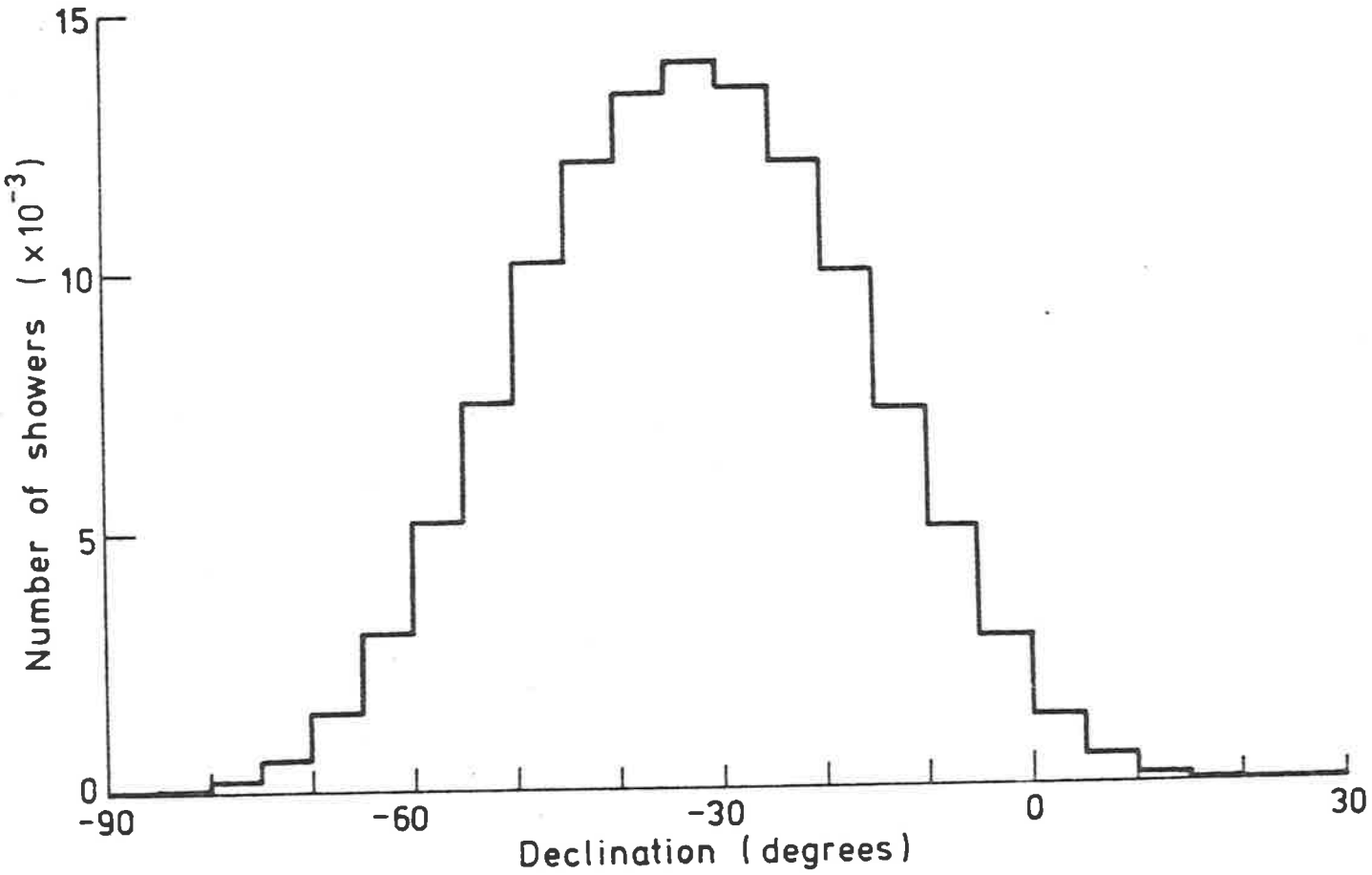

Figure 5.16 The declination distribution of events detected at Buckland Park

details of which are not available. Therefore no attempt has been made to theoretically evaluate the distribution.

To test the independence of the anisotropy to the declination, the data have been arbitrarily divided into two declination strips - North (from -5 to -30°) and South (from -35° to -60°) and analysed for Right Ascension variations. This technique was first performed using the whole data set, excluding only showers with poor analysis or recording errors. The results are shown in table 5.13 below. It is clear that these results give no indication of variations of the amplitude of the sidereal anisotropy and the phases show excellent agreement. Statistical tests on the number of events from each declination strip cannot easily be used to determine a flux variation since these declination ranges are not equally exposed to the Buckland Park array, the zenith corresponding to a declination of about 34.5°. Also, the slightly non-uniform North-South azimuth distribution of the array interferes with this comparison. As a rough check however, the numbers are compatible with equal probability of events from either declination strip at the 95% significance level.

In view of the energy dependence found earlier, this should be investigated in the declination dependence. To this end, the size bins N_1 and N_4 have been analysed for declination variations of the Right Ascension anisotropy. This analysis uses the same three years of data checked earlier, with equivalent vertical sizes and triggering

Table 5.13 Declination Dependence of All Showers (in RA)

	No. of Events	First Harmonic			Second Harmonic		
		Amp (%)	Phase (hr)	Prob	Amp. (%)	Phase (hr)	Prob.
North	47826	1.03	08.6	28.0	0.86	02.6	41.1
South	48276	0.92	08.9	36.2	1.11	04.2	22.8

probability near 100%. The results, shown in table 5.14 are difficult to interpret because of the rather sparse statistics and arbitrary data division. Thus, genuine sidereal amplitudes at the sizes indicated are difficult to justify on the basis of the propagation of the primary particles or other anisotropy measurements. The consistency of the phases with the earlier measurements presented is interesting although the 12 hour phase change associated with large amplitude variation in the high energy first harmonic should be carefully examined. It is obvious that much better statistics are required before conclusions about the declination dependence of the Right Ascension anisotropy can be drawn. It should also be emphasized that these declination bins are drawn only from the Southern Hemisphere.

5.5 Other Measurements on the Flux

5.5.1 Declination Anisotropy

As shown in the previous section, the determination of the array declination distribution is a non-trivial problem. As a result, estimates of the deviation from isotropy of the cosmic ray flux as a function of declination are not easily made. This is especially so if details of the structure of the anisotropy are required. Simple estimates of the flux difference from different declinations may however be made.

Table 5.14 Declination Dependence of Right Ascension for Shower Size

		Bins N_1 and N_4					
N_1	No. of Events	First Harmonic			Second Harmonic		
		Amp(%)	Phase(hr)	Prob.	Amp(%)	Phase(hr)	Prob.
North	1972	5.50	17.74	22.5	0.66	02.87	97.9
South	2232	9.55	19.64	0.1	3.75	04.08	45.7
N_4							
North	6074	4.58	09.25	4.1	2.68	02.66	33.5
South	5966	0.95	21.23	87.5	5.38	05.56	1.3

Two identical but distinct regions of the sky have been investigated by taking Buckland Park data from two azimuthal quadrants about the Northerly and Southerly directions, the azimuthal angles of acceptance being 325^{o} to 45^{o} and 135^{o} to 225^{o} (Clay and Gerhardy 1982b). To ensure that the declinations of these data groups were distinct, accepted events were also restricted to those arriving from zenith angles between 28^{o} and 40^{o}. These restrictions defined two clearly distinct event populations in terms of declination as seen in figure 5.17. To avoid variations in the showers accepted due to collecting area effects, the events used were confined to well analysed showers within the size range from $2.3*10^{5}$ particles to $1.8*10^{6}$ particles. Because of the large zenith angle, these showers were considerably attenuated from their equivalent vertical sizes and the mean energy was estimated to be about 10^{16} eV.

The total number of events accepted from four years of data was 7909. Of these 4079 were detected in the Southerly quadrant and 3830 in the Northerly quadrant. Although near symmetry, when tested statistically, the hypothesis of equal probabilities of arrival from each direction was rejected at the 1% significance level.

This result suggests a declination anisotropy of about 3% with maximum towards Southern declinations. It should be noted that the azimuth angle distribution discussed in Chapter 2 has a first harmonic with the phase of maximum in the

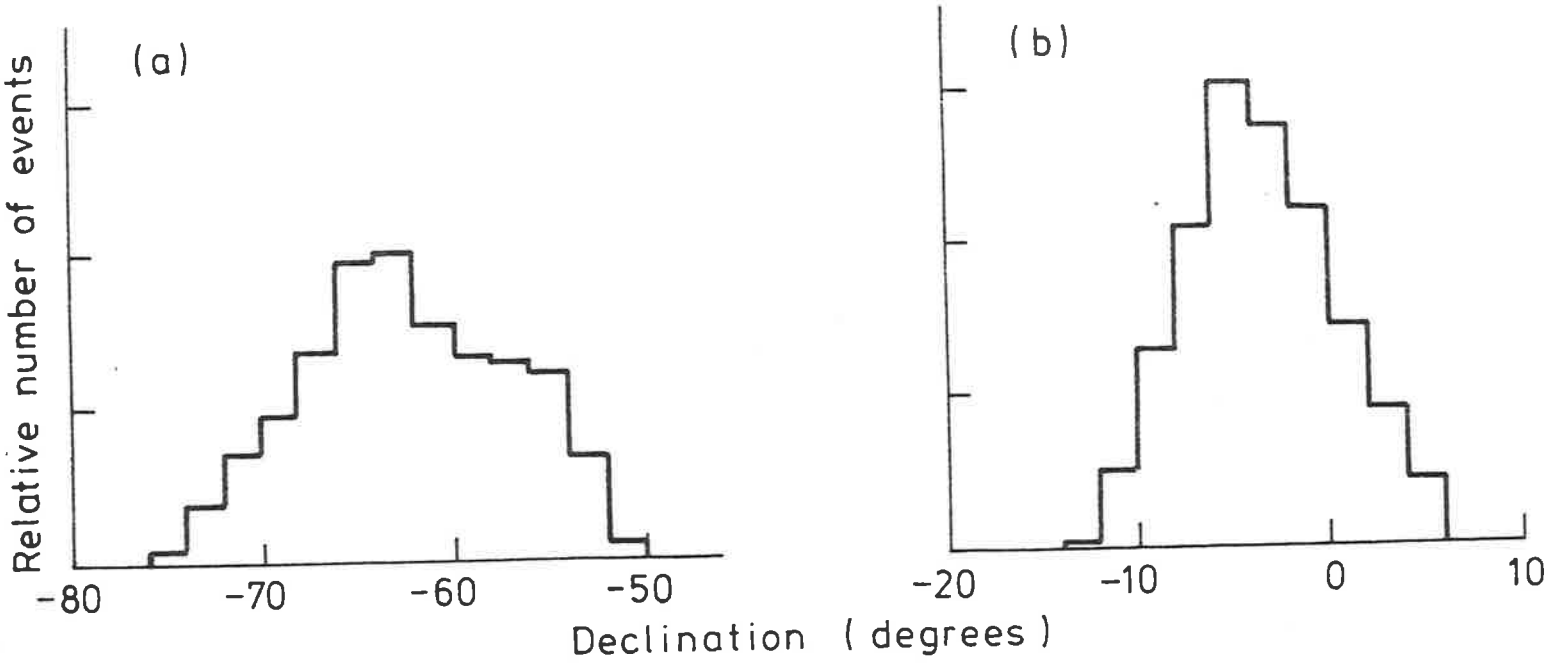

Figure 5.17 The declination distribution of shower arrival directions for the two lobes of selected showers. (a) the southerly beam (b) the northerly beam

Northerly direction, probably resulting from imbalance in the fast timing system. The effect of this asymmetry is to amplify the probability of flux variations in the declination distribution.

Further information on the declination variation of the cosmic ray flux can be obtained using data from other observatories. In Chapter 3, the size spectrum obtained by the Akeno array (latitude 35^{o} N) was compared to that measured at Buckland Park (latitude 35^{o} S). After differences in calibration and analysis have been removed, the resulting intensity difference is less than 10%, placing an upper limit on the flux anisotropy at the declinations observed of about 5%.

Both these results suggest a slight flux enhancement from Southerly declinations.

5.5.2 Event Arrival Time Intervals

The time spacing of cosmic ray events is generally considered to be close to random due to the source distribution and the randomizing effect of the galactic magnetic field on charged particles during propagation from their sources. However a number of experimentalists (Bhat et al 1979, Bhat et al 1980, Badino et al 1980) have found evidence which suggests time correlations in the arrivals of events on scales of less than a minute for cosmic rays with

primary energies of greater than about 10^{14} eV.

This surprising result has few possible interpretations. The most likely possibility is that the primary particles are neutral particles, probably gamma rays, from a single source with relatively small dimensions. Possible candidates for these are pulsars (Gibson et al 1982) and gamma ray burstars (although these are rather rare). For measurable time correlations to occur, these sources would be required to contribute a significant proportion of the cosmic ray flux at these energies and directional anisotropies should be clearly measurable in point source searches. If the correlated events are produced by charged particle primaries, small scale smoothness of the galactic magnetic field is required. In this case, particles produced (or accelerated) nearly simultaneously at a source of small dimensions would not be randomized by scattering, but would propagate together along the field lines and be detected at the Earth in bunches. The important points in these conjectures are the small scales of the sources and the smoothness of the magnetic field since even very small irregularities over the interstellar distances would destroy the correlation at the Earth. Although the intensive anisotropy measurements at these primary energies have produced little support for these results, (see Section 5.2) point sources at these energies would be very difficult to resolve due to the meagre directional information provided by arrays which use atmospheric collimation.

The Buckland Park data (at slightly higher energies)

have been analysed for corroborative evidence for these time correlations (Clay and Gerhardy 1980b). Since the time of each detected event is recorded by the array to an accuracy of about one second, the data record may be searched for time correlations by an examination of the relative event arrival times. The arrival time distribution for 17 months of data from Buckland Park is shown in figure 5.18 in 40 second bins. To allow for the recording time required by subsidiary experiments, a dead-time of 30 seconds is built into the recording system, although the detection logic remains active. This dead-time precludes the detection of correlations in the arrival times of less than 30 seconds, the region where correlations were detected by Bhat et al (1979). A parallel recording system using a Commodore PET microcomputer which recorded the time intervals between all events satisfying the triggering conditions was used to overcome this problem. These data are shown in figure 5.19.

For random events, the probability distribution of times is given by an exponential (as for radioactive decay):

$$p(t)=k.\exp(-t/T) \qquad (5.14)$$

where t is the time between events and T is the mean interval. This form was fitted to the data in figures 5.18 and 5.19 resulting in the solid lines on the figures. Although some events (about 7%) are lost in the dead-time from the first bin in figure 5.18, these are replaced by a similar number from intervals where the first event occurs during the

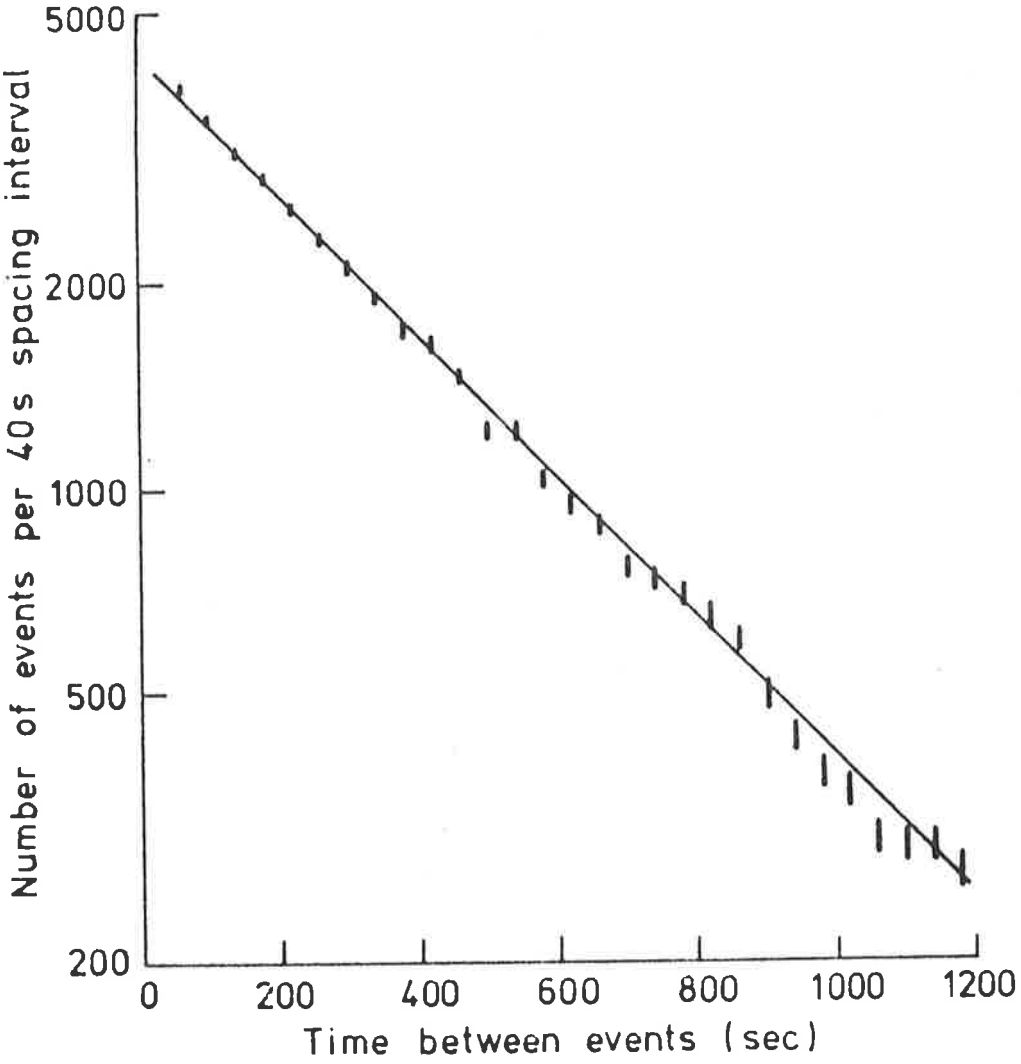

Figure 5.18 The distribution of time intervals between events as recorded by the Buckland Park array. These data have been binned in 40s intervals. In this mode of operation the array has a built in dead time of 30 s.

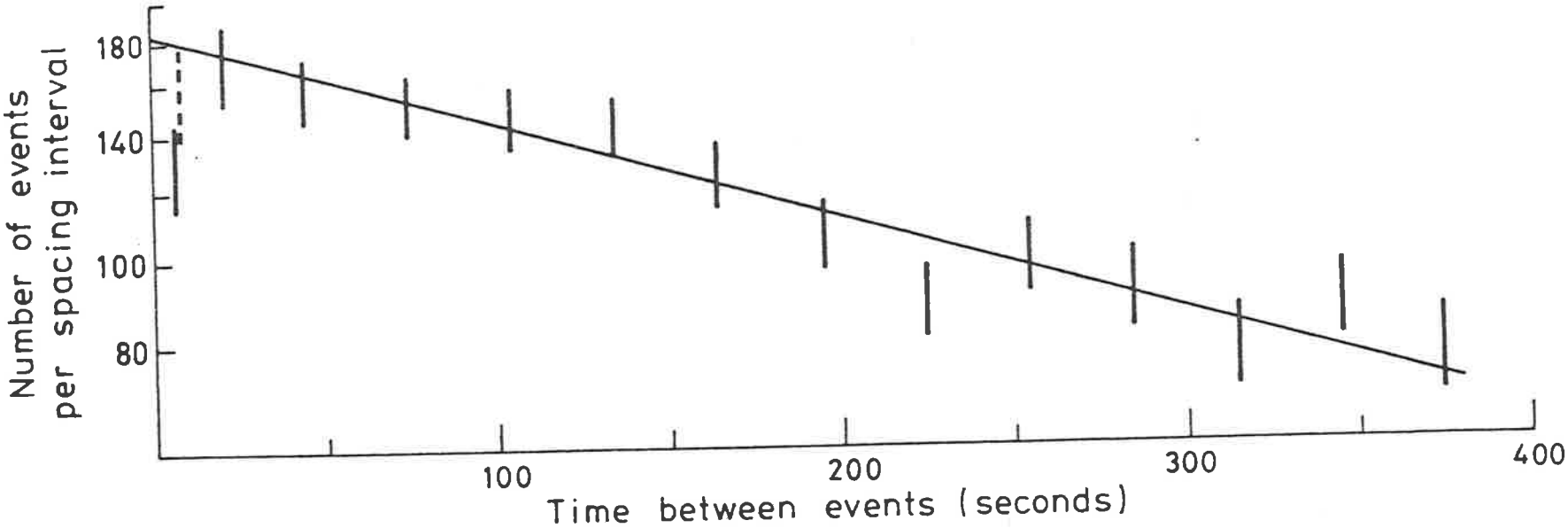

Figure 5.19 The distribution of time intervals between events using a counting system (Commodore PET) with a minimal dead time. The first bin is corrected for dead time effects (dashed line)

dead-time. Thus the argument for randomness of the intervals is not significantly affected. Similarly, some data is lost in the PET dead time although this is much less than 1 second. A correction for this effect is given in figure 5.19.

The exponential best fits to the data are characterized by the mean intervals. These are:

Intervals	Mean Interval
all data	415+-4 s
t<=200 s	395+-22 s
440 s<t<1200 s	418+-8 s

An extra benefit associated with the measurement of the mean time intervals was derived from the consistency of this parameter over the time periods measured. Long term fluctuations in the mean interval were within statistical expectations, confirming the stability of the array required for anisotropy measurements.

Excesses in the small time interval bins are within the statistical range expected i.e. within a standard deviation. No support is therefore found for correlated events. Since the region of the sky viewed and the energy range are different to those of the other observers, the null results may be due to an energy cutoff or change in the radius of gyration or simply because the source, if the primary particles are neutral, is not within the region of the sky viewed by the array. Clay and Dawson (1981) have conducted a

similar search to that reported here, but at the energies suggested by Bhat et al (i.e. above 10^{14} eV), but also find no evidence for correlated events.

5.5.3 Gamma Ray Primaries near 10^{16} eV

If gamma rays form a significant component of the high energy cosmic ray flux, some correlations of their arrival directions with astronomical objects might be expected. In response to high energy photons, the atmosphere produces cascades of particles similar to the EAS produced by charged particles, the difference being that only an electromagnetic component is produced. At low energies the cascades die out high in the atmosphere, but for energetic photons (greater than about 10^{13} eV) the showers may be detected at sea level. Grindlay et al (1975) have used the Cerenkov radiation produced by the cascades with primary energies greater than $3*10^{11}$ eV to look for correlations of the directions of the primaries with known possible energetic sources such as pulsars, X-ray sources and active galaxies. Although the shower itself at these energies is unlikely to reach sea level, the Cerenkov radiation produced is little attenuated and can be easily detected. Care was taken to exclude showers with charged particle primaries from the events collected and a number of correlations were found.

At the energies accessible to the Buckland Park array, it was thought that possible gamma ray sources should include

the highest energy gamma ray events - gamma ray bursts. These are identified as sharp increases, with short durations (about 10 seconds), in the counting rate of spacecraft-mounted scintillator detectors sensitive to high energy photons. They occur irregularly and the maximum energies detected (above about 1 MeV) are limited by the detector sizes. The actual sources of the bursts are unknown and none of the detected bursts have been positively identified with known astronomical objects, although the most notable event detected (March 5, 1979), with an intensity much larger than the normal events, has been tentatively linked to a supernova remnant (N49) in the Large Magellanic Cloud. This identification is in doubt however, since at that distance, the energy of the burst integrated over the whole sky is dauntingly large. Physical mechanisms for the burst production include pulsars and their magnetic fields (e.g. Katz 1982).

Directional information on bursts derives from two possible methods. The most accurate information is obtained from triangulation using the relative detection times by three or more non-coplanar spacecraft (Evans et al 1979) although lower numbers of satellites may give information if alternative arrival directions can be eliminated by for example the Earth's shadow. Alternatively, if a single spacecraft has a number of anisotropic detectors, the response of each of these to a burst can give lower grade directional data (Mazets and Golinetskii 1981).

A search of air shower data from Buckland Park for

correlations with known gamma ray bursts has been made (Clay et al 1982c). The bursts investigated come from a list of 94 events occurring between May 1978 and May 1979. Of these 43 were immediately eliminated because their arrival coordinates were inaccessible to the Buckland Park array, or they coincided with off-times for the array. Of the remainder, only three had well defined arrival directions and times which could be compared with the recorded array data. The large March 5, 1979 event was also included although the zenith angle of this event would have been 63^{o} as observed by the array. However, very high energy photons (greater than 10^{18} eV) would have been detected. Details of these four events are given in table 5.14.

The celestial coordinates of EAS events detected within +-30 minutes of the local time coinciding with these bursts were calculated and are plotted in figure 5.20 (a), (b), (c) and (d). From these data, no EAS can be positively identified with any of the bursts, that is for all the bursts less than one photon per burst was detected.

Using the known collecting area of the array, upper limits may be placed on the photon flux. Above 10^{16} ev for events (a), (b) and (c), the photon flux at the Earth was less than $4*10^{-5}$ m^{-2}. The large zenith angle of event (d) reduces the array collecting area by foreshortening, and also the energy required for detection is much greater. Therefore, the only upper limit on the photon flux is for greater than 10^{18} eV with an upper limit of about $7*10^{-5}$ m^{-2}.

Table 5.15 Gamma Ray Bursts within Array 'Beam'

	Date	Time(UT)	Energy Flux (E 30keV) ergs cm^{-2}	Arrival Directions R.A. (hr)	dec.(^{0})
(a)	2 Jan 1979	17.56	$6.5*10^{-6}$	6.79	-76.0
(b)	31 Mar 1979	21.03	$7.9*10^{-4}$	19.48	- 5.88
(c)	2 Apr 1979	09.42	$3.7*10^{-5}$	7.83	-55.8
(d)	5 Mar 1979	15.52	$1.3*10^{-3}$	5.45	-66.07

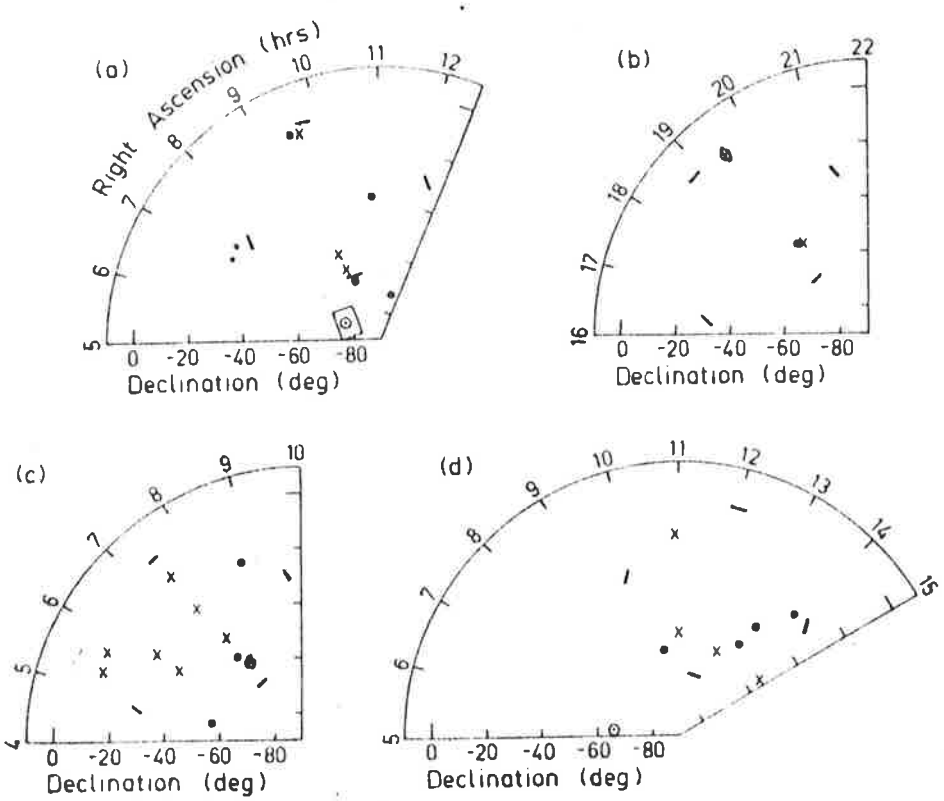

Figure 5.20 Arrival directions of cosmic ray showers detected within ± 30 minutes of gamma ray bursts. Circles (surrounded by error box) - direction of burst, crosses - arrival directions of showers within ± 15 minutes of burst, dots - arrival directions of remaining events within ± 30 minutes. The solid lines indicate the effective array beam. The bursts follow the naming of table 5.14.

These limits suggest that only a very small cosmic ray flux component comes from gamma ray bursts.

CHAPTER SIX

DISCUSSION OF RESULTS

6.1 The Spectral Shape

Conclusions about the shape of the primary energy spectrum between 10^{15} eV and 10^{17} eV cannot be made without a knowledge of the mass composition of the primary particles - a topic which until recently was the subject of considerable controversy (Thornton and Clay 1979, Orford and Turver 1980), although the situation now appears to be clearer (Andam et al 1982, Hillas 1981). Until accurate extrapolations to the top of the atmosphere are possible, it is important that the size spectrum be well known.

The array density spectrum presented here clearly shows a rapid change in the power law index. In the region corresponding to median shower sizes between about 10^5 particles and $4*10^5$ particles, the integral spectral index changes from about 1.4 to about 1.9 after which it remains constant up to at least 10^7 particles . Allowing for some smearing of the size spectrum shape in the density spectrum (Allan priv. comm. 1979, Wenneberg 1982), this indicates a sharp change in the shower size spectrum near $3*10^5$ particles. This result is in agreement with the Buckland Park

size spectrum measured using assumed lateral distributions, although the sharpness of the change deduced from the array density spectrum is not apparent. The size spectrum shows a fairly gradual change in the power law index from about 1.3 to 2.0 in the size range from 10^5 particles to 10^7 particles. Although there is quantitative agreement about the amplitude of the spectral change, the difference between these spectra suggests variations in the lateral distribution of particles in these showers.

These variations in the lateral distribution are demonstrated by the variation of the average lateral age parameter of the showers detected. It should be emphasized however, that this measure of the lateral distribution change is only qualitative. The work of Capdevielle and Gawin (1982) shows that the lateral age parameter is itself a function of the core distance so that the value fitted to the age parameter is a function of the detector positions. If a detector distance parameter can be defined by some statistical weighting of the particle density measured by each detector (in the same way that density measurements are weighted for determining the shower core position), since the array collecting area varies with shower size, it can be seen that this distance parameter will vary slowly (because of the array geometry) with shower size. Hence the distance corresponding to this heaviest weight for the fitting of the lateral age parameter also varies. Fortunately, the calculations of Capdevielle and Gawin (1982) indicate that between core distances of 10 metres and 100 metres, changes in the age

parameter are slow so that the qualitative conclusions hold. It may be then, that the lateral distribution function (NKG) used in the present work is not sufficiently accurate to show the detailed structure of the shower size spectrum. Modifications to the NKG function have been used for example at Akeno (Hara et al 1979a), however for the details required to be observed, this should also include provisions for rapid changes over the size interval indicated.

Support for these changes in shower development come especially from depth (in the atmosphere) of shower maximum measurements presented by for example Thornton and Clay (1979). These indicate that the depth of maximum increases in the region between 10^5 particles and 10^7 particles much more rapidly than can be accounted for by conventional composition and nuclear interaction models. Linsley and Watson (1981a) have interpreted this as a change in the logarithmic mean primary mass number, $\langle \ln A \rangle$, from 4 (+-2) at $1.6*10^{15}$ eV to 0 (+0.6,-0) at $3*10^{16}$ eV, that is a change in the mean composition from predominantly iron primaries to predominantly proton primaries with the nuclear interactions following scaling with rising hadron - air cross sections. However this is not the only possible interpretation, and Clay and Gregory (priv. comm. 1982) have suggested the possibility of a change in the nuclear interactions near 10^{15} eV (about 10^3 GeV in centre of mass) to explain the spectral features. McCaughan (1982c) has also suggested changes in the nature of the interactions at near 10^{15} eV to explain the results of density spectrum measurements made at

various altitudes near the shower cores and he has shown that these interaction changes may masquerade as changes in the primary composition.

The suggestion of interaction changes is supported by measurements of the shower frequency absorption length. Bourdeau et al (1980) showed that the absorption length was sensitive to the nuclear interaction model and mass composition. A number of models and varying compositions were used to derive the dependence of the absorption length on shower size, however the measured results were not sufficiently refined for the rejection of many of the models. The data presented here has error limits of less than 5% and places stringent conditions on the available theories. From the calculations of Bourdeau et al, the best model is a CKP model with rising proton-air cross sections and proton primaries. However the fit of this model to the observations remains poor. The list of models used by Bourdeau et al was not exhaustive however, and the Linsley and Watson result cannot be eliminated.

6.2 The Anisotropy

Measurements of the anisotropy in the medium energy flux are in good agreement especially in phase with the compilation of Linsley and Watson (1977), although the accurate determination of the amplitude is hampered by relatively low statistics. This is rather interesting since

that compilation was dominated by experiments viewing the Northern sky. The only comparable experiment, the early counting rate experiments of Farley and Storey (1954, 1957) also show agreement with these data although the rapid phase change from maximum at about 19.00 hours RA to about 10.00 hours RA at energy near 10^{16} eV is not so obvious. The significance of these observations is indicated by the comment of Linsley (Pollock 1978) mentioned earlier with good phase agreement but relatively poor amplitude agreement.

Mass composition and the detailed shape of the energy spectrum in this region are important for information on the origin of these particles. The feature of the spectrum, the 'knee' or 'bump' near $3*10^{15}$ eV has had a number of interpretations (which were discussed in Chapter 1) ranging from rigidity dependent leakage of primary particles from a leaky box model (Peters 1961) to the injection of a second component from pulsars (Karakula et al 1974) into the spectrum.

Both models have difficulties, an important one in the leaky box model being the primary mass change from heavy to light discussed in the previous section. This change is the reverse of that expected for leakage unless the proton leakage occurs at lower energies than expected (due to a weaker galactic magnetic field). If this was the case, a second proton component, perhaps extragalactic, would have to become important at just above 10^{16} eV. Evidence from the increasing anisotropy with energy (Lloyd-Evans 1982) however,

indicates that this is not likely until above 10^{17} eV.

Similarly, the general shape of the spectrum including a pulsar component is in agreement with that expected from conventional shower development models with proton primaries. However, if the depth of maximum data does indicate a change in the mass composition with the iron component being produced by pulsars , the peak of the 'bump' is moved upwards in energy from about $3*10^{15}$ eV by a factor of about 34 (see equation 1.1). This result obviously presents problems, the only obvious solution being that the Ostriker and Gunn (1969) mechanism is incorrect.

The change in mass composition at the 'knee' which has been proposed is attractive from the point of view of the anisotropy measurements, since the change in the phase of maximum could then be explained by the change in the radius of gyration of the primary particles in the galactic magnetic field if the primary sources remain the same. Also, if the mass change is in the direction indicated, the radius of gyration of the particles (from equation 5.1) would be rapidly increasing in the transition region, suggesting a rapid increase in the amplitude of the anisotropy. This increase is quite compatible with the empirical increase (as $E^{0.5}$) suggested by Linsley and Watson (1977).

Although no clear information on the origin of the particles in this energy interval is available from the anisotropy data, the apparent steady increase in the amplitude

indicated by the compilation of these data argue in favour of a galactic origin.

6.3 Conclusions

At the present time, the least well defined part of the cosmic ray spectrum is the energy region between 10^{15} eV and 10^{17} eV (ignoring the low statistics above 10^{19} eV). Although it is clear that rapid changes of some description take place, it cannot yet be determined whether or not these are changes in the primary composition or nuclear physics occurring at these energies, or both. It is most important then, that the question of composition near the spectral 'knee' be resolved.

The measurements of the anisotropy presented here indicate that the flux from the Southern sky is changing rapidly in direction as well as in isotropy. For clarification, the statistics should be extended to reduce the noise level to the region of 0.1% requiring of the order of $4*10^6$ events. At the present rate of data collection this is impractical for the Buckland Park array. However in combination with other arrays, statistics approaching these might be achievable. As well as the rough structure given by harmonic analysis, some finer details might then be accessible.

In combination with detailed magnetic field

information and a reliable energy spectrum, it may then be possible to determine the origin of these obscure particles.

APPENDIX 1

Shower Arrival Direction Analysis

Given fast timing detector locations at $\underline{r_i}$ (x_i, y_i) and relative arrival times of the shower front at the detectors of t_i, the shower axis is defined by the direction cosines (l,m,n) (or arrival directions θ (zenith angle) and ϕ (azimuth angle)). Assuming a plane shower front and horizontal array (z-coordinate is zero), since the shower travels at the speed of light, c, then:

$$c.t_i = l.x_i + m.y_i$$

The direction cosines are then determined by minimizing the least squares fit:

$$S = \sum_i (c.t_i - l.x_i - m.y_i)^2$$

i.e.
$$\partial S/\partial l = 2.\sum_i (c.t_i - l.x_i - m.y_i).x_i$$
$$\partial S/\partial m = 2.\sum_i (c.t_i - l.x_i - m.y_i).y_i$$
$$= 0 \quad \text{for } S = \text{minimum.}$$

therefore
$$c.\sum_i t_i.x_i - l.\sum_i (x_i)^2 - m.\sum_i x_i.y_i = 0$$

and
$$c.\sum_i t_i.y_i - l.\sum_i x_i.y_i - m.\sum_i (y_i)^2 = 0$$

for the symmetrical fast timing array:

$$\sum_i x_i = \sum_i y_i = \sum_i x_i.y_i = 0$$

hence
$$l = c.\sum_i t_i.x_i / \sum_i (x_i)^2$$

$$m = c \cdot \sum_i t_i \cdot y_i / \sum_i (y_i)^2$$

$$n = (1 - l^2 - m^2)\,0.5$$

The shower arrival directions are then given by:

$$\Theta = \arccos(n)$$

$$\phi = 90^{o} - \arctan(l/m)$$

APPENDIX 2

Core Location and Shower Size Analysis

Given density detector locations at $\underline{r_i}$ (x_i,y_i) and measured densities ρ_i, it is required to determine the shower parameters, N_e (the shower size), and (x,y) the core location using the lateral distribution function:

$$\rho(r)=a.N_e.\exp(-r/r_0)/r$$

where r_0 and a are constants. This can be rewritten as:

$$\rho(r)=A.\exp(-r')/r'$$

where $$r'=r/r_0$$

The problem is solved by least squares minimization of:

$$R=\sum_i w_i.(\rho_i-A.\exp(-r_i')/r_i')^2$$

where w_i the weight is set to $1/\rho_i$. The core location is first chosen by a weighted mean of the densities i.e.:

$$x=\sum_i x_i.\rho_i/\sum_i \rho_i$$
$$y=\sum_i y_i.\rho_i/\sum_i \rho_i$$

Minimizing R, dR/dA=0, hence:

$$A = \sum_i (w_i . \rho_i . \exp(-r_i')/r_i') / \sum_i w_i . (\exp(-r_i')/r_i)^2$$

The shower size, N_e, is then determined from A by the normalization of the lateral distribution function:

$$N_e = \int_0^{2\pi} \int_0^{\infty} \rho(r) . r . dr . d$$

This evaluates the shower size, N_e for core location (x,y). The final analysis is completed by minimizing R as a function of the core location, that is, the gradient of the 'R surface' is calculated and the core location moved in the direction of the minimum with gradually reducing step sizes.

APPENDIX 3

Harmonic Analysis (see Chapman and Bartels 1940, Linsley 1975a,b)

For a series of measurements resulting in N equal amplitudes with phases $\phi_1, \phi_2, \ldots\ldots \phi_N$, the m^{th} Fourier harmonic is characterized by an amplitude r and phase Θ given by:

$$r=(a^2+b^2)^{0.5}, \qquad \Theta=\arctan(b/a)$$

where $$a=(2/N).\sum_i \cos(m\phi_i), \qquad b=(2/N).\sum_i \sin(m\phi_i)$$

with Θ found in the appropriate quadrant, i.e.

if	a,b>0	Θ in 1st quadrant
	a<0,b>0	2nd quadrant
	a,b<0	3rd quadrant
	a>0,b<0	4th quadrant

If N>>0 and the phases ϕ_i are randomly distributed between 0 and 2π, the probability of obtaining an amplitude between R and R+dR and phase between Θ and $\Theta+d\Theta$ is given by:

$$w(R,\Theta)dRd\Theta=(NR/4\pi).\exp(-NR^2/4)dRd\Theta$$

hence the probability of obtaining an amplitude greater than or equal to R is:

$$W(>=R)=\exp(-NR^2/4)=\exp(-k_0)$$

The probability distributions for R and Θ approach Gaussian for N large enough with widths:

$$\sigma_R=(2/N)^{0.5} \qquad \sigma_\Theta=(2k_0)^{-0.5}=\sigma_R/R$$

The RMS amplitude due to noise fluctuations may be defined for $k_0=1$ as (Edge et al 1978):

$$r_{RMS}=2/N^{0.5}$$

Harmonic analysis of the cosmic ray flux data was carried out by sorting the data into h bins each containing n_i events with an exposure time t_i. The components a and b were then defined by:

$$a=((2/h).\sum_i(n_i/t_i).\cos(m\phi_i))/<r>$$

$$b=((2/h).\sum_i(n_i/t_i).\sin(m\ _i))/<r>$$

where $<r>=<n_i/t_i>$

r and Θ are then defined as before.

If the exposure times are non-uniform, the probability contours in the a, b plane are elliptical compared with the circular symmetry for even exposure. The probability is still defined as before, however k_0 is modified but may be approximated by (Pollock 1978):

$$k_0 = r.(a^2+b^2)/4.\langle n_i^2/t_i^2\rangle$$

If $\underline{r} = \underline{s} + \underline{x}$ where $\underline{r}$ is the measured vector, $\underline{s}$ is the true vector and $\underline{x}$ is the Rayleigh fluctuation, then if $k_0 >> 1$ $\underline{x}$ is unimportant, however as $k_0 \rightarrow 1$ $\underline{r}$ tends to overestimate $\underline{s}$ and for $k_0 >= 1.5$, $\langle s \rangle$ may be approximated by (Linsley 1975a):

$$\langle s \rangle = r.(1-1/(2k_0))^{0.5}$$

below which point the approximation begins to break down due to a tendancy for $\underline{r}$ to underestimate $\underline{s}$. Figure A.1 drawn from Linsley (1975a) shows confidence limits and expectancy for s/r. The best estimate of Θ is the observed phase. The 95% error in Θ is also shown in A.1 as a function of k_0.

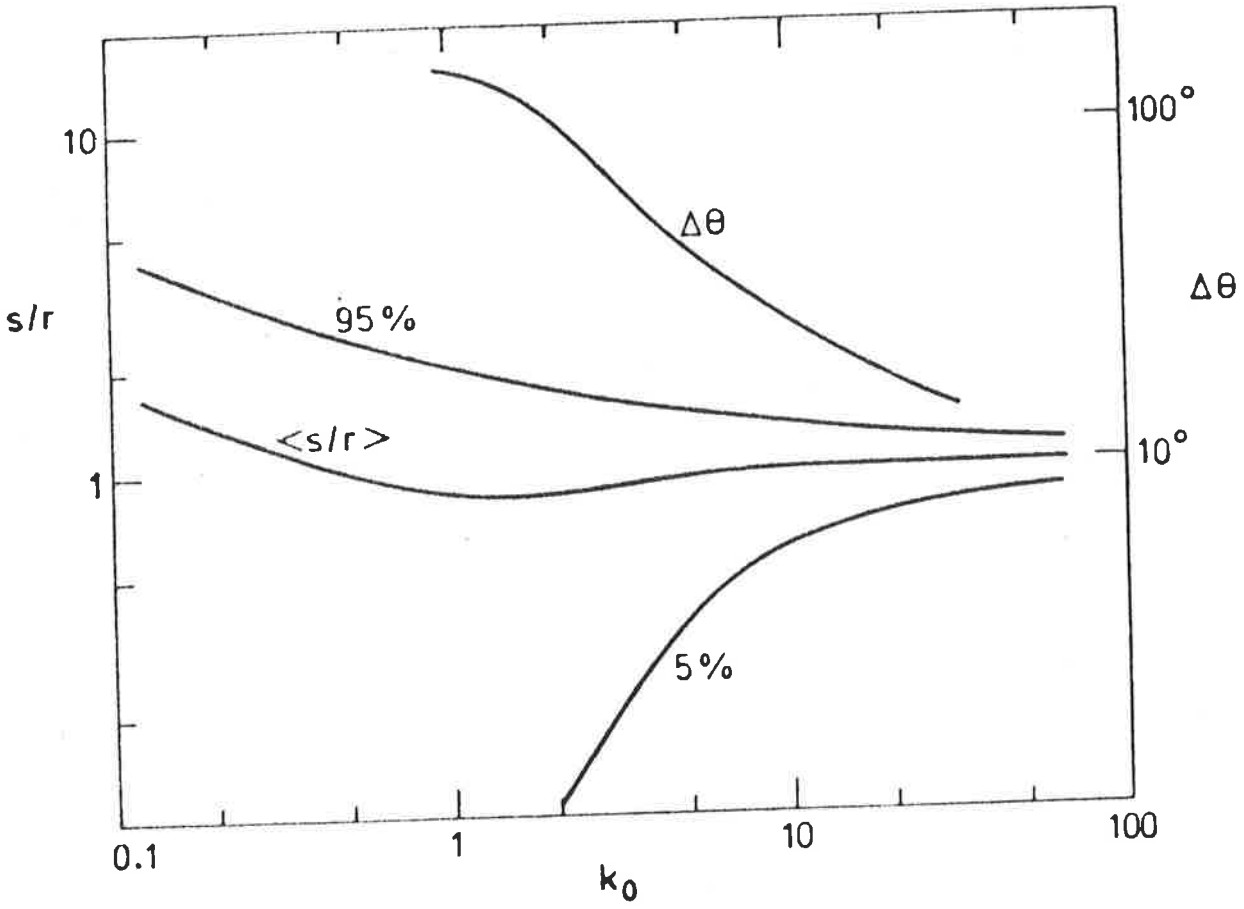

Figure A.1 The best estimate and confidence limits for the ratio of genuine to measured amplitudes. $\Delta\theta$ is the 95% confidence level for the phase . This diagram comes from the data of Linsley (1975a)

REFERENCES

(Note: The initials PICCR stand for - The Proceedings of the International Conference on Cosmic Rays)

Abdullah M.M., Ashton F., Fatemi J., 17th PICCR (Paris) 6 , 151, 1981.

Aguirre C., J. Phys. A 7 , 1474, 1974.

Alexeenko V.V., Chudakov A.E., Gulieva E.N., Sborshikov V.G., 17th PICCR (Paris) 2 , 146, 1981.

Allan H.R. and Davies S.T., 16th PICCR (Kyoto) 8 , 371, 1979.

Allkofer O.C., Bella G., Bohm E., Carstensen K., Dau W.D., Entis A., Greve W., Hartmann G., Jokisch H., Klemke G., Leugers B., Oren Y., Seidman A., Uhr R.C., Yeivin Y., 15th PICCR (Plovdiv) 9 , 62, 1977a.

Allkofer O.C., Bella G., Dau W.D., Fahnders E., Jokisch H., Kaleschke G.P., Klemke G., Oren Y., Virni U., Sauerland K., Seidman A., Schmidtke G., Uhr R.C., 15th PICCR (Plovdiv) 9 , 67, 1977b.

Andam A.A., Chantler M.P., Craig M.A.B., McComb T.J.L., Orford K.J., Turver K.E., Walley G.M., 17th PICCR (Paris) 11 , 281, 1981.

Andam A.A., Chantler M.P., Craig M.A.B., McComb T.J.L., Orford K.J., Turver K.E., Walley G.M., Phys. Rev. D 26 , 23, 1982.

Andrews D., Edge D.M., Evans A.C., Reid R.J.O., Tennent R.M., Watson A.A., Wilson J.G., Wray A.M., 12th PICCR (Hobart) 3 , 995, 1971.

Antonov R.A., Ivanenko I.P., Somosudov B.E., Tulinova Z.I., 12th PICCR (Hobart) 6 , 2194, 1971.

Antonov R.A., Astafiev V.A., Ivanenko I.P., Kapylova T.M., 15th PICCR (Plovdiv) 8 , 137, 1977.

Asakimori K., Jogo N., Kameda T., Maeda T., Mizushima K., Toyoda Y., Yashida M., 16th PICCR (Kyoto) 8 , 247, 1979.

Ashton F. and Nejabat H., 17th PICCR (Paris) 6 , 172, 1981.

Ashton F. and Parvaresh A., 14th PICCR (Munich) 8 , 2719, 1975.

Ashton F., Parvaresh A., Saleh A.J., 14th PICCR (Munich) 8 , 2831, 1975.

Auger P.P., Maze R., Ehrenfest P.Jr., Freon A., J. Phys. Radium 10 , 39, 1939.

Badino G., Galeotti P., Periale L., Saavedra O., Nuovo Cim. Lett. 28 (s2), 93, 1980.

Bell A.R., Mon. Not. Roy. Ast. Soc 182 , 147, 1978a.

Bell A.R., Mon. Not. Roy. Ast. Soc. 182 , 443, 1978b.

Bell M.C., Kota J., Wolfendale A.W., J. Phys. A 7 , 420, 1974.

Bennett S., Delvaille J., Greisen K., Kendziorski F., J. Phys. Soc. Japan 17 (Supp. A3), 196, 1962.

Bergeson H.E., Groom D.E., West W.J., 14th PICCR (Munich) 2 , 581, 1975a.

Bergeson H.E., Boone J.C., Cassiday G.L., 14th PICCR (Munich) 9 , 3059, 1975b.

Bergeson H.E., Boone J.C., Cassiday G.L., 14th PICCR (Munich) 8 , 3064, 1975c.

Bergeson H.E., Cassiday G.L., Cooper D.A., 14th PICCR (Munich) 9 , 3397, 1975d.

Bergeson H.E., Cutler D.J., Davis J.F., Groom D.E., 16th PICCR (Kyoto) 4 , 188, 1979a.

Bergeson H.E., Cutler D.J., Davis J.F., Groom D.E., 16th PICCR (Kyoto) 4 , 194, 1979b.

Bhat C.L., Sarma P.R., Sapru M.L., Kaul C.L., 16th PICCR (Kyoto) 8 , 57, 1979.

Bhat C.L., Sapru M.L., Kaul C.L., Nature 288 , 146, 1980.

Boehm E., 15th PICCR (Plovdiv) 8 , 29, 1977.

Boehm E. and Steinmann E., 16th PICCR (Kyoto) 8 , 294, 1979.

Bourdeau M.F., Capdevielle J.N., Gawin J., Procureur J., 16th PICCR (Kyoto) 9 , 143, 1979.

Bourdeau M.F., Capdevielle J.N., Gawin J., Procureur J., J.Phys. G 6 , 401, 1980.

Bower A.J., Cunningham G., England C.D., Lloyd-Evans J., Reid R.J.O., Walker R., Watson A.A., 17th PICCR (Paris) 2 , 113, 1981.

Bradt H., Clark G., La Pointe M., Domingo V., Escobar I., Kamata K., Murakami K., Suga K., Toyoda Y., 9th PICCR (London) 2 , 715, 1965.

Bray A.D., Goorevich L., Horton L., McCusker C.B.A., Peak L.S., Rapp P., Ulrichs J., Winn M.M., 14th PICCR (Munich) 2 , 609, 1975.

Bray A.D., Horton L., McCusker C.B.A., Peak L.S., Ulrichs J., Winn M.M., 17th PICCR (Paris) 11 , 239, 1981.

Brecher K. and Burbidge G., Ap. J. 174 , 253, 1972.

Broadbent D., Kellermann E.W., Hakeem M.A., Proc. Phys. Soc. A63 , 864, 1950.

Brooke G., Hayman P.J., Kamiya Y., Wolfendale A.W., Proc. Phys. Soc. 83 , 853 , 1964.

Burbidge G. and Brecher K., Comm. Ap. Space Sci. 3 , 140, 1971.

Capdevielle J.N. and Gawin J., J. Phys. G 8 , 1317, 1982.

Casse M., 17th PICCR (Paris) 13 , 111, 1981.

Catz Ph., Gawin J., Grochalska B., Hibner J., Hochart J.P., Milleret G., Stanczyk J., Wdowczyk J. 14th PICCR (Munich) 12 , 4329, 1975.

Chantler M.P., Craig M.A.B., McComb T.J.L., Orford K.J., Turver K.E., Walley G.M., J. Phys. G 8 , L51, 1982.

Chapman S. and Bartels J., Geomagnetism, Vol. 2, Oxford Uni. Press, 1940.

Chitnis E.V., Sarabhai V.A., Clark G.W., Phys. Rev. 119 , 1085, 1960.

Cini G., Proc. Int. Cos. Ray Symp. on H.E. Mod., Tokyo, p101, 1976.

Citron A. and Stiller G., Nuovo Cim. Sup. 8 , 675, 1958.

Clark G.W., Phys. Rev. 108 , 450, 1957.

Clark G.W., Earl J., Kraushaar W., Linsley J., Rossi B., Scherb F., Nuovo Cim. 8 (Sup. 2), 623, 1958.

Clark G.W., Earl J., Kraushaar W.L., Linsley J., Rossi B.B., Scherb F., Scott D,W., Phys. Rev. 122 , 637, 1961.

Clay J., Physica 9 , 897, 1942.

Clay R.W. and Dawson B.R., Aust. J. Phys. 34 , 591, 1981.

Clay R.W. and Gerhardy P.R., J. Phys. G 6 , 909, 1980a.

Clay R.W. and Gerhardy P.R., Aust. J. Phys. 33 , 753, 1980b.

Clay R.W. and Gerhardy P.R., Nuovo Cim. 4C , 26, 1981a.

Clay R.W. and Gerhardy P.R., J. Phys. G 7 , L33, 1981b.

Clay R.W. and Gerhardy P.R., Aust. J. Phys. 35 , 59, 1982a.

Clay R.W. and Gerhardy P.R., Aust. J. Phys. 35 , 441, 1982b.

Clay R.W., Gerhardy P.R., Gregory A.G., 17th PICCR (Paris) 6 , 309, 1981a.

Clay R.W., Gerhardy P.R., Liebing D.F., Thornton G.J., Patterson J.R., Nuovo Cim. 4C , 668, 1981b.

Clay R.W., Wenneberg M.E., Gregory A.G., preprint 1982b.

Clay R.W., Gerhardy P.R., Gregory A.G., Ast. Space Sci. 83 , 279, 1982c.

Clay R.W. and Gregory A.G., Nuc. Inst. Meth. 153 , 467, 1978.

Cleghorn T.F., Freier P.S., Waddington C.J., Canadian J. Phys. 46 , s572, 1968.

Cocconi G., Handbuch der Physik XLVI(1) , 215, 1961.

Cocconi G., Loverdo A., Tongiorgi V., Phys. Rev. 70 , 841, 1946.

Cocconi G. and Tongiorgi V.C., Phys. Rev. 75 , 1058, 1949.

Colgate S.A. and Johnson M.H., Phys. Rev. Lett. 5 , 235, 1960.

Compton A.H. and Getting I.A., Phys. Rev. 47 , 817, 1935.

Cowsik R., Tonwar S.C., Viswanath P.R., Ellsworth R.W., Goodman J.A., Ito A.S., Streitmatter R.E., Yodh G.B., 17th PICCR (Paris) 2 , 120, 1981.

Cowsik R. and Wilson L.W., 13th PICCR (Denver) 1 , 500, 1973.

Coy R.N., England C.D., Pearce D., Reid R.J.O., Watson A.A., 17th PICCR (Paris) 6 , 43, 1981a.

Coy R.N., Lloyd-Evans J., Patel M., Reid R.J.O., Watson A.A., 17th PICCR (Paris) 9 , 183, 1981b.

Cranshaw T.E. and Galbraith W., Phil. Mag. 45 , 1109, 1954.

Cranshaw T.E. and Galbraith W., Phil. Mag. 2, 804, 1957.

Cranshaw T.E., De Beer J.F., Galbraith W., Hillas A.M., Norris S., Porter N.A., Phil. Mag. 3 , 811, 1958.

Crawshaw J.K. and Elliot H., Proc. Phys. Soc. A69 , 102,

1956.

Crouch P.C., Ph.D. Thesis, University of Adelaide, 1979.

Crouch P.C., Gerhardy P.R., Patterson J.R., Clay R.W., Gregory A.G., Nuc. Inst. Meth. 179 , 467, 1981.

Danilova T.V., Kabanova N.V., Nesterova N.M., Nikolskaya N.M., Nikolsky S.I., Katsarsky L.M., Kirov I.N., Stamenov J.N., Janminchev V.D., 15th PICCR (Plovdiv) 8 , 129, 1977.

Das A.K. and De A.K., J. Phys. G 6 , 411, 1980.

Daudin J., Auger P., Cachon A., Daudin A., Nuovo Cim. 3 , 1017, 1956.

Davies R.D., I.A.U. Symp. 20, 1964.

Davies S.T., Elliot H., Marsden R.G., Thambyapillai T., Dutt J.C., Planet. Space Sci. 27 , 733, 1979a.

Davies S.T., Elliot H., Thambyapillai T., 16th PICCR (Kyoto) 4 , 210, 1979b.

Davis L.Jr., Phys. Rev. 96 , 743, 1954.

Dawson B.R., Hons. Thesis, University of Adelaide, 1980.

De Beer J.F., Holyoak B., Wdowczyk J., Wolfendale A.W., Proc. Phys. Soc. 89 , 567, 1966.

Dedenko L.G., Kabanova N.V., Stamenov J.N., 16th PICCR (Kyoto) 8 , 320, 1979.

Delvaille J., Kendziorski F., Greisen K., J. Phys. Soc. Japan 17 (Sup. A3), 76, 1962.

Dixon H.E. and Turver K.E., Proc. R. Soc. A339 , 171, 1974.

Dobrotin N.A., Zacepin G.T., Nikolskij S.I., Hristiansen G.B., Nuovo Cim. Sup. 3 , 635, 1956.

Duperier A., Proc. Phys. Soc. A62 , 684, 1949.

Duperier A., J. Atmos. Terr. Phys. 1 , 296, 1951.

Dutt J. and Thambyapillai T., J. Atmos. Terr. Phys. 27 , 349, 1965.

Dyakonov M.N., Knurenko S.P., Kolosov V.A., Krasilnikov D.D., Kulakovskaya V.P., Kuzmin A.I., Orlov V.A., Sleptsov I.Ye., Yefimov N.N., Yegorov T.A., Nikolsky S.I., 13th PICCR (Denver) 4 , 2389, 1973.

Dyakonov M.N., Egorov T.A., Egorova V.P., Ivanov A.A., Knurenko S.P., Kozlov V.G., Kolosov V.A., Krasilnikov A.D., Krasilnikov D.D., Lishchenuk F.F., Pavlov V.N., Sidorov R.G.,

Sleptsov I.Ye., Nikolskii S.I., 17th PICCR (Paris) 6 , 106, 1981.

Edge D.M., Pollock A.M.T., Reid R.J.O., Watson A.A., Wilson J.G., J. Phys. G 4 , 133, 1978.

Efimov N.N., Krasilnikov D.D., Nifontov M.A., Shamsutdinova F.K., J. Phys. Soc. Japan 17 (Sup. A3), 232, 1962.

Elbert J.W., Keuffel J.W., Lowe G.H., Morrison J.L., 13th PICCR (Denver) 1 , 213, 1973.

Erlykin A.D., Kulichenko A.K., Machavariani S.K., 13th PICCR (Denver) 4 , 2500, 1973.

Evans W.D., Glore J.P., Klebesadel R.W., Laros J.G., Tech E.R., Science 205 , 119, 1979.

Farley F.S.M. and Storey J.R., Proc. Phys. Soc. A67 , 996, 1954.

Farley F.S.M. and Storey J.R., Proc. Phys. Soc. B70 , 840, 1957.

Fenton A.G., Proc. Int. Cos. Ray Symp. on H.E. Mod., Tokyo, p308, 1976.

Fenton A.G. and Fenton K.B., Proc. Int. Cos. Ray Symp. on H.E. Mod., Tokyo, p313, 1976.

Fenton A.G., Fenton K.B., Humble J.E., 15th PICCR (Plovdiv) 11 , 242, 1977.

Feynman R.P., Phys. Rev. Lett. 23 , 1415, 1969.

Gaisser T.K., 15th PICCR (Plovdiv) 10 , 267, 1977.

Gaisser T.K., Stanev T., Freier P., Waddington C.J., Phys. Rev. D 25 , 2341, 1982.

Gerhardy P.R., Clay R.W., Gregory A.G., Liebing D.F., Patterson J.R., Prescott J.R., 17th PICCR (Paris) 6 , 162, 1981.

Gibson A.I., Harrison A.B., Kirkman I.W., Lotts A.P., Macrae J.H., Orford K.J.,Turver K.E., Walmsley M., Nature 296 , 833, 1982.

Ginzburg V.L. and Syrovatskii S.I., The Origin of Cosmic Rays, Macmillan, New York, 1964.

Gombosi T., Kota J., Somogyi A.J., Varga A., Betev B., Katsarski L., Kavlakov S., Khirov I., 14th PICCR (Munich) 2 , 586, 1975.

Gombosi T., Kota J., Somogyi A.J., Varga A., Betev B., Katsarski L., Kavlakov S., Khirov I., 15th PICCR (Plovdiv) 2 ,

167, 1977.

Gregory J.C., Holynski R., Jurak A., Wolter W., Wosiek B., Dake S., Fuki M., Tominaga T., Friedlander E.M., Heckman H.H., Huggett R.W., Hunter S.D., Jones W.V. , Takahashi Y., Parnell T.A., Watts J.W., Miyamura O., Burnett T.H., Lord J.J., Wilkes R.J., Hayashi O., Iwai J., Tabuki T., 17th PICCR (Paris) 9 , 154, 1981.

Greisen K., Prog. Cos. Ray. Phys. III , 1, 1956.

Greisen K., Ann. Rev. Nuc. Sci. 10 , 63, 1960.

Greisen K., Phys. Rev. Lett. 16 , 748, 1966.

Grigorov N.L., Nesterov V.E., Radoport I.D., Savenko I.A., Skiridin G.A., 9th PICCR (London) 1 , 50, 1965.

Grigorov N.L., Rapoport I.D., Savenko I.A., Nesterov V.E., Prokhin V.L., 12th PICCR (Hobart) 5 , 1760, 1971.

Grindlay J., Helmken H.F., Hanbury-Brown R., Davis J., Allen L.R., Ap. J. 201 , 82, 1975.

Hammond R.T., Orford K.J., Protheroe R.J., Shearer J.A.L., Turver K.E., Waddoup W.P., Wellby D.W., Nuovo Cim. 1C , 315, 1978.

Hara T., Hatano Y., Hasabe N., Hayashida N., Jogo N., Kamata K., Kawaguchi S., Kifune T., Nagano M., Tanahashi G., 16th PICCR (Kyoto) 13 , 148, 1979a.

Hara T., Hatano Y., Hasabe N., Hayashida N., Jogo N., Kamata K., Kawaguchi S., Kifune T., Nagano M., Tanahashi G., 16th PICCR (Kyoto) 13 , 154, 1979b.

Hayakawa S., Cosmic Ray Physics, Wiley, New York, 1969.

Heiles C., Ann. Rev. Ast. Ap. 14 , 1, 1976.

Hillas A.M., 16th PICCR (Kyoto) 8 , 7, 1979a.

Hillas A.M., 16th PICCR (Kyoto) 9 , 13, 1979b.

Hillas A.M., Aust. J. Phys. 33 , 911, 1980.

Hillas A.M., 17th PICCR (Paris) 13 , 69, 1981.

Hillas A.M., School of Cosmic Ray Astrophysics, ~~Enrice~~ Erice, 1982.

Hillas A.M., Hollows J.D., Hunter H.W., Marsden D.J., 12th PICCR (Hobart) 5 , 1007, 1971.

Hillas A.M. and Ouldridge M., Nature 253 , 609, 1975a.

Hillas A.M. and Ouldridge M., 14th PICCR (Munich) 12 , 4160, 1975b.

Hodson A.L., Proc. Phys. Soc. A64 , 69, 1951.

Hodson A.L., Proc. Phys. Soc. A66 , 49, 1953.

Humble J.E. and Fenton A.G., 15th PICCR (Plovdiv) 11 , 245, 1977.

James F. and Roos M., Computer Phys. Comm. 10 , 343, 1975.

Janossy L., Cosmic Rays, Oxford Uni. Press., 1948.

Kalmykov N.N., Nechin Yu.A., Prosin V.V., Fomin Yu.A., Khristiansen G.B., Berezhko I.A., Grigorev V.M., Efimov N.N., 16th PICCR (Kyoto) 9 , 73, 1979.

Karakula S., Osborne J.L., Wdowczyk J., J. Phys. A 7 , 437, 1971.

Karakula S., Osborne J.L., Roberts E., Tkaczyk W., 12th PICCR (Hobart) 1 , 310, 1974.

Katsumata I., J. Phys. Soc. Japan 19 , 800, 1964.

Katz J.I., Ap. J. 260 , 371, 1982.

Kempa J., Wdowczyk J., Wolfendale A.W., J. Phys. A 7 , 1213, 1974.

Khristiansen G.B., Abrosimov A.T., Astrashkevitch V.B., Kulikov G.V., Solovieva V.I., Fomin Yu.A., Khrenov B.A., 9th PICCR (London) 2 , 799, 1965.

Khristiansen G.B., Kulikov G.V., Solovieva V.I., Aliev N., Makhmudov R.I., Sharibdzhanov R.I., Sirodzhev N., 16th PICCR (Kyoto) 8 , 365, 1979.

Khristiansen G.B., Kulikov G.V., Solovieva V.I., 17th PICCR (Paris) 6 , 39, 1981.

Kiraly P.J., Kota J., Osborne J.L., Stapley N.R., Wolfendale A.W., Riv. Nuovo Cim. 2 , 1, 1979.

Kiraly P.J., Osborne J.L., White M., Wolfendale A.W., 14th PICCR (Munich) 2 , 612, 1975.

Kiraly P.J. and White M., J. Phys. A 8 , 1336, 1975.

Klemke G., Bella G., Dau W.D., Jokisch H., Oren Y., Liland A., Carstensen K., Allkofer O.C., 17th PICCR (Paris) 9 , 150, 1981.

Kota J., Nature 260 , 507, 1976a.

Kota J., Proc. Int. Cos. Ray Symp. on H.E. Mod., Tokyo, p279, 1976b.

Krasilnikov D.D., Efimov N.N., Nifontov M.A., J. Phys. Soc.

Japan 17 (Sup. A3), 230, 1962.

Krasilnikov D.D., Kuzmin A.I., Linsley J., Orlov V.A., Reid R.J.O., Watson A.A., Wilson J.G., J. Phys. A 7 , L176, 1974.

Krasilnikov D.D., Egorov T.A., Ivanov A.A., Kershenholz I.M., Kozlov V.I., Makarov K.N., Mikhailov A.A., Orlov V.A., Starostin S.K., 15th PICCR (Plovdiv) 2 , 189, 1977.

Krasilnikov D.D. 16th PICCR (Kyoto) 8 , 26, 1979.

Kuhlmann J.D. and Clay R.W, 17th PICCR (Paris) 6 , 96, 1981.

Kuzmichev L.A., Mandritskaya K.V., Osipova E.A., Rakobolskaya I.V., Sokolskaya N.V., Sudov A.S., Tulinova N.I., Varkovitskaya A. Ya., Zatsepin V.I., 17th PICCR (Paris) 2 , 103, 1981.

La Pointe M., Kamata K., Gaebler J., Escobar I., Domingo V., Suga K., Murakami K., Toyoda Y., Shibata S., Canadian J. Phys. 46 , 568, 1968.

Lapikens J., Lloyd-Evans J., Pollock A.M.T., Reid R.J.O., Watson A.A., 16th PICCR (Kyoto) 8 , 19, 1979.

Liebing D.F., Clay R.W., Gregory A.G., Patterson J.R., Prescott J.R., Thornton G.J., 17th PICCR (Paris) 6 , 90, 1981.

Linsley J., Phys. Rev. Lett. 34 , 1530, 1975a.

Linsley J., 14th PICCR (Munich) 2 , 592, 1975b.

Linsley J., 14th PICCR (Munich) 2 , 598, 1975c.

Linsley J., Proc. I.U.P.A.P./I.A.U. Symp. 94, 1980.

Linsley J. and Watson A.A., 15th PICCR (Plovdiv) 2 , 188, 1977.

Linsley J. and Watson A.A., Phys. Rev. Lett. 46 , 459, 1981a.

Linsley J. and Watson A.A., 17th PICCR (Paris) 2 , 137, 1981b.

Lloyd-Evans J., Ph.D. Thesis, University of Leeds, 1982.

Lloyd-Evans J., Pollock A.M.T., Watson A.A., 16th PICCR (Kyoto) 13 , 130, 1979.

Longair M.S., High Energy Astrophysics, Cambridge Uni. Press., 1981.

Lowe G.H., Bergeson H.E., Keuffel J.W., Sandberg V.D., Ozaki S., 13th PICCR (Denver) 3 , 1878, 1973.

Lyons P.R.A., Ph.D. Thesis, University of Tasmania, 1979.

Manchester R.N., Ap. J. 188 , 637, 1974.

Marsden R.G., Elliot H., Hynds R.J., Thambyapillai T., Nature 260 , 491, 1976.

Mathewson D.S., Ap. J. (Lett.) 153 , L47, 1968.

Mazets E.P. and Golenetskii S.V., Ap. Space Sci. 75 , 47, 1981.

McCaughan J.B.T., Ph.D. Thesis, University of Sydney, 1973.

McCaughan J.B.T., J. Phys. G 8 , 413, 1982a.

McCaughan J.B.T., J. Phys. G 8 , 433, 1982b.

McCaughan J.B.T., preprint, Aust. Inst. Phys. 5th Congress, Cos. Ray Workshop, 1982.

McCaughan J.B.T., McCusker C.B.A., Seet S.H., Wand R.H., O'Donnell B., Prescott J.R., Wilson B.G., Nuovo Cim. 38 , 697, 1965.

McCusker C.B.A. and Winn M.M., J. Phys. G 5 , 159, 1979.

Mitsui K., Kitamura T., Minorikawa Y., 17th PICCR (Paris) 9 , 158, 1981.

Miyake S., Ito N., Kawakami S., Hayashi Y., Awaji N., 16th PICCR (Kyoto) 13 , 170, 1979.

Moliere G., Cosmic Radiation, Dover, New York, 1946.

Nagashima K., Sakakibara S., Fujimoto K., Fujii Z., Ueno H., Kondo I., 15th PICCR (Plovdiv) 2 , 154, 1977.

Nikolsky S.I., Kabanova N.V., Stamenov I.N., Janminchev V.D., 16th PICCR (Kyoto) 8 , 335, 1979.

Nikolsky S.I., Nikolskaya N.M., Stamenov I.N., Ushev S.Z., 17th PICCR (Paris) 2 , 129, 1981.

Nishimura J., Handbuch der Physik XLVI(2) , 1, 1967.

Nishimura J. and Kamata K., Prog. Theor. Phys. 5 , 899, 1950.

Nishimura J. and Kamata K., Prog. Theor. Phys. 6 , 262, 1951a.

Nishimura J. and Kamata K., Prog. Theor. Phys. 6 , 628, 1951b.

Norman R.J., Proc. Phys. Soc. A69 , 804, 1956.

Orford K.J. and Turver K.E., Phys. Rev. Lett. 44 , 959,

1980.

Ostriker J.P. and Gunn J.E., Phys. Rev. Lett. 22 , 728, 1969.

Peters B., Nuovo Cim. 22 , 800, 1961.

Phillipps S., Kearsey S., Osborne J.L., Haslam C.G.T., Stoffel H., Ast. Ap. 103 , 405, 1981.

Pollock A.M.T., Ph.D. Thesis, University of Leeds, 1978.

Prescott J.R., Proc. Phys. Soc. A69 , 870, 1956.

Protheroe R.J., Ph.D. Thesis, University of Durham, 1977.

Ramana Murthy P.V. and Subramanian A., Phys. Lett. 37B , 646, 1972a.

Ramana Murthy P.V. and Subramanian A., Proc. Indian Acad. Sci. 76A , 1,1972b.

Rayleigh, Lord, (Strutt J.W.) Phil. Mag. 10 , 73, 1880.

Reid R.J.O., Gopaulsingh K., Page D.E., Idnurm M., McCusker C.B.A., Malos J., Millar D.D., Winterton G., J. Phys. Soc. Japan 17 (Sup. A3), 234, 1962.

Sakakibara S., J. Geomag. Geoelect. (Japan) 17 , 99, 1965.

Sakakibara S., Ueno H., Fujimoto K., Fujii Z., Kondo I., Nagashima K., 16th PICCR (Kyoto) 4 , 216, 1979.

Sekido Y., Nagashima K., Kondo I., Sakakibara S., Proc. Int. Cos. Ray Symp. on H.E. Mod., Tokyo, p302, 1976.

Singer S.F., Phys. Rev. 81 , 579, 1951.

Staubert R., Ph.D. Thesis, University of Kiel, 1968.

Strong A.W., Wdowczyk J., Wolfendale A.W., J. Phys. A 7 , 1489, 1974a.

Strong A.W., Wdowczyk J., Wolfendale A.W., J. Phys. A 7 , 1767, 1974b.

Syrovatskii S.I., Comm. Ap. Space Sci. 3 , 155, 1971.

Thambyapillai T., Proc. NATO Adv. Study Inst. 14 , 37, 1974.

Thornton G.J. and Clay R.W., Phys. Rev. Lett. 43 , 1622, 1979.

Thornton G.J. and Clay R.W., Phys. Rev. D 23 , 2090, 1981.

Trefall H., Nature 171 , 888, 1953.

Trefall H., Proc. Phys. Soc. A68 , 625, 1955a.

Trefall H., Proc. Phys. Soc. A68 , 893, 1955b.

Trefall H., Proc. Phys. Soc. A68 , 953, 1955c.

Vernov S.N., Goryunov N.N., Dmitriyev V.A., Kulikov G.V., Nechin Yu. A., Khristiansen G.B., 6th PICCR (Moscow) 2 , 115, 1960.

Waddington C.J. and Freier P.S., 13th PICCR (Denver) 4 , 2449, 1973.

Watson A.A., Proc. NATO Adv. Study Inst. 14 , 61, 1974.

Watson A.A., Proc. 1st Moriond Ap. Meeting, 1981.

Wdowczyk J., Cosmic Rays at Ground Level, ed Wolfendale A.W., Inst. of Phys, London, p137, 1973.

Wdowczyk J. and Wolfendale A.W., Nature 281 , 356, 1979.

Wenneberg M.E., M.Sc.Eng. Thesis, University of Gothenberg, 1982.

Wolfendale A.W., 15th PICCR (Plovdiv) 10 , 235, 1977.

Zatsepin G.T. and Kuzmin V.A., Soviet Phys. JETP 4 , 114, 1966.